THE UNIVERSITY OF CALGARY

The Development of VISAT - A Mobile Survey System For GIS Applications

by

Naser El-Sheimy

A DISSERTATION

SUBMITTED TO THE FACULTY OF GRADUATE STUDIES

IN PARTIAL FULFILLMENT OF THE REQUIREMENTS FOR THE

DEGREE OF DOCTOR OF PHILOSOPHY

DEPARTMENT OF GEOMATICS ENGINEERING

CALGARY, ALBERTA

SEPTEMBER, 1996

ii

ABSTRACT

During the last decade, the demand for Geographic Information Systems (GIS) in management and design applications has greatly increased. The realization of a GIS in many application areas still suffers from data acquisition problems. To be of value to the user, a GIS must be updated regularly, so that the information in the database correctly represents the real world. However, the acquisition of up-to-date GIS data by conventional survey techniques is prohibitive in cost and has therefore limited the applicability and usefulness of GIS to potential users. Described in this thesis is an attempt to overcome this problem by employing a mobile highway survey system and an associated workstation for georeferenced images.

The total system consists of a data acquisition system, called VISAT, and a data processing system, called VISAT Station. In this thesis, only the first component will be addressed. The data acquisition system has been designed and implemented in cooperation between The University of Calgary (UofC) and GEOFIT Inc. The system can be used to create and selectively update GIS databases very quickly and inexpensively. The system derives its name, **VISAT,** from the fact that it utilizes **V**ideo images, an **INS** system, and the GPS **Sat**ellite system. The system integrates a cluster of Charge-Coupled-Devices (CCD) cameras, an Inertial Navigation System (INS), and satellite receivers of the Global Positioning System (GPS). The system carrier is currently a van, but the use of the system in airborne or marine mode can be realized in a similar way. For the van application, the overall objective was the development of a precise mobile highway

survey system that could be operated at a speed of 60 km per hour and could achieve an accuracy of 0.3 m (RMS) with respect to the given control framework and a relative accuracy of 0.1 m (RMS) for points within a 35 m radius. This accuracy was required in all environments including inner cities, where a stand-alone GPS is not reliable. Sensor integration has been optimized to reliably reach the accuracy requirements in different environments. Data flow optimization has been done with the objective of facilitating the subsequent feature extraction process and transfer into a GIS system.

System testing indicates that highway velocities of 60 km/h can be maintained with adequate data transfer and target positioning in a post-processing mode with the VISAT Station software. Extensive tests in city centers, suburban areas, and rural areas have shown that the run-to-run and day-to-day repeatability achieved is about 10 cm (RMS) in horizontal and about 5 cm (RMS) in height and that the expected absolute positioning accuracy of 30 cm is surpassed in many cases.

ACKNOWLEDGEMENTS

TABLE OF CONTENTS

Page

CHAPTER

LIST OF FIGURES

LIST OF TABLES

NOTATION

1. CONVENTIONS

1.1 Vectors and matrices are typed in boldface.

1.2 Vectors are represented by lower-case letters.

1.3 Matrices are represented by upper-case letters.

1.4 "Vector" means components of a vector. A superscript indicates the particular

frame in which the vector is represented, e.g.,

$$\boldsymbol{r}^b = \begin{bmatrix} r_x^b & r_y^b & r_z^b \end{bmatrix}^T.$$

1.5 Rotation Matrix **R** are specified by two indices such that the transformation

from the b-frame to the c-frame is given by

$$\boldsymbol{r}^c = \boldsymbol{R}_b^c \cdot \boldsymbol{r}^b$$

1.6 Angular velocity of the m-frame with respect to the i-frame coordinated in the

b-frame is described by

$$\boldsymbol{\omega}_{im}^b = \begin{bmatrix} \omega_x & \omega_y & \omega_z \end{bmatrix}^T$$

or by the corresponding skew-symmetric matrix

$$\boldsymbol{\Omega}_{im}^b = \begin{bmatrix} 0 & -\omega_z & \omega_y \\ \omega_z & 0 & -\omega_x \\ -\omega_y & \omega_x & 0 \end{bmatrix}.$$

2. COORDINATE FRAMES

- Operational inertial frame (i-frame)

    - origin : at the mass center of the Earth.

    - x-axis : towards the mean vernal equinox.

    - y-axis : completes a right-handed system.

    - z-axis : coincident with the mean rotation axis of the Earth..

- Earth-fixed frame(e-frame)

    - origin : center of mass of the Earth.

    - x-axis : orthogonal to the z-axis, in the mean Greenwich

      meridian plane.

    - y-axis : completes a right-handed system.

    - z-axis : direction of mean spin axis of the Earth.

The rotation of the e-frame with respect to the i-frame is given by

$$\omega_{ie}^e = \begin{pmatrix} 0 \\ 0 \\ \omega_{Earth} \end{pmatrix} = \begin{pmatrix} 0 \\ 0 \\ 7.2921158x10^{-5} \dfrac{rad}{\sec} \end{pmatrix}$$

- Local-Level frame (LL-frame)

    - origin : at topocenter.

    - x-axis : ellipsoidal east.

    - y-axis : ellipsoidal north.

- z-axis : pointing up along the ellipsoidal normal

The transformation matrix between the LL-frame and the e-frame is given by

$$R_{LL}^{e} = \begin{pmatrix} -\sin\lambda & -\sin\phi\cos\lambda & \cos\phi\cos\lambda \\ \cos\lambda & -\sin\phi\sin\lambda & \cos\phi\sin\lambda \\ 0 & \cos\phi & \sin\phi \end{pmatrix}$$

where,

ϕ is the geodetic latitude

λ is the geodetic longitude

- Body frame (b-frame)

  - origin : at center of accelerometer proof masses. Assumed to be identical with center of rotation of rotated sensor unit.

  - x-axis : pointing to the right-handed side when looking forward.

  - y-axis : pointing forward along the longitudinal.

  - z-axis : completes a right-handed system.

The transformation matrix between the b-frame and the LL-frame is given by

$$R_{b}^{LL} = \begin{pmatrix} \cos(y)\cos(r) - \sin(y)\sin(p)\sin(r) & -\sin(y)\cos(p) & \cos(y)\sin(r) + \sin(y)\sin(p)\cos(r) \\ \sin(y)\cos(r) + \cos(y)\sin(p)\sin(r) & \cos(y)\cos(p) & \sin(y)\sin(r) - \cos(y)\sin(p)\cos(r) \\ -\cos(p)\sin(r) & \sin(p) & \cos(p)\cos(r) \end{pmatrix}$$

where,

(r, p, y) are the three Euler angles defined as:

r   roll, around y-axis, positive counter-clockwise when seen from the positive end of the axis

        p   pitch, around x-axis, positive counter-clockwise when seen from the positive end of the axis

        y   yaw, around z-axis, positive counter-clockwise when seen from the positive end of the axis

3. ACRONYMS

- 3-D   Three dimensional
- ABS   Anti-lock Braking-System
- ADC   Analog-to-Digital Converter
- C/A Code   Coarse/Acquisition Code
- AVLN   Automatic Vehicle Location and Navigation
- CCD   Charge Coupled Devices
- CCIR   Commite Consultatif International des Radiocommunications
- CEP   Circular Error Probable
- CPU   Central Processing Unit
- DBMS   Data Base Management System
- DD   Double Difference
- DOP   Dilution of Precision
- DR   Dead Reckoning
- EIA   Electronics Industries Association

- FOV   Field of View
- GCP   Ground Control Point
- GPS   Global Positioning System
- Hz   Hertz
- HSYNC   The video image's Horizontal Synchronization signal
- INS   Inertial Navigation System
- IMU   Inertial Measuring Unit
- IRQ   Interrupt Request
- ITS   Intelligent Transportation Systems
- IVHS   Intelligent Vehicle Highway Systems
- NTSC   National Television Systems Committee
- OTF   On The Fly
- PC   Personal Computer
- P Code   Precise Code
- PLL   Phase-Locked-Loop
- PPS   Pulse Per Second (of the GPS receiver)
- RAM   Random Access Memory
- RMS   Root Mean Square
- RTC   Real Time Clock
- RAID   Redundant Array of Independent Disks
- SCSI   Small Computer System Interface
- UTM   Universal Transverse Mercator

- VGA   Video Graphics Array

- VISAT   **V**ideo-**I**nertial-**SAT**ellite

- VSYNC   The video image's Vertical Synchronization signal

- WL   Wide Lane

- ZUPT   Zero Velocity Update

List of Figures

List of Tables

CHAPTER 1

INTRODUCTION

1.1 Background

With the continuing growth of urban centers on a world-wide scale, the demand of city planners for up-to-date information is increasing at a rapid rate. This has led to the establishment of spatially-referenced Geographic Information Systems (GIS) for a variety of applications. The information needed is expensive to obtain by conventional methods. These methods are therefore not well suited for rapid updating. In addition, conventional methods often supply only pointwise information and are therefore not suited to answer the increasingly complex questions concerning the interaction of different factors in urban centers and their time dependencies. Satellite remote sensing and aerial photogrammetry are two methods which can provide a variety of GIS information at high rates and reasonable cost. However, in the first case the associated accuracy is not currently sufficient for many applications, and in the second case the near vertical field of view provides only part of the information needed.

Furthermore, the quality and type of information required by the user is changing. Quite often the user prefers a cartographically less perfect product (e.g. map substitute) that contains the most recent information rather than a product of very high cartographic standard but with contents that is not up-to-date. Also, the demands for user specific maps or data, and for non-cartographic products such as reports, images, graphs, and answers to questions are steadily increasing. This requires mapping organizations to be more sensitive to user needs and to put in place more flexible information revision processes which can be optimally achieved using information technology only.

With the advances made in satellite and inertial georeferencing techniques and the ready availability of digital imaging sensors, a considerable portion of GIS information can potentially be acquired from moving vehicles. The advantage of kinematic-mode data collection is that the survey can be performed much faster and therefore more economically.

1.2 Vehicle Navigation Systems

Land vehicle navigation has advanced significantly over the past ten years. This has been due largely to the advancement of navigation and computer related technologies (Krakiwsky, 1991). During this period, land vehicle navigation has been known as, or associated with, Automatic Vehicle Location and Navigation (AVLN), Intelligent Vehicle

Highway Systems (IVHS), Intelligent Transportation Systems (ITS) and ,more recently, Mobile Mapping Systems (MMS).

In recent years there has been an explosion in the number, type and diversity of system designs and application areas. A total of 280 distinct land AVLN systems have been documented in Krakiwsky et. al. (1995). These systems can be classified into five types: Autonomous, Fleet Management, Advisory, Inventory and Mapping, and Portable. Table 1.1 lists the characteristics and applications of these systems.

Positioning, locating, and navigating are distinct processes in these AVLN systems. Positioning is determining coordinates in a fixed coordinate system (Krakiwsky and Wells, 1971). Coordinates by themselves do little to tell the average person where they are. Locating is the process of putting coordinates into a frame of reference that is more useful. Typically, a map with topographical features, navigational aids, roads, street addresses, etc. is used to determine location (Bullock, 1995). Navigation regards the provision of directional information on how to travel from the vehicle's present position to a given destination or a set of waypoints (Harris, 1988).

Classical AVLN systems used to be single-sensor systems either using satellite-based sensors (e.g., Global Positioning System(GPS)), land-radio-station techniques (e.g., Loran C), road-facility infrastructures (e.g., beacons), or a dead reckoning (DR) sensors (e.g., compass and odometery) (Abousalem, 1993). For high accuracy applications, integrated navigation sensors, such as GPS/INS, were employed. The cost of such systems is higher

than that of single-sensor systems, however, the integration is a trade-off between cost on the one hand and performance, versatility, accuracy, and reliability on the other (Wong et. al., 1988). Truly, it is the application itself which inherently defines the system's specific requirements and limitations and likewise governs the various navigational and informational strategies to be incorporated. For example, the integration of navigation sensors with sighting devices, e.g. digital cameras and laser imaging, extends the application of AVLN systems to inventory and mobile mapping.

1.3 History of Mobile Mapping Systems

Starting with the development of the Mobile Highway Inventory System (MHIS) by a number of Canadian provinces and some US states in 1983, surveying from a moving van has become more and more sophisticated and is now at a point where it matches classical survey methods in accuracy and far surpasses them in economy. In the classical approach, discrete static measurements are used to fix the position of individual points which are then used to derive highway features of interest. In the kinematic approach, a combination of navigation and imaging sensors are used to record all visible features along a highway corridor from a moving van. This information is then used to form a continuous three-dimensional (3-D) model of the highway corridor from which all features of interest can be extracted and stored in a 3-D GIS Systems (Schwarz et. al. (1993a)).

Table 1.1 : List of AVLN Systems Characteristics and Applications (Sources: Krakiwsky

et. al. 1995, Abousalem (1993), and Bullock (1995))

System	Characteristics	Applications
1. Autonomous	Stand-alone vehicles with positioning device and a map database.	Used in personal vehicles for on-line guidance and assistance; basically replacing paper maps and yellow pages.
2. Fleet Management	♦ Fleets of vehicles linked to a control center via communications link. ♦ Although positioning sensors are available in the vehicles, the map databases are not necessary. ♦ The control center is responsible for the transmission of the necessary information to the vehicle on call.	Civic applications, such as police, fire fleets, ambulance, delivery services, etc.
3. Advisory	♦ A blend of autonomous and fleet management architecture. ♦ Not controlled by a dispatcher center, but part of a fleet that is being served by a traffic control center. ♦ The control center is a mobile service center. ♦ Vehicles receive updated information regarding traffic and weather information without the control center being able to identify them.	♦ Used for access to route information, such as real-time traffic information, turn restrictions, one-way streets, and, in some systems, weather conditions. ♦ Essential to minimize route travel time and to prevent and avoid traffic congestion.
4. Inventory and Mapping	♦ Autonomous vehicles equipped with navigation and imaging sensors. ♦ May have a communications link with a control center.	Used in the inventory of road conditions, mapping, and general GIS applications.
5. Portable	Autonomous systems that are not permanently installed in a vehicle.	Used by tourists, hikers, real estate agents, hunters, business travelers, and others.

The initial MHIS had these capabilities only in an embryonic stage. It used gyroscopes, accelerometers, and a wheel odometer to fix the location of the vehicle, and video cameras to document features in the highway corridor. The positioning accuracy of this survey van was rather poor and the video images were not digitized for measurement purposes. However, it provided a good visual record of highway features and their approximate locations. In 1988, a major step forward was made when a new positioning and orientation component was tested for the Alberta MHIS. Satellite methods (i.e. differential GPS) were employed to improve the positioning accuracy and an inertial strapdown system was used to bridge GPS outages and to provide the capability for accurate camera orientation. Results of these tests showed that positioning of the vehicle was possible with an accuracy of 0.2 to 0.3 m while moving at a speed of 50 to 70 km per hour (for details, see Lapucha, 1990). A proposal to further develop this system into a precise highway survey system was discussed by Lapucha et. al. (1990).

The next major step was made when the information contained in the video images was itself incorporated into the measurement process. This idea is basic to the highway van developed by the Ohio State University's Center of Mapping and the GEOVAN system operated by GEOSPAN Corp.. Both systems work with an array of video cameras. The video information is stored and individual images are digitized post-mission. If digital images of the same object are available from two different positions, then the 3-D position of the object with respect to the camera reference can be obtained. As long as the distances between object and camera reference are short, high positioning accuracy can be achieved. In order to maintain this accuracy along the whole trajectory, the position and

orientation of the cameras has to be determined with a similar accuracy. Little information has been published on how the orientation of the images is obtained in the above mentioned systems or how the different data streams are time-tagged. It is, therefore, difficult to assess the overall accuracy of these systems at this stage.

In this thesis, the further development of mobile multi-sensor systems for inventory and mapping is described. While this work was pursued at The University of Calgary, similar ideas were developed by other research groups. Table 1.1 lists other developed Mobile Mapping Systems (MMS) and their hardware structures. Their accuracy is typically in the 1-2 m range. This was not sufficient for the development of the system described in this thesis which required accuracy of 0.3 m or better. For detailed information on the other systems, the following references should be consulted Bossler et. al. (1993), Halverson (1992), Pottle (1995), Baraniak (1994), ROADWARE (1994), and Ash (1995).

Table 1.1 : List of Existing MMS and Their Hardware Structure

Van		Positioning				Cameras		Accuracy (m)
Name	Developer	GPS	INS	DR	Gyros	CCD	VHS	
GPS Van	OSU	♦		♦	♦	2	2	±1 (x, y) ±2 (h)
GeoVAN	GeoSPAN	♦	♦				8	±1
GPSVision	Lambda	♦		♦	♦	2		±1 (x, y) ±2 (h)
ARAN	Roadware	♦		♦		2	1	1-5
GIM	Navsys	♦	♦				1	±1-3
TruckMAP	JECA	♦			♦	1	1	±1-2
ITC	Infrared Tech.	♦					1	-

1.4 Research Objectives

The main objective of this thesis is the development of a fast and accurate survey system which operates from a moving vehicle. The system described was developed as part of The University of Calgary's research on precise multi-sensor mobile surveying systems for general mapping and GIS applications. The system is named **VISAT**, alluding to the fact that it integrates <u>**V**</u>ideo cameras, an <u>**I**</u>nertial system, and <u>**SAT**</u>ellite GPS receivers. The VISAT concept integrates ideas mentioned previously with the requirements for an accurate and versatile GIS. More specifically, a precise mobile survey system had to be developed that could be operated at speeds of up to 60 km per hour and achieve a positioning accuracy of 0.3 m (RMS) with respect to the given control framework and a relative accuracy of 0.1 m (RMS) for points within a 35 m radius; sensor integration had to be optimized to reach these requirements; and data flow had to be streamlined to facilitate the subsequent feature extraction process and transfer into a GIS. The specified accuracy was required in all environments, including inner cities, which made it impossible to use GPS alone for positioning. The data capturing and storage process had to be separated from the feature extraction process for the GIS. Thus, the development of a stand-alone workstation was an important requirement in the overall system concept.

Under the overall objective, the following tasks had to be addressed :

- Choose suitable hardware for the system,
- Develop GPS/INS/Video integration, synchronization, and logging software,
- Develop a georeferencing model for video images,

8

- Develop calibration software for the integrated system,

- Investigate the main factors affecting the final accuracy of the VISAT system,

- Implement real-time and post-mission quality control, and

- Test the production system in different operational environments.

1.5 Thesis Outline

In Chapter 2, the concept and the major components of the VISAT system are described. Hardware limitations and the integration of GPS and INS with video cameras are outlined. The underlying principle of extracting 3-D coordinates from the video images through the use of INS/GPS data is briefly discussed.

In Chapter 3, techniques of integrating multi-sensor data for mapping applications will be discussed. It is understood that multi-sensor integration implies different mathematical and physical models. Essential components of multi-sensor systems for mapping applications will be discussed and a general model for georeferencing of multi-sensor data will be presented.

In Chapter 4, the calibration of all sensors of the integrated system will be presented as an essential requirement to ensure accurate 3-D positioning. System calibration includes the determination of camera parameters which define the internal geometry of the camera.

They are termed the inner orientation parameters. The relative location and orientation between the camera cluster and the navigation sensors (GPS and INS) are defined by the relative orientation parameters. The relative orientation parameters will be used in the georeferencing process for the transformation of the 2-D image coordinates into the 3-D object coordinates. In this chapter, an overview of imaging with CCD cameras will be given as an introduction to the general requirements of their calibration. Mathematical models of integrating the navigation sensor output in the calibration procedure will be discussed.

In Chapter 5, the factors affecting the accuracy of the 3-D coordinates are discussed. The final accuracy of 3-D coordinates computed from the VISAT system is a function of the complete processing chain, which involves GPS position, INS position/attitude, system synchronization, system calibration, pixel size, pointing accuracy, and van speed. The procedure of 3-D coordinate computation will be discussed, followed by a discussion of the factors affecting the accuracy. The expected accuracy of the 3-D coordinates and the contribution of each component to the error budget will conclude the chapter.

In Chapter 6, the results of system testing are presented. The system was tested in Calgary, Montreal, and Quebec City over a total 500 km of roads. The test areas included open areas, urban centers with narrow roads, and minor and major highways with a number of overpasses. A detailed analysis of these tests will be given.

Finally, Chapter 7 draws conclusions from the research work conducted and gives recommendations for future work.

Some of the material presented in Chapters 3, 5, and 6 has been previously published in papers. In those cases where the candidate has been the author or a co-author of these papers, quotations are not indicated as such, but are simply referenced.

CHAPTER 2

SYSTEM OVERVIEW

This chapter presents the system concept and the major components of the VISAT system, and highlights some of the hardware limitations and integration problems. It also introduces the principle of extracting 3-D coordinates from video images through the use of INS/GPS data.

2.1 System Concept

Figure 2.1 shows the conceptual design and data flow of the VISAT system in schematic form. The total system consists of a data acquisition system, called VISAT Log, a georeferencing processor, called GEORef, and a measuring and processing system, called VISAT Station. The georeferencing processor consists of an image processing module, called ImgProc, and navigation processor, called KINGSPAD. The VISAT Station implements the concept of storing georeferenced digital images as the basic unit for 3-D coordinate determination. By combining an arbitrary number of such units, which may be from different time periods, the specific information required is obtained. The system can be used to selectively update and create precise GIS databases very quickly and inexpensively. Currently, the system carrier is a van (Figure 2.2), but other carriers such as ships or aircraft can also be used.

The VISAT System
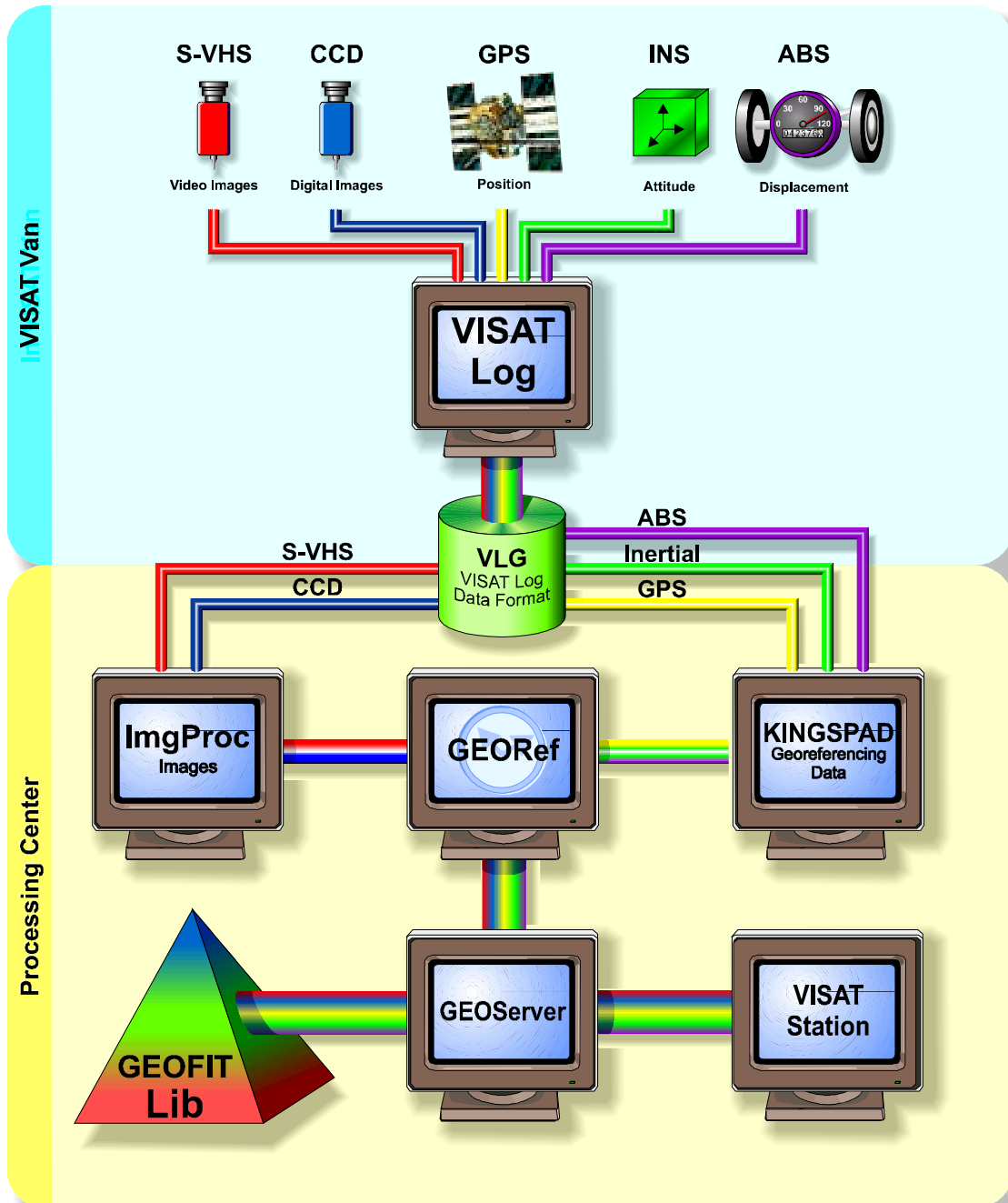
Figure 2.1 : The VISAT System
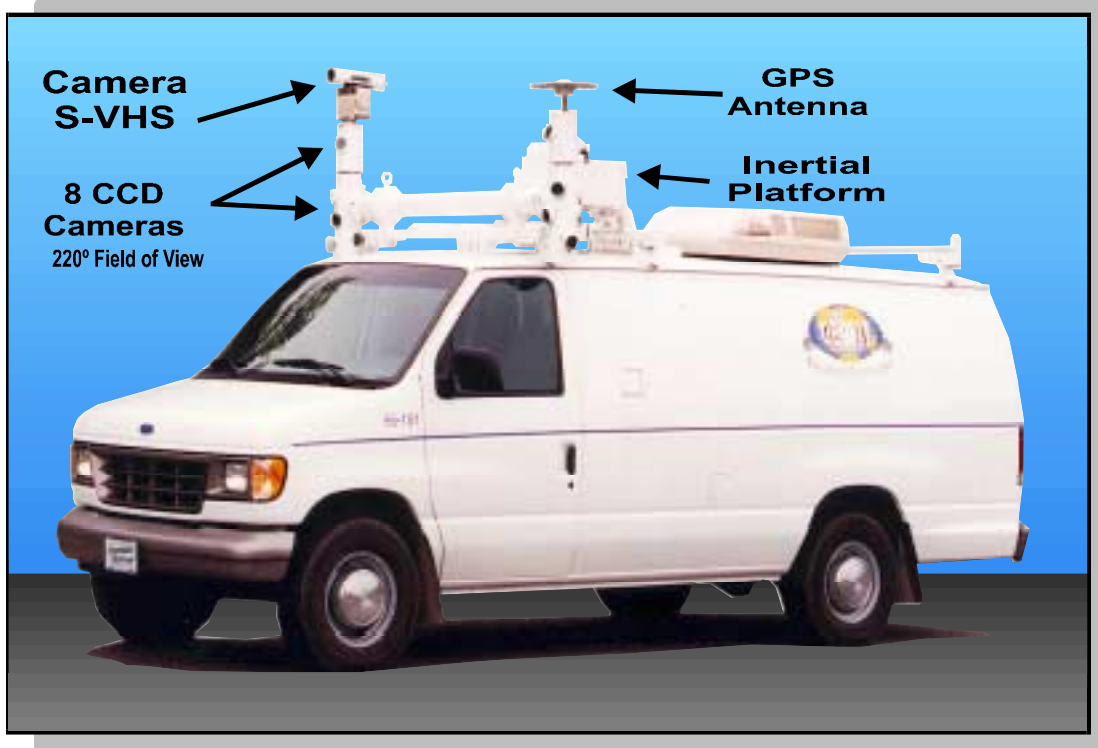
Figure 2.2: The VISAT Van

The overall objective of the VISAT development was the design of a precise mobile survey system, for road inventory and general cadastral GIS applications, that could be operated at speeds of up to 60 km per hour and would achieve an accuracy of 0.3 m (RMS) with respect to the given control framework and a relative accuracy of 0.1 m (RMS) for points within a 35 m radius.

The system data acquisition components are a strapdown INS system, two L1/L2 GPS receivers, a cluster of video cameras, an Antilock-Braking-System (ABS) pick-up, an image control unit, and a S-VHS camera. The function of each component can be subdivided into primary and secondary tasks. In terms of primary functions, the camera

cluster provides 3-D positioning with respect to the VISAT reference, which in most cases is the perspective center of one of the cameras. The position of this reference with respect to the existing control is determined by differential GPS techniques, while the camera orientation in 3-D space is given by the INS. The ABS system will trigger the cameras at constant distance intervals using the VISAT controller trigger channel. In terms of secondary functions, the camera cluster provides redundancy, i.e. more than two images of the same object; the GPS controls the INS error propagation; and the INS, when used in positioning mode, bridges GPS outages, corrects GPS cycle slips, and gives precise interpolation between GPS fixes. The ABS data can be used to update the INS data in case of GPS signal blockage.

Surveying by VISAT, therefore, consists essentially of three parts (Figure 2.3): data acquisition, georeferencing, and 3-D positioning for GIS. The acquisition of synchronized GPS, INS, ABS, and image data has been fully automated to minimize field time while maintaining data quality. Position and orientation of the moving VISAT reference is obtained in the georeferencing process which requires GPS/INS data input and is currently performed in post-mission mode. Positioning of objects in the road corridor with respect to the VISAT reference is done in post-mission using two or more oriented camera images. The result of this operation can directly be used to update or create GIS databases. A brief description of each component is given in the subsequent sections.

<div align="center">

Data Acquisition	Georeferencing	Measurements & GIS
Automated collection of GPS, INS, and CCD image data	Put position and attitude stamp on images	Obtain 3-D coordinates of all important features and store them as GIS elements

</div>
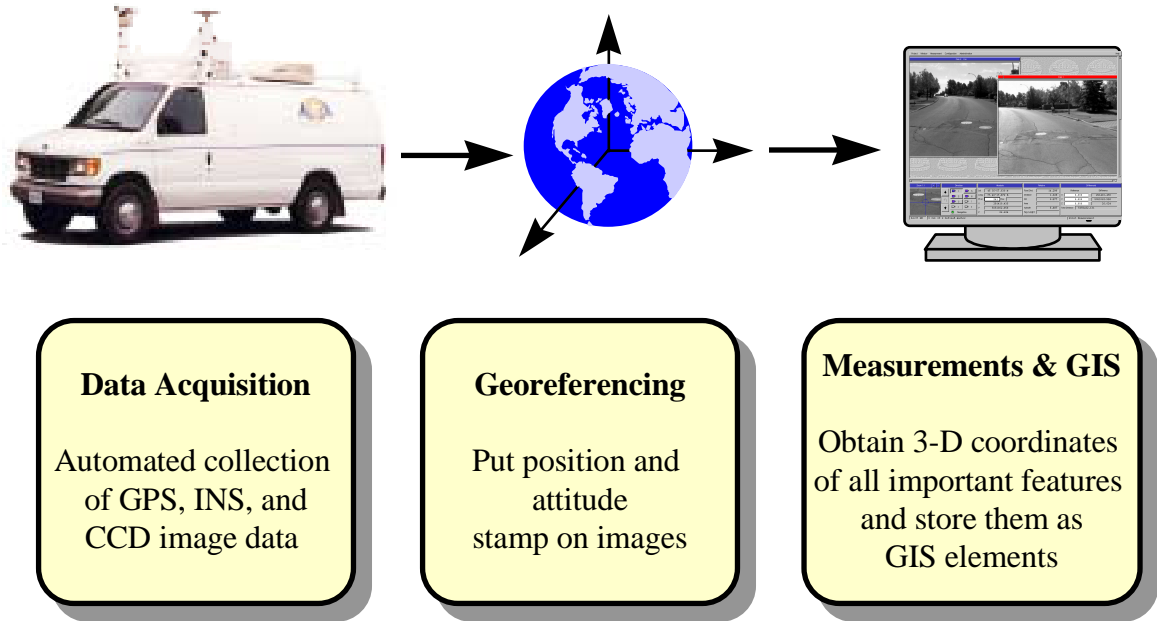
Figure 2.3 : The VISAT System Data Flow

2.2 Hardware and Data Acquisition

2.2.1. The VISAT Navigation Component

Determining the navigation information (position and orientation) of the VISAT reference in 3-D space is in principle a problem of trajectory determination. The general motion of each camera in space can be described by six parameters. They are typically chosen as three position and three orientation parameters. Measuring systems used for VISAT trajectory determination must, therefore, have the capability to sense six independent quantities from which these parameters are derived.

A conceptually simple implementation of this concept is a strapdown inertial measuring unit. It consists of three gyroscopes which are used to sense angular velocity, and three accelerometers which are used to sense specific force. The first set of measurements is integrated in time to provide orientation changes of the vehicle relative to its initial orientation. The second data set is used to derive vehicle acceleration with respect to three orthogonal axes which after double integration with respect to time gives position differences relative to an initial position. Thus, a strapdown inertial measuring unit can, in principle, provide all information needed for this specific application. In practice, due to the double integration, the time-dependent position errors will quickly exceed the accuracy specifications for VISAT. Frequent updating is, therefore, needed to achieve the required accuracy. One of the typical update measurements is the Zero-Velocity-Update (ZUPT) which is simply obtained by stopping the vehicle. Disadvantages of using ZUPTs are:

- the system will be limited to semi-kinematic applications;

- on highways and high-traffic roads, it is not possible to stop the vehicle without interrupting the traffic flow;

- the production rate, which is critical in many projects, will be reduced.

For more details, see El-Sheimy and Schwarz (1994).

GPS is another measuring system that can be used for trajectory determination. To reach the accuracy required, it has to be used in differential mode, i.e. with one receiver stationary at an initial known point and the other receiver in the moving vehicle. The system output in this case are ranges and range rates between satellite and receiver,

17

derived from carrier phase data. These measurements can be used to determine position and velocity of the vehicle with respect to the initial point. Both of these vectors are given in an earth-fixed coordinate system, so that it is, in principle, possible to derive orientation changes by differencing techniques. Thus, GPS can also provide the information needed for this specific application. Its major drawback is the problem of cycle slips which are in essence gross errors leading to a discontinuity in the trajectory. In addition, the range and range rate measurements are not truly independent, and the current data density and accuracy are not sufficient to meet the accuracy requirements for VISAT orientation.

The navigation component of the VISAT system consists of two Ashtech Z12 GPS receivers, a Honeywell Laser-Ref III strapdown INS, and an ABS pickup. The combination of the three measuring systems offers a number of advantages. In the absence of cycle slips and signal blockage, the precise positioning accuracy of differential GPS can be used to provide frequent updates for the inertial system. The inertial sensor orientation information and precise position and velocity over short time intervals allow the detection and correction of cycle slips. The ABS data can be used to update the INS if the GPS signal is blocked for periods longer than the INS bridging level required to recover the GPS ambiguities. In general, the fact that redundant measurements are available for the determination of the six required trajectory parameters greatly enhances the reliability of the system. See Appendix (1) for technical description of the INS Laser-Ref III and the Ashtech Z-12 receiver.

2.2.2 The VISAT Imaging Component

The imaging component of the VISAT system consists of eight video cameras, of the COHU 4980 series, with a resolution of 640 x 480 pixels (see Appendix (1) for technical specification of the cameras). The cameras are housed in a pressurized case and mounted inside two fixed-base towers on top of the VISAT van, thus eliminating any chance of camera movement during the survey. Six of these cameras are arranged in such a way that they provide a 220-degree horizontal field of view (FOV) and 37 degrees vertical FOV. The other two cameras are dedicated to special high features, e.g. power lines.

Problems that have to be addressed when integrating the CCD cameras with the INS/GPS systems are due to current hardware limitations. They are :

1. Most of the frame grabbers on the market can capture at most images from 3-4 cameras in a multiplexing mode. In this mode, the time delay between images from different cameras is of the order of 0.1 sec. During this delay the van will move at least 1-1.5 m, hence the advantages of having fixed-base between the cameras is lost. This will affect the final accuracy since any small errors of the INS/GPS will be amplified due to the small baseline between the cameras.

2. The existing off-the-shelf image processing systems which capture up to six images simultaneously require all the cameras to be synchronized. Synchronizing eight cameras requires special hardware which is not currently available on the market.

3. In order to capture and record six images simultaneously every 5-6 m (0.4 sec at 60 km/h), the data transfer rate between the frame grabber and the system memory should be of the order of 3-4 MB/sec. This requires a 32-bit bus digitizing board which is quite rare on the market. See Table 2.2 for more details about the time taken by each component of the VISAT system.

4. The limited transfer rate of most hard disks will consume most of the logging computer central processing unit (CPU) time especially when transferring the image data.

In order to solve the problem of grabbing six images simultaneously the Matrox IMAGE-CLD has been chosen. The IMAGE-CLD is a color digitizer which can grab up to three images simultaneously from three synchronized monochrome cameras. Two such boards can be installed in one computer without having a conflict with other hardware, such as the Video Graphics Array (VGA) address. The COHU 4980 has genlock capabilities, externally synchronized to an external sync generator. The external sync can be the composite sync signal of another camera (sync containing both horizontal and vertical sync pulses of the Video signal). Therefore, one of the cameras can provide the synchronization by applying the composite sync to the other cameras genlock boards. The IMAGE-CLD is interfaced to the baseboard, a Matrox IMAGE-640, which works as a temporary storage and an interface between the digitizer and the host computer. The IMAGE-640 has an EISA bus interface which provides a full 32-bit data interface to the host interface and fast image transfer.

Table 2.1 : VISAT Data Capture and Write Cycle.

Cycle	Hardware	Time (msec)	% of Cycle	Comments
Data Capture (Total time = 100.6 msec)	1. GPS	3.4	3.6	1. Read, decode, and write.
	2. INS	5.1	5.1	2. Read, decode, and write.
	3. ABS	0.1	0.1	3. Receive and write.
	4. CCD	91.2	91.1	4. Capture five images.
	5. Keyboard	0.1	0.1	5. Keyboard interrupts.
Image (Total Time = 387 msec)	1. Read	237.5	61.4	1. Read from the imaging board.
	2. Write	149.2	38.6	2. Write to the hard disk.
Total time		487.6		

To synchronize the eight cameras, a video signal controller (VISAT Controller) has been designed. The controller can handle up to 16 cameras and redirect eight of them in real-time according to eight predefined user configurations. This allows the addition of more cameras in the future. The controller also includes two dedicated input channels for the ABS data and the GPS receiver Pulse Per Second (PPS). With these data the controller can perform the following:

• receive the ABS data and interrupts, and count the number of ABS pulses between two consecutive GPS PPS,

• trigger the cameras at a certain predefined user distance; thus all the images within the survey mission are equally spaced,

- switch off/on the cameras if the van stops at a traffic signals,

- stamp any distance-dependent events automatically with the GPS time, e.g. start/end of INS ZUPTs, start/end of GPS static periods,

- provide the sync signal required for synchronizing the eight output images,

- send a warning message to the driver's remote warning panel, to stop the system for an INS ZUPT in case of frequent GPS signal blockages.

All cameras are externally synchronized so that any image record (six images) is related to one position of the van. The images grabbed from these cameras are compressed in real-time using a file system format and then stored to a RAID (Redundant Array of Independent Disks). The RAID can store up to 17 Gbyte of data, which correspond to 110,000 images. To speed up the RAID SCSI disk transfer rate, an EISA cashing SCSI adapter has been used to transfer the data from the system memory to the RAID with a special low-level SCSI access format. Each image record is stamped with the GPS time indicating the time of grabbing the images. This time is used in post-mission to georeference the video images using the GPS/INS position and attitude data as described in Chapter 3.

The imaging component of the VISAT van includes one S-VHS video camera. The camera can be zoomed and tilted in real-time in any direction using a control unit inside the van. The images are coded with the GPS time on the audio track of the video tape. The color images are used in applications which do not currently require metric applications.

2.2.3 System Integration

In the vehicle, all the sensors are interfaced to a standard PC-486 in a decentralized manner, which controls the different tasks through program interrupt processes. Figure 2.4 shows a block diagram of the VISAT system hardware interfaced to the PC.

The VISAT hardware is controlled by the real-time data logging software **VLog** (**V**ISAT **Log**ging). The VLog has been written in such a way that it can manipulate different hardware components in a decentralized manner (see Figure 2.5 for the VLog hardware initialization window). The output files from the VLog software are the input to the processing software.

The VLog software performs the following functions through an interrupt process (El-Sheimy and Schwarz, 1994):

- Storing the INS position and attitude information at a data rate of 50 Hz. The INS is interfaced to the computer through an ARINC-429 serial board. At present the board issues 50 interrupts per second through IRQ 5;

- Storing the GPS position and velocity at a data rate of 2 Hz (2 k byte/sec). With the RS-232 data from the GPS receiver, every byte issues one interrupt. The CPU may have to service up to 2000 interrupts (bytes) per second. To avoid problems with this large number of interrupts, an intelligent RS-232 board with its own CPU and buffer is used, much like the ARINC. With this smart board, the GPS data can be grabbed once per second, thereby reducing the number of GPS data interrupts;

8 CCD
Cameras

GPS

INS

PPS   RS232

RS170

Arinc   429

Serial Board

2 A/D Frame Grabbers

VISAT
Controller

Arinc Board

Logging Computer

ABS

Navigation
Data

Image
Data
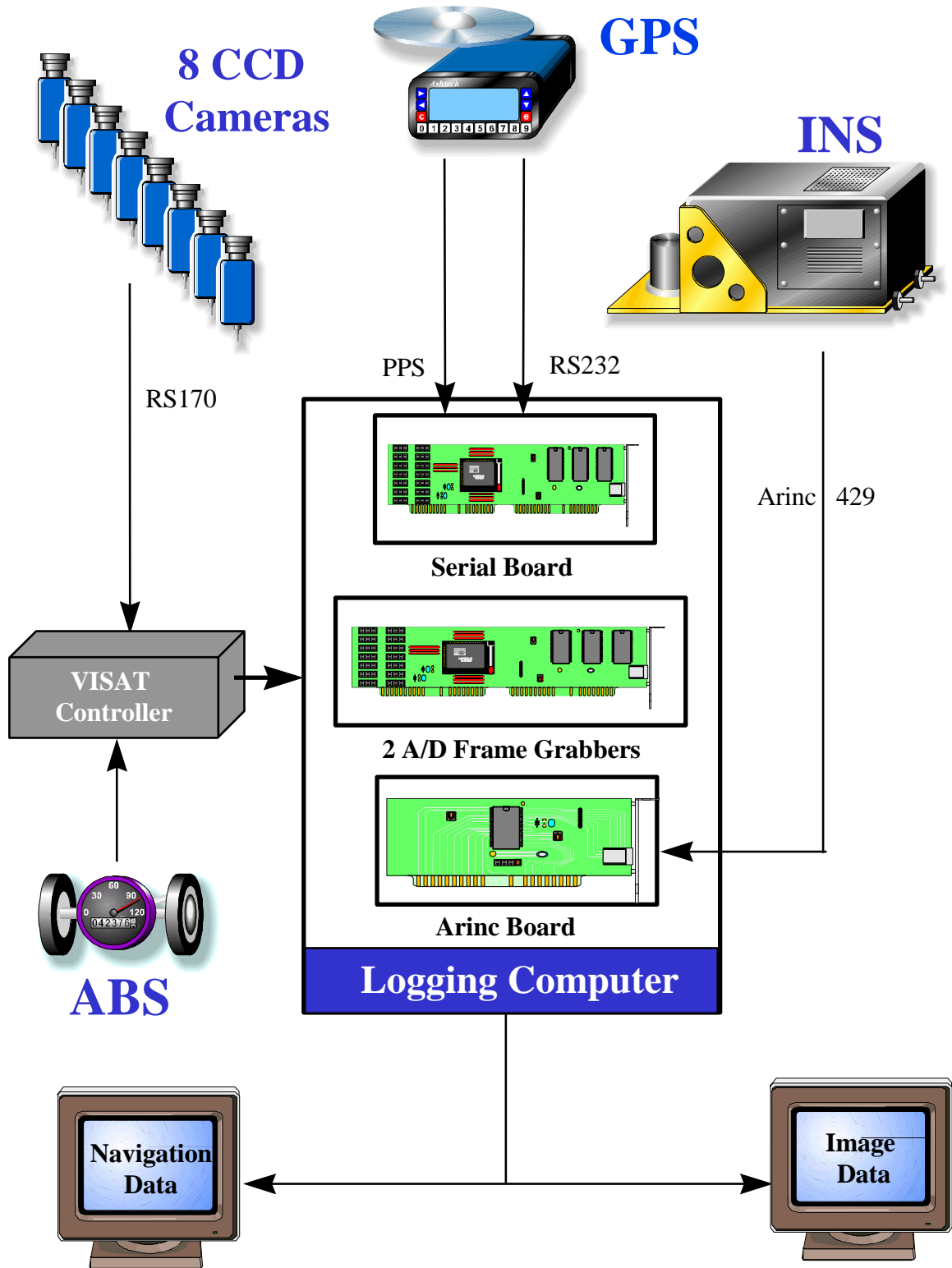
Figure 2.4 : The VISAT System Hardware
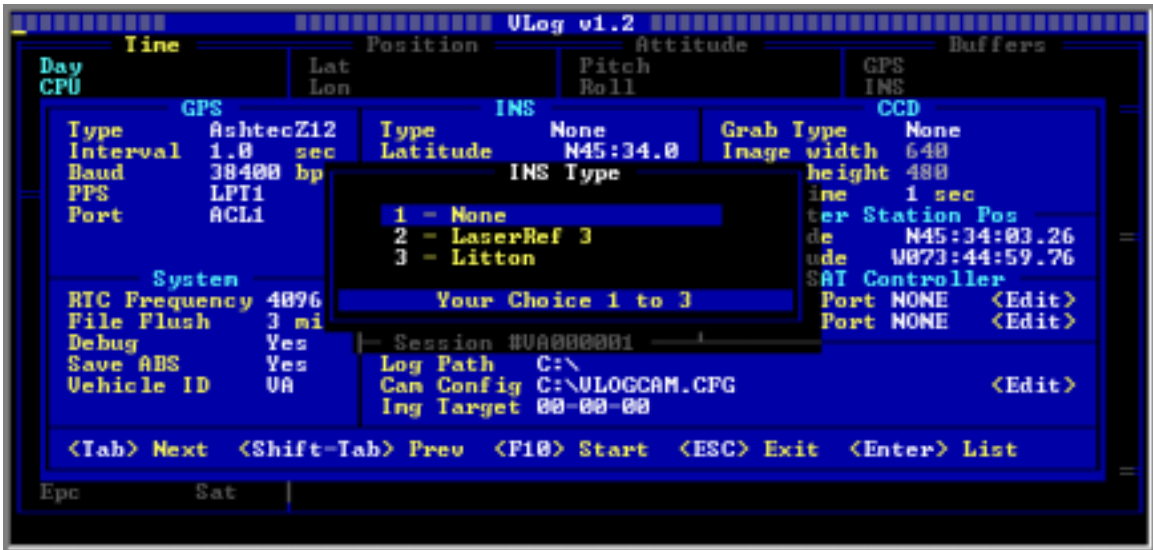
Figure 2.5 : VLog Hardware Initialization Window (See the VISAT Van Operation Manual, 1995)

- Storing the satellite ephemeries for post processing of the GPS data;

- Updating the computer CPU real-time clock upon receiving the PPS pulse from the GPS receiver. The PPS pulse can be activated through any parallel port depending on user requirements;

- Storing any special events, e.g. camera switch off/on. User and system messages are stored in a file with a time tag to allow post-processing of special events;

- Grabbing and storing up to six simultaneous images every 0.4 sec. The program allows different camera configurations and different recording distances; both can be changed in real time. The images are stored in such a way that all images grabbed at the same time will have a header file that contains the necessary information for georeferencing them. This header will be filled after processing the INS and GPS data using the KINGSPAD software;

- Guiding the operator by a user-friendly monitor which contains all the important information, such as video images, position, velocity, attitude, number of grabbed images, the available computer disk space, the active hard disk, number of locked satellites, satellites that have dropped or are affected by cycle slips, etc. ;

- Switching the cameras off and on in order to limit the storage requirements. This feature is very important in situations when the vehicle has to stop, for example at traffic signals or when maneuvering between different survey areas.

- Applying a suite of real-time quality control actions to the GPS and INS data streams.

2.3 Positioning of the VISAT System

To optimally combine GPS and INS data for positioning, a Kalman filtering scheme is used (Schwarz et. al., 1990). Software developed at The University of Calgary allows to do this by either a centralized or decentralized Kalman filter in the **KINGSPAD** software (**KIN**ematic **G**eodetic **S**ystem for **P**osition and **A**ttitude **D**etermination). In the centralized case, a common state vector is used to model both the INS and the GPS errors. In this case, the INS measurements are used to determine the reference trajectory, and the GPS measurements to update the solution and estimate the state vector components. In the decentralized case, two filters are run simultaneously and interact only occasionally. The GPS data are Kalman filtered to obtain estimates of position and velocity which are then used as quasi-observations to update the INS Kalman filter. At the same time, the GPS

data are continuously checked for cycle slips. For more details on the mathematical formulation and Kalman filtering alternatives, see Wei and Schwarz (1990a).

The KINGSPAD software performs the following functions:

- Processing the data in three different modes, that is, pure GPS, pure INS, and hybrid INS/GPS;

- Processing static, semi-kinematic, and kinematic data;

- Defining which GPS data will be used to update the INS, namely, position, velocity, or position/velocity;

- Viewing individual space vehicle (SV) data, thus allowing the rejection of specific a SV in the GPS processor;

- Selecting the GPS update rate according to a specific application (e.g., airborne, land application);

- Computing the updated INS position, velocity, and attitude at 64 Hz to suit different applications;

- Applying rapid static integer ambiguity resolution techniques for short baselines (i.e., under 7 km);

- Applying 'on-the-fly' (OTF) ambiguity techniques for kinematic processing of GPS data;

- Providing a suite of bridging procedures in case of GPS outages;

- Applying backward smoothing of INS data for minimizing the INS drift characteristics;

- Output survey coordinates according to a user-defined format (e.g., geographic coordinates Φ, λ, h, UTM, 3TM).

The output from the KINGSPAD program will be used to georeference (position and orient) the video images as described in Chapter 3.

2.4 The VISAT Station

The digital images acquired from the VISAT van are associated with positions of exposure stations and orientation of camera axes as determined by the GPS and INS data. Thus, the images are georeferenced. Subsequently, 3-D coordinates of objects are needed in many applications. In addition, geometric information and attributes of thematic objects such as control points, utility lines and land parcels are needed to form GIS elements for thematic layers. This requires that the image information of measured objects be extracted and their locations be precisely determined by digital (softcopy) photogrammetry. Furthermore, the results of the measurements can be organized in such a way that they can be incorporated into GIS.

The data processing unit, i.e. the VISAT Station, is implemented on a SUN SPARC workstation and consists of five subsystems, for more details about the VISAT Station see Li et. al. (1994) and the VISAT Station User Manual (1996). The subsystems are :

- Graphic User Interface (GUI),

- Measurement Module,

- Data Base Management System (DBMS) Module,

- Navigation Window Module, and

- GIS Module.

The GUI provides a user-friendly environment for image processing, object measurement, and display. It interfaces the operator with the system in such a way that:

- the photogrammetric measuring procedure is well integrated into the system and is task-oriented, and

- the measurement process is menu-driven, and thus the system is transparent to users.

The Measurement Module enables the measurement of objects appearing in the images and generates GIS elements (Figure 2.6). An unlimited number of images can be displayed. Through forward and backward scroll buttons, images along the track line of the survey van can be displayed and selected. Corresponding image points of an object in different images can be measured with various zooming factors to increase the measurement accuracy. To measure a point, the operator moves the cursor to the point in the first image. If accepted, the target area can be zoomed with various factors (e.g. 2, 4, 8, and 16 times). In addition, epipolar lines are displayed on the other images to assist the operator in identifying the corresponding point in the second image. After photogrammetric triangulation, the system gives 3-D coordinates and accuracy estimate of the measured points in 3D object space. Any number of image points may be used to photogrammetrically triangulate a point. An object to be measured can be defined as a

GIS element such as a point, arc, or polygon by selecting a menu item. A photogrammetric measuring procedure, associated with the menu item and function buttons, gives geometric entities of the chosen GIS element. Attributes associated with the elements can be either input through pop-up menus or by typing in a text window. Results of the measurements are shown in real time on a base map displayed by the GIS module.
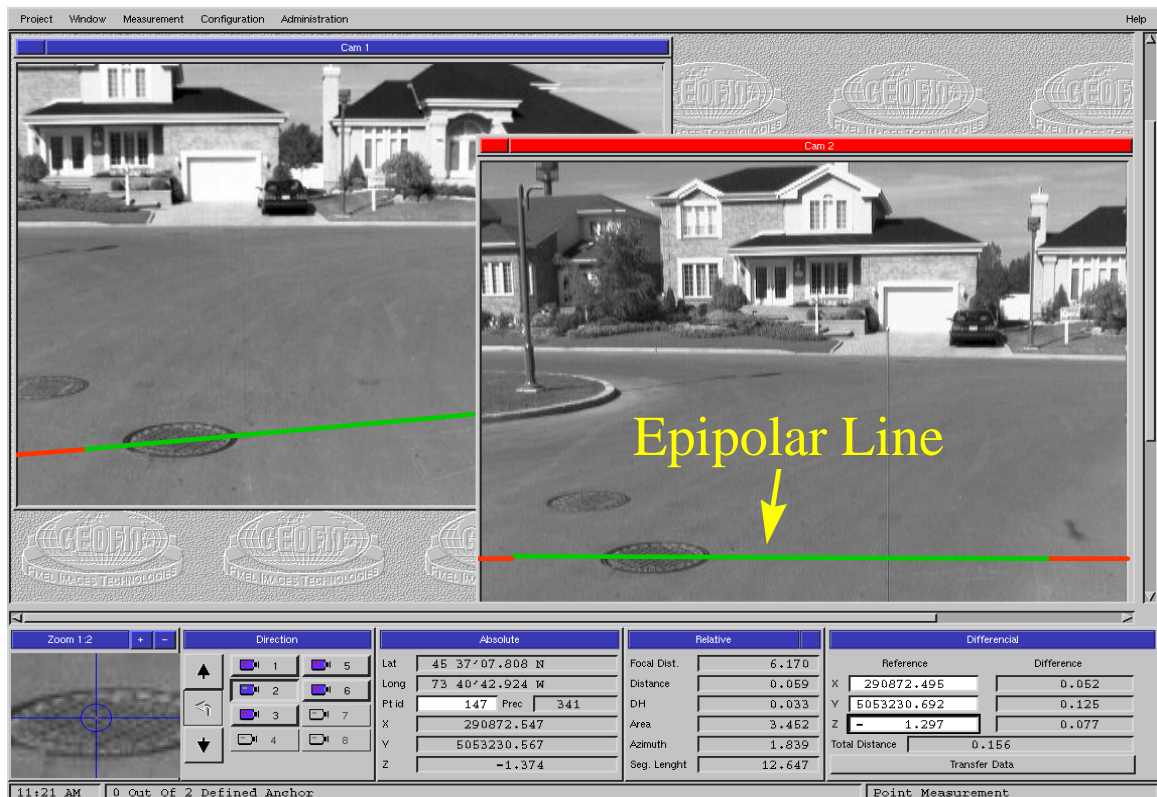
Figure 2.6: The VISAT Station

The GIS module displays the measured elements from the Measurement Module; the elements may be linked to a base map in a local coordinate system, for example State Plane, UTM or 3TM. The base map expressed in either vector or raster format can be

displayed as a reference for the images in the CAD/GIS Module. The route line of the VISAT van can be overlaid on the base map for easy image reference and access. GIS elements of points, arcs, and polygons that are measured are displayed immediately on the base map. Basic editing functions of zoom, pan, update, and delete are provided.

The DBMS is responsible for managing the VISAT image library as well as the user link. It is also used for searching images in a specific area along the track line. The image frames are searchable according to location, time, project, or map window. Since the operator has to decide whether the measurement made should be classified as point, arc, or polygon with attributes, the measurement results can be stored in a GIS database very easily. Input of these data to various GIS systems can be realized by format conversions. The operator may select and measure objects according to a specific theme. Subsequently, the measured elements can be saved as one layer, for example a layer of control points or power towers. Layers of other themes can also be formed. One layer may also contain different thematic objects depending on applications and GIS to be used subsequently.

CHAPTER 3

GEOREFERENCING OF MULTI-SENSOR DATA

This chapter will introduce the integration of multi-sensor data for mapping applications. In general, multi-sensor integration implies different mathematical and physical models depending on the specific sensors used. A general model for georeferencing of mapping sensor data using GPS/INS data is presented here.

3.1 Indirect Georeferencing of Photogrammetric Data

Aerial remote sensing, more specifically aerial photogrammetry, in its classical form of film-based optical sensors (analogue) has been widely used for high accuracy mapping applications at all scales. Ground Control Points (GCPs) were the only required source of information for providing the georeferencing parameters and suppressing undesirable error propagation. In general, the necessity for GCPs was so evident that all operation methods relied on it. Even with the major changes in photogrammetry from analogue to analytical and then to the digital mode of operation, it was taken for granted that GCPs were the only source for providing reliable georeferencing information. External georeferencing information was therefore labeled as auxiliary data, indicating that they

were only useful in minimizing the number of GCPs. The drawback of indirect georeferencing is the cost associated with the establishment of the GCPs. They usually represents a significant portion of the overall budget. In some cases, this cost can be prohibitive, especially when imagery is to be acquired and georeferenced in remote areas such as areas found in many developing countries, for more details see Schwarz et. al., (1993). The use of the GCPs also often puts operational constraints on a specific flight mission.

The use of **auxiliary position and navigation sensor** data in the georeferencing process has been extensively studied for several decades. The output of these sensors is used to determine the six parameters of exterior orientation, either completely or partially, and thus to eliminate the need for a dense GCP network. These sensors include airborne radar profile recorders (APR), gyros, horizon cameras, statoscope, Hiran, and Shiran. However, at this stage the use of the auxiliary data was intended only to support the georeferencing process by reducing the number of GCPs. Also, the accuracy achieved with most of these auxiliary data was limited. Thus, during the last two decades the use of such auxiliary data in the georeferencing process has almost disappeared completely from photogrammetry, except for the statoscope, for more details see Ackermann (1995).

This situation changed fundamentally when GPS data were included in the block adjustment of aerial triangulation. In principle, the use of GPS data made block triangulation entirely independent of GCPs. For the first time in the history of photogrammetry, the georeferencing process became autonomous, as GCPs were not

necessarily required any more (Ackermann, 1995). However, this is only true for the block triangulation scheme with over-lapping images. Other sensors, cannot be fully georeferenced by GPS alone. Well-known examples of which are pushbroom digital scanners, laser scanners, and imaging radar systems, which are important in kinematic mapping applications.

Georeferencing of pushbroom imagery, for example, requires the instantaneous position and attitude information of each scan line. GCPs alone are not sufficient to resolve all the three positions and three orientations parameters associated with each scan line, of which there may be thousands in a single image. Also, the data rate of most available GPS receivers is not high enough to support the data rate required for airborne pushbroom scanners (about 20-40 lines/sec). Other restrictions of GPS come from the operational environment of kinematic close-range terrestrial mapping systems, especially in urban centers where stand-alone GPS, due to frequent signal blockage, cannot reach the accuracy requirements of such application. Also, for non-imaging sensors such as imaging radar systems, the use of GPS in stand-alone mode will not be feasible, since no support by block formation is easily realized.

Only recently has direct georeferencing become possible by integrating GPS and INS, such that all the exterior orientation information has become available with sufficient accuracy at any instant of time (Schwarz et. al., 1993). The integration of GPS/INS puts the georeferencing of photogrammetric data on a new level and frees it from operational

restrictions. Together with digital data recording and data processing, it initiates the era of multi-sensor systems.

3.2 Direct Georeferencing of Imaging Data

Multi-sensor systems have become an emerging trend in mapping applications because they allow a task-oriented implementation of geodetic concepts at the measurement level (Schwarz and El-Sheimy, 1996). Examples of such systems can be found in airborne remote sensing (Cosandier et. al. (1992) and Seige (1994)), airborne gravimetry (Wei and Schwarz (1995), Hein (1995)), airborne laser scanning (Wagner (1995)), and mobile mapping vans and trains (El-Sheimy and Schwarz (1993), Bossler et. al. (1993), and Blaho and Toth (1995)). All of these systems have a common feature in that the sensors necessary to solve a specific problem are mounted on a common platform. By synchronizing the data streams accurately, the solution of a specific problem is possible by using data from one integrated measurement process only. The post-mission integration of results from a number of disjoint measurement processes and the unavoidable errors inherent in such a process are avoided. This results in greater conceptual clarity, task-oriented system design and data flow optimization, and also offers in most cases the potential for real-time solution, which is becoming more important in many applications.

The trend towards multi-sensor systems in geomatics is fuelled by the demand for fast and cost-effective data acquisition and by technological developments which satisfies this demand. Two developments are especially important in this context: Digital imaging and precise navigation. Digital imaging sensors considerably reduce the data processing effort by eliminating the digitizing step. They also opens the way towards new and flexible designs of the processing chain, making ample use of mathematical software tools readily available. In the form of digital frame cameras, they are inexpensive enough to make redundancy a major design tool. In the form of pushbroom scanners, they provide additional layers of information, not available from optical cameras.

Precise navigation has developed to a point where it can provide the solution of the exterior orientation problem without the use of GCPs or block adjustment procedures; for details of the principle, see Schwarz et al. (1984); for results and practical considerations see Lapine (1990), Cannon (1991) and Skaloud et. al. (1994). Since results are available in a digital form, data fusion with the imaging data is easy and real-time applications are possible in principle. Operational flexibility is greatly enhanced in all cases where a block structure is not needed. Costs are considerably reduced, especially in areas where little or no ground control is available. Current accuracy is sufficient for many mapping applications, see for instance Schwarz (1995). The potential to solve even high-accuracy cadastral applications certainly exists.

Combining these two developments, the concept of the georeferenced image as the basic photogrammetric unit emerges. This means that each image is stamped with its

georeferencing parameters, namely three positions and three orientations, and can be combined with any other georeferenced image of the same scene by using geometric constraints, such as epipolar geometry or object-space matching. This is a qualitatively new step because the georeferencing parameters for each image are obtained in a direct way by independent measurement. This is conceptually different from the notion that a block of connected images and sufficient ground control is needed to solve the georeferencing problem. The direct method, in contrast, does not require connectivity information within a block of images to solve the georeferencing problem, and thus offers much greater flexibility. It is especially intriguing to consider its use for mapping applications which use either digital frame cameras, pushbroom scanners, or laser scanners as imaging components.

3.3 Components of Multi-Sensor Systems

In the following, common features in the design and analysis of multi-sensor systems will be discussed. System design and analysis comprises the following steps as a minimum; for more details see Schwarz and El-Sheimy (1996):

- Data acquisition

- Kinematic Modeling

- Synchronization

- Calibration

- Georeferencing

- Integration and data fusion

- Quality control

- Data flow optimization and automation.

The conceptual layout and data flow of a multi-sensor system for mapping applications is shown in Figure 3.1. The selection of sensors for such a system obviously depends on system requirements, such as accuracy, reliability, operational flexibility, and range of applications. The data acquisition module has, therefore, to be designed keeping both the carrier vehicle and the intended applications in mind. The data acquisition module contains navigation sensors and imaging sensors. Navigation sensors are used to solve the georeferencing problem. Although a number of different systems are used in general navigation, the rather stringent requirements in terms of accuracy and environment make the integration of an INS with GPS receivers the core of any sensor combination for an accurate mobile mapping system for short range applications. This combination also offers considerable redundancy and makes the use of additional sensors for reliability purposes usually unnecessary. However, the addition of an odometer type device, such as the ABS, for close-range applications may be useful for operational reasons, as for instance keeping a fixed distance between camera exposures.
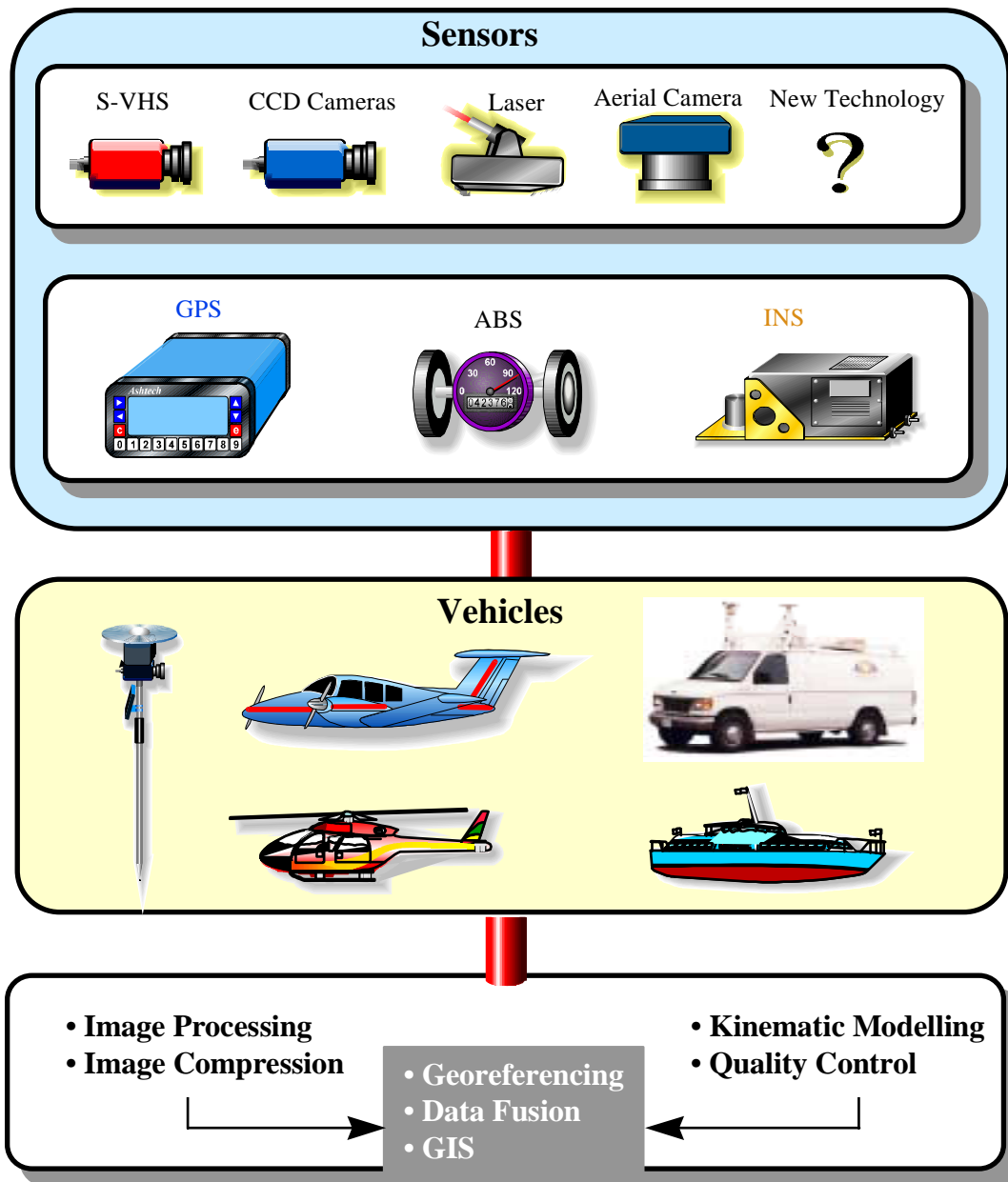
Figure 3.1: Multi-Sensor Integration for Mapping Application

Imaging sensors may be subdivided based on the way they contribute to the information about the object space. They may provide descriptive information, as for instance grey scales, or geometric information, as for instance direction or range from the camera to the

object. Table 3.1 summarizes the contribution of sensors typically used in multi-sensor systems for mapping applications.

Table 3.1 : Summary of Mapping Related Sensors

Type of sensor	Type of information	Characteristics
Analogue aerial cameras	Descriptive/Geometric	Photos; high geometric accuracy
Multi-spectral linear scanners (Pushbroom)	Descriptive/Geometric	Multi-spectral images, geometric accuracy depends on sensor resolution
CCD cameras	Descriptive/Geometric	Images; geometric accuracy depends on sensor resolution
Imaging laser	Descriptive/Geometric	Image + Distance between the object and the sensor
Laser Profiles, Laser Scanners	Descriptive/Geometric	Distance between the object and the sensor, scanning angle
Impulse radar	Descriptive/Geometric	Thickness of objects (mainly used for pavement structure voids)
Ultra sonic sensors	Geometric	Distance between the object and the sensor. Road rutting measurement, and cross-section profile measurement
GPS positioning and attitude determination	Geometric	High accuracy position and medium accuracy attitude, global reference
Inertial sensors	Geometric	Low-to-high accuracy relative position and attitude.
Odometers	Geometric	Distances.

The selected sensor configuration requires a certain data processing sequence. Part of the processing will have to be performed in real time, such as data compression for the imaging data and initial quality control processing for the navigation data. Most of the data, however, will immediately be stored for post-mission use. In post-mission, the data processing hierarchy is determined by the fact that all mapping data have to be georeferenced first before they can be used in the integration process. The first step is, therefore, the georeferencing of all mapping data and their storage in a multimedia data base.

In mapping applications, photogrammetric methods have been increasing in importance, due to the use of CCD cameras. CCD sensors have overcome two major disadvantages of film-based photographic cameras: single-frame, slow-rate photography and highly specialized processing equipment. Recent trends in CCD technology are characterized by increased resolution, color image acquisition, and improved radiometric quality (anti-blooming, reduced cross-talk). Another important development which supports the use of CCD cameras in photogrammetric applications is the advancement of fast analogue-to-digital conversion (ADC). Frame grabbers integrated with high-speed computer buses and processing hardware have become a standard commodity. Compared to analogue/analytical plotters used in conventional photogrammetry, the use of state-of-the-art computer image boards greatly simplifies measurements. More information about CCD cameras will be given in Chapter 4. To determine 3-D coordinates of objects visible in CCD camera images, the following information is needed for a pair of cameras:

- Position of the camera perspective center at exposure time (3 parameters per image),

- Camera orientation at exposure time (3 parameters per image),

- Interior geometry of the camera sensor, and

- Lens distortion parameters.

The first two sets of parameters are known as exterior orientation parameters, while the other two sets are known as interior orientation parameters. The general problem in photogrammetry, aerial and terrestrial, is the determination of the camera's interior and exterior orientation parameters. The exterior orientation parameters are determined by a combination of GPS and INS, the interior orientation parameters by field or laboratory calibration. This means that exterior orientation is tied to a real-time measurement process and its parameters change quickly. In contrast, interior orientation is obtained by using a static field calibration procedure and can be considered as more or less constant for a period of time. Thus, it can be done before or after the mission and is not generally affected by the data acquisition process. More details about the interior orientation calibration will be given in Chapter 4.

Real-time georeferencing is possible, in principle, because the interior orientation can be done before the run and the exterior orientation parameters can be computed in real time. However, it is not advisable in applications where frequent loss of lock to GPS satellites occurs. In such cases, real-time georeferencing will be much poorer in accuracy and reliability than post-mission processing. The principle of georeferencing will be discussed in more detail in Section 3.5.

Implied in the georeferencing process is the synchronization of the different data streams. The accuracy of georeferencing is dependent on the accuracy with which this can be achieved. The synchronization accuracy needed is dependent on the required system performance and on the speed with which the survey vehicle moves. It is, therefore, much more critical for airborne applications than for marine and land vehicle applications. Fortunately, GPS provides a well-defined time signal to which the other sensors can be slaved. Still, the implementation of sensor synchronization is not a trivial process and should be done with care. More details about system synchronization will given in Chapter 5.

Model integration and data fusion comprises all steps necessary to extract the desired result from the georeferenced images. If the objective is to extract 3-D coordinates of objects in the images, then the application of geometric constraints, the handling of redundant images of the same object, and the fusion of data of different type and quality are important considerations. Figures 3.2 and 3.3 show typical examples of data fusion in mapping application. Figure 3.2 shows the example of a mobile mapping system which uses digital images and laser profile data for the imaging component and GPS, INS, and ABS data for georeferencing the two other data types. Figure 3.3 shows the example of an airborne mapping system which uses digital full-frame images, multi-spectral pushbroom and laser profile data for the imaging component, and GPS and INS data for georeferencing the three other data types. The objective may, however, be much wider than object coordinates. Data fusion generally means that data from various sources and

different nature are merged together to provide a versatile resource for mapping applications, a typical example could be a combination of the two systems shown in Figures 3.2 and 3.3. Therefore, data fusion in its general sense means images of different scale, geometry, and radiometric characteristics can be combined together. Model integration and data fusion are closely related to the issue of quality control because in most system designs accuracy of the final results is but one issue. Reliability and economics are usually equally important considerations and a well-designed system will be balanced with a view to these, sometimes conflicting, requirements.
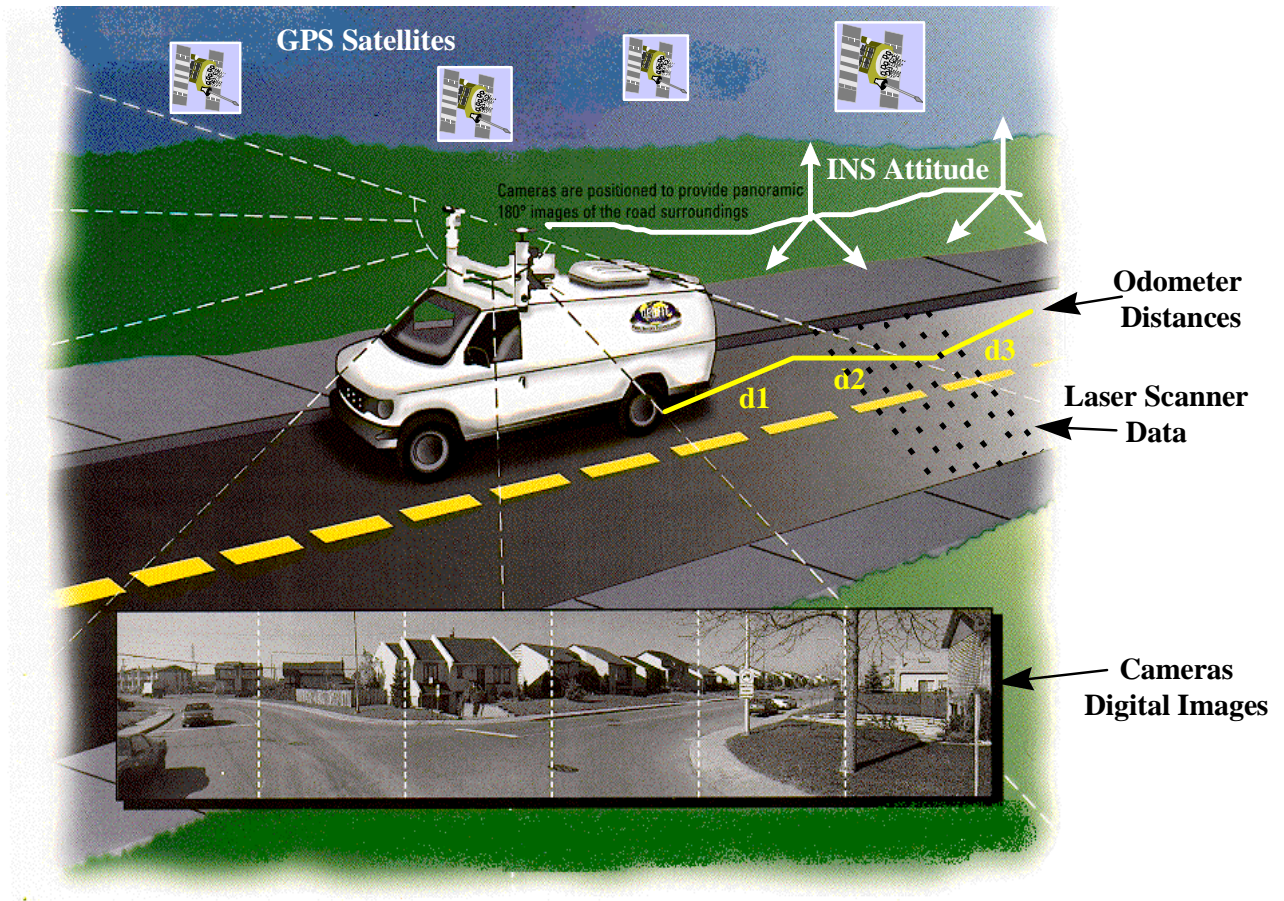
Figure 3.2 : An Example of Data Fusion in Close-Range Applications
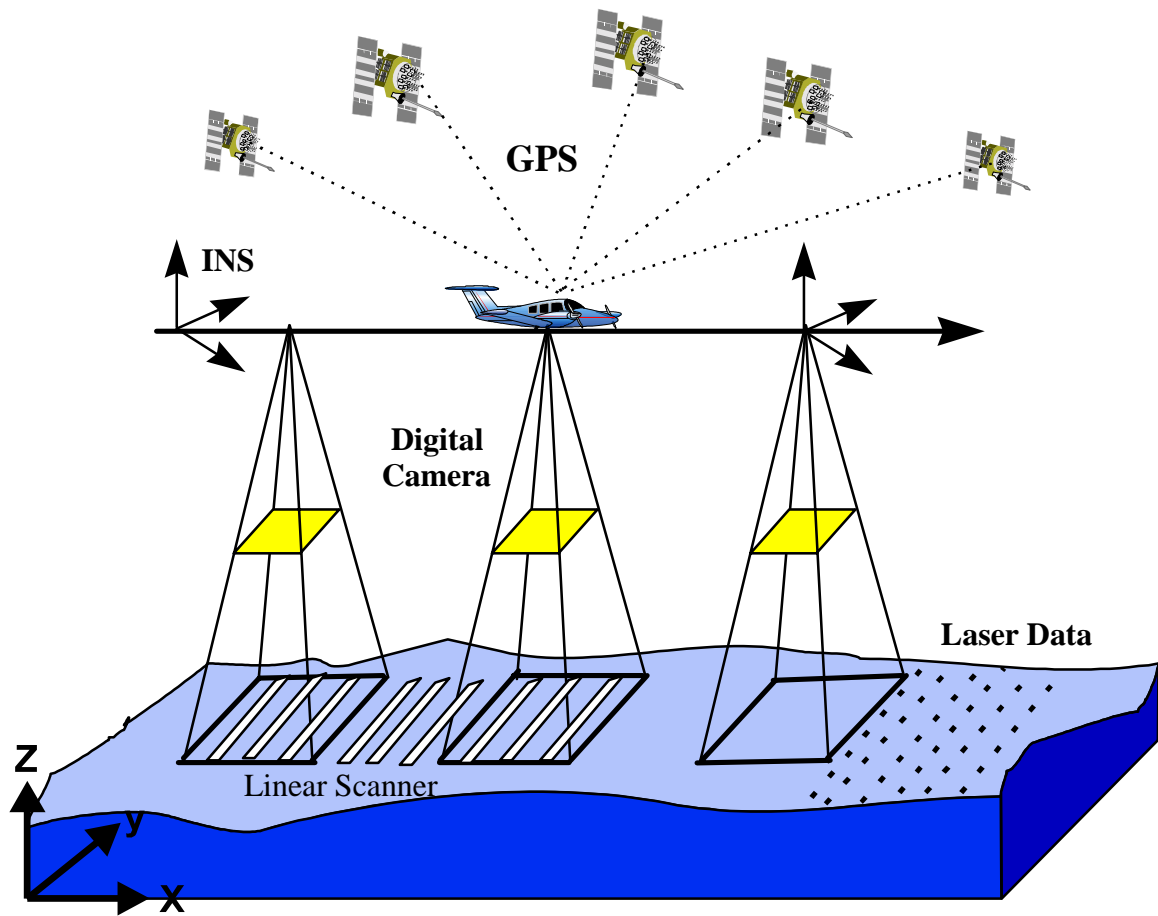
Figure 3.3: An Example of Data Fusion in Airborne Applications

Quality control usually has a real-time component and a post-mission component. In real-time, one wants to decide whether a specific set of data is sufficient to provide the required accuracy with a certain level of probability. In post-missions, one wants to know the percentage of measurements for which the required accuracy has actually been achieved. If the results of real-time prediction differ considerably from the results of post-mission analysis, the real-time model needs improvement. This can only come from the analysis of large discrepancies between predicted and post-mission results. Thus, each real-time model includes a certain amount of expert knowledge that has been gained in

post-mission analysis. It is the art of real-time quality control to combine this expert knowledge with minimum information on the measurement process and still to arrive at reliable predictions. Such predictions would normally contain an acceptable level of poor data without requiring a large number of re-surveys. More details about the quality control module will be given in Chapter 5. Quality control results will be discussed in Chapter 6.

Data flow optimization and automation are on the one hand based on the mathematical description and the integration model of the system and on the other hand, they are completely separate from it. When addressing optimization and automation, assumption is usually made that the underlying mathematics of the process is well understood, but that the process of arriving at the results is too slow and requires too much human interaction. The emphasis in this step is therefore on speeding up the process of arriving at the required result, including all essential parameters that describe its quality, and on the automation of all processes that require human expert knowledge and interaction. Very often, the automation process is the more difficult one to accomplish because the further it goes, the more complex it becomes, and the likelihood that it will show a curve of diminishing return is very high. It is, therefore, not surprising that complete automation is rarely achieved, but that a reasonable level of automation is defined which will cover most of the cases that occur with a certain frequency. More details about data optimization and automation will be given in Section 3.6.

3.4 Kinematic Modeling

Kinematic modeling is the determination of a rigid body's trajectory from measurements relative to some reference coordinate frame. It, thus, combines elements of modeling, estimation, and interpolation. Modeling relates the observable to the trajectory. Estimation uses actual observation, i.e., it adds an error process to the model and solves the resulting estimation problem in some optimal sense. Interpolation connects the discrete points resulting from the estimation process and generates a trajectory by formulating some appropriate smoothness condition (Schwarz, 1993b).

A rigid body is a body with finite dimensions, which maintains the property that the relative positions of all its points, defined in a coordinate frame within the body, remain the same under rotation and translation (Goldstein, 1980). The general motion of a rigid body in space can be described by six parameters. They are typically chosen as three position and three orientation parameters. The modeling of rigid body motion in 3-D space can be described by an equation of the form:

$$r_i^m = r_b^m(t) + R_b^m(t) \cdot a^b \tag{3.1}$$

where,

r_i^m are the coordinates of point (i) in the m-frame,

$r_b^m(t)$ are the coordinates of the center of mass (b) the rigid body in

                the m-frame at time (t),

$R_b^m(t)$ is the rotation matrix between the b-frame and the m-frame at time (t),

a^b is the fixed distance between point (i) and the center of mass of the rigid body.

The right-hand side of Equation 3.1 consists of a translation vector $r_b^m(t)$ and a rotational component $(R_b^m(t) \cdot a^b)$. The vector a^b can be any vector fixed in the rigid body with its origin at the center of mass of the rigid body. Its rotation is equivalent to the rotation about the center of mass of the rigid body.

Figure 3.4 illustrates the basic concept. The coordinate "b-frame" is fixed to the body and rotates in time with respect to the coordinate m-frame in which the translation vector r_i^m is expressed. The m-frame is, in principle, arbitrary and, thus, can be chosen to simplify the problem formulation. The m-frame can be a system of curvilinear geodetic coordinates (latitude, longitude, height), a system of UTM or 3TM coordinates, or any other earth-fixed coordinate system.

As discussed in Section 2.2.1, determining the position and orientation of the rigid body in 3-D space is, in principle, a problem of trajectory determination which requires measuring systems with the capability to sense six independent quantities from which these parameters can be derived. Most notable among them is INS and receivers linking into the GPS.
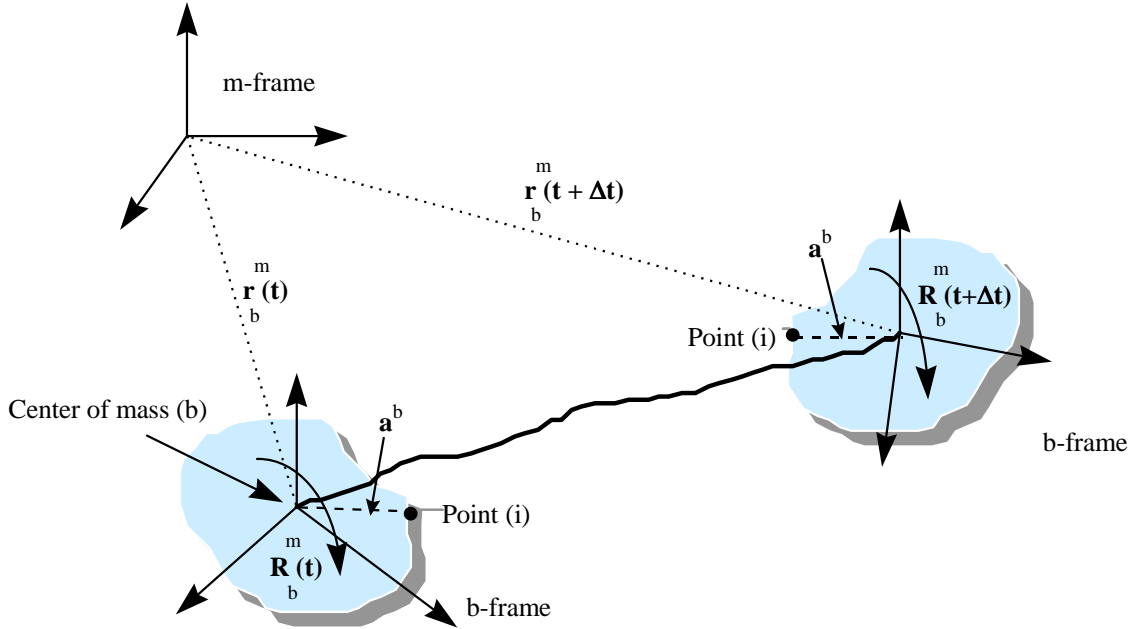
Figure 3.4 : Modeling Rigid Body Motion in Space

In general, the INS consists of three gyroscopes and three accelerometers. Gyroscopes are used to sense angular velocity ω_{ib}^b which describes the rotation of the b-frame with respect to the i-frame, coordinated in the b-frame. The i-frame is a properly defined inertial reference frame in the Newtonian sense and, thus, can be considered as being non-accelerating and non-rotating. Accelerometers are used to sense specific force f^b in the b-frame. The first set of measurements, the angular velocities ω_{ib}^b, are integrated in time to provide orientation changes of the body relative to its initial orientation. The second data set, the specific force measurements f^b, are used to derive body acceleration which, after double integration with respect to time, give position differences relative to an initial position. Specific force and angular velocity can be used to determine all parameters required for trajectory determination by solving the following system of differential equations (see Schwarz and Wei (1990b)) :

$$
\begin{pmatrix} \dot{r}^m \\ \dot{v}^m \\ \dot{R}_b^m \end{pmatrix} = \begin{pmatrix} D^{-1}v^m \\ R_b^m \cdot f^b - (2\Omega_{ie}^m + \Omega_{em}^m) \cdot v^m + g^m \\ R_b^m \cdot (\Omega_{ib}^b - \Omega_{im}^b) \end{pmatrix}
\tag{3.2}
$$

To solve the system, the observables f^b and ω_{ib}^b are needed as well as the scaling matrix D^{-1}, the gravity vector g^m, the Earth rotation rate ω_{ie}^m and the dimensions of the implied reference ellipsoid. The gravity vector is normally approximated by the normal gravity field, while the Earth's rotation is assumed to be known with sufficient accuracy. The scaling matrix D^{-1} is obtained in the integration process using the implied reference ellipsoid. For more details see Schwarz et. al. (1993b).

GPS is another measuring system that can be used for trajectory determination. The system output in this case are ranges and range rates between the satellites and receiver, derived from carrier phase data. The models that relate the position and velocity with the measurements are well known, see Wells et. al. (1986) and Lachapelle (1995). In GPS stand-alone mode, a multi-antenna system can be used to provide both position and attitude. The feasibility of attitude determination using multi-antenna systems has been shown for applications not requiring the highest accuracy, see Cannon et. al. (1992), Cohen and Parkinson (1992), and El-Mowafy and Schwarz (1994). Similar to the INS model, the GPS trajectory equation can be written in state vector form :

$$
\begin{pmatrix} \dot{r}^m_m \\ \dot{v}^m_m \\ \dot{R}^m_b \end{pmatrix} = \begin{pmatrix} v^m \\ 0 \\ R^m_b \cdot \Omega^b_{mb} \end{pmatrix} \qquad\qquad (3.3)
$$

In this equation, the angular velocities in the body frame are obtained by differencing between antennas, satellites, and epochs. Note that the translation parameters of the trajectory are obtained by differencing between the master station receiver and the rover receiver, while the rotational parameters are obtained by differencing between the rover receivers only. Other models can be found in Schwarz et. al. (1989).

Thus, both INS and GPS are, in principle, capable of determining position and attitude of the rigid body. In practice, due to the double integration of the INS acceleration data, the time-dependent position errors will quickly exceed the accuracy specifications for many trajectory determination applications. Frequent updating is, therefore, needed to achieve the required accuracies. GPS on the other hand, can deliver excellent position accuracy, but has the problem of cycle slips, which are in essence gross errors leading to a discontinuity in the trajectory. In addition, the range and range rate measurements are not truly independent, and the current data density and accuracy are not sufficient to meet the accuracy requirements for VISAT orientation.

The combination of the two measuring systems, therefore, offers a number of advantages. In the absence of cycle slips, the excellent positioning accuracy of differential GPS can be used to provide frequent updates for the inertial system. The inertial sensors orientation

information and the precise short-term position and velocity can be used for cycle slip detection and correction. In general, the fact that nine independent measurements are available for the determination of the six required trajectory parameters greatly enhances the reliability of the system.

To optimally combine the redundant information, a Kalman filtering scheme is used whereby the inertial state vector is regularly updated by GPS measurement. Two integration strategies can be implemented at the software level using the Kalman filter approach. In the first one, a common state vector is used to model both the INS and the GPS errors. This is often called the centralized filter approach. It has been applied with good success in Wong et. al. (1988) and Cannon (1991). In the second approach, different filters are run simultaneously and interact only occasionally. This is often called the decentralized filter approach. For a discussion of the algorithm, see Hashemipour et. al. (1988) and for its implementation, see Wei and Schwarz (1990a). It has advantages in terms of data integrity and speed, but is more complex in terms of program management.

3.5 A Unified Approach for Georeferencing Multi-Sensor Data Using GPS/INS

The integration of multi-sensor data requires a unified model for georeferencing such data. Unified in this context means that the model can be applied to most, if not all, sensor data without the need to account for a different set of parameters for each sensor. Such a model is very important for the fusion of different sensor data. For the sake of simplicity, the unified georeferencing model will be derived for a camera system which

can be used in both airborne and close-range applications. Modifications required for other sensors will be given when necessary.

Georeferencing of images can be defined as the problem of transforming the 3-D coordinate vector r^c of the camera frame (c-frame) to the 3-D coordinate vector r^m of the mapping frame (m-frame) in which the results are required. The m-frame, as mentioned before, can be any earth-fixed coordinate system such as curvilinear geodetic coordinates (latitude, longitude, height), UTM, or 3TM coordinates. The major steps in this transformation are depicted in Figure 3.5 for the airborne case, where the carrier could be an airplane or a helicopter.
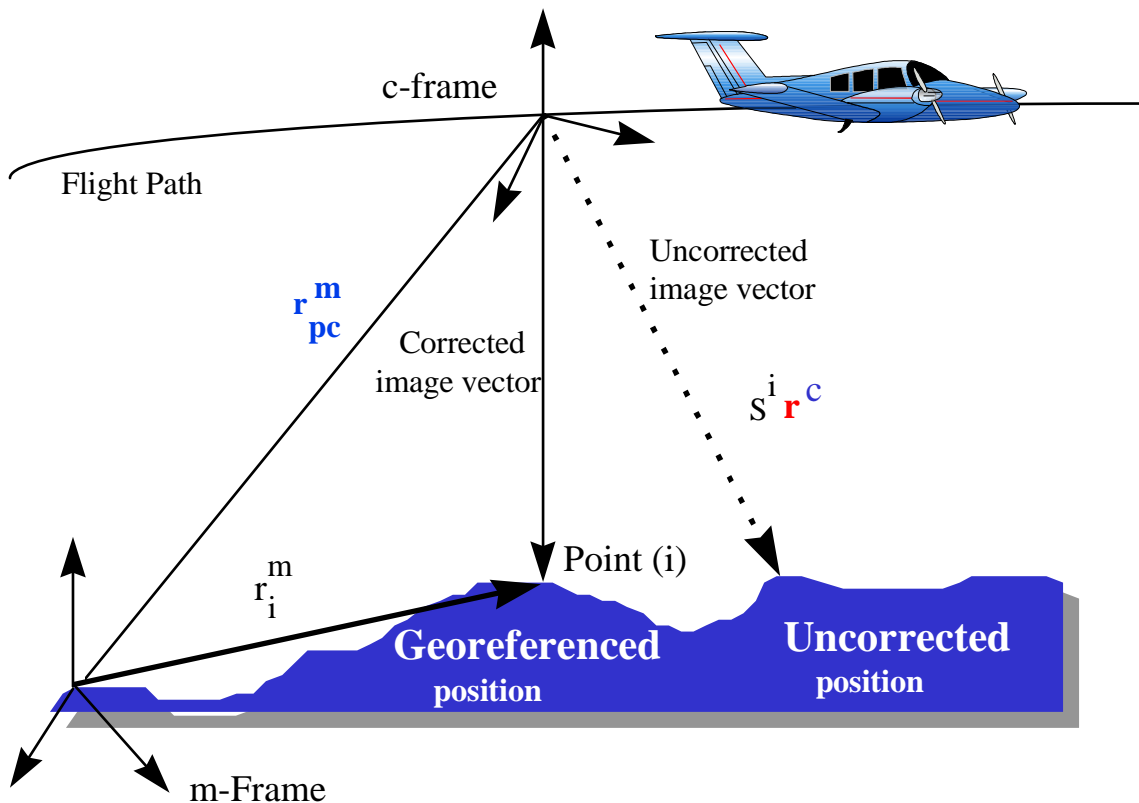
Figure 3.5: Georeferencing of Airborne Sensing Data (see Schwarz et. al., 1994)

The camera coordinate system, c-frame, changes position and orientation with respect to the m-frame. Georeferencing is possible if at any instant of time (t) the position of the camera projective centers (p.c.) in the m-frame, i.e. $r_{pc}^{m}(t)$, and the rotation matrix between the c-frame and the m-frame $R_{c}^{m}(t)$ have been determined. The georeferencing equation can then be written for any object point (i) as :

$$r_{i}^{m} = r_{pc}^{m}(t) + s^{i} \bullet R_{c}^{m}(t) \bullet r^{c} \tag{3.4}$$

where

r_{i}^{m} is the position vector of an object (i) in the chosen mapping frame;

r_{pc}^{m} is the coordinate vector from the origin of the mapping frame to the center of the position sensor on the moving vehicle, given in the m-frame;

R_{c}^{m} is the 3-D transformation matrix which rotates the c-frame into the m-frame;

(t)   is the measurement epoch, i.e. the time of capturing the images in this case;

r^{c} is the vector of image coordinates given in the c-frame;

s^{i} is a scale factor specific to a one-point/one-camera combination which relates the image coordinates to the object coordinates.

Equation 3.4 is, however, only a first approximation of the actual situation. It implies that the coordinates of the projective center of the camera can be directly determined. This is usually not the case because the navigation sensors - GPS antenna/INS center- cannot

share the same location in space with the imaging sensors. Thus, small translations and rotations between the different centers have to be considered. The actual situation is shown in Figure 3.6. It has been assumed that the camera is mounted in the cargo area of the airplane, that the positioning sensor, a GPS antenna is mounted on top of the airplane, and that the attitude sensor, an inertial measuring unit is mounted in the interior of the aircraft, somewhere close to the camera. In this case, aircraft position and attitude are defined by the INS center and the internal axes of the inertial measuring unit (b-frame). Similarly, Figure 3.7 shows the actual situation for the close-range case.

If the vector between the origin of the INS body frame (b-frame) and the camera is given in the b-frame as a^b, $r^m_{pc}(t)$ can be written as :

$$r^m_{pc}(t) = r^m_{INS}(t) + R^m_b(t) \cdot a^b \qquad (3.5)$$

where

- $r^m_{INS}(t)$ is the vector of interpolated coordinates of the INS in the m-frame

  at time (t), and

- a^b is the constant vector between the camera perspective center and the center

  of the INS b-frame, usually determined before the mission by calibration.
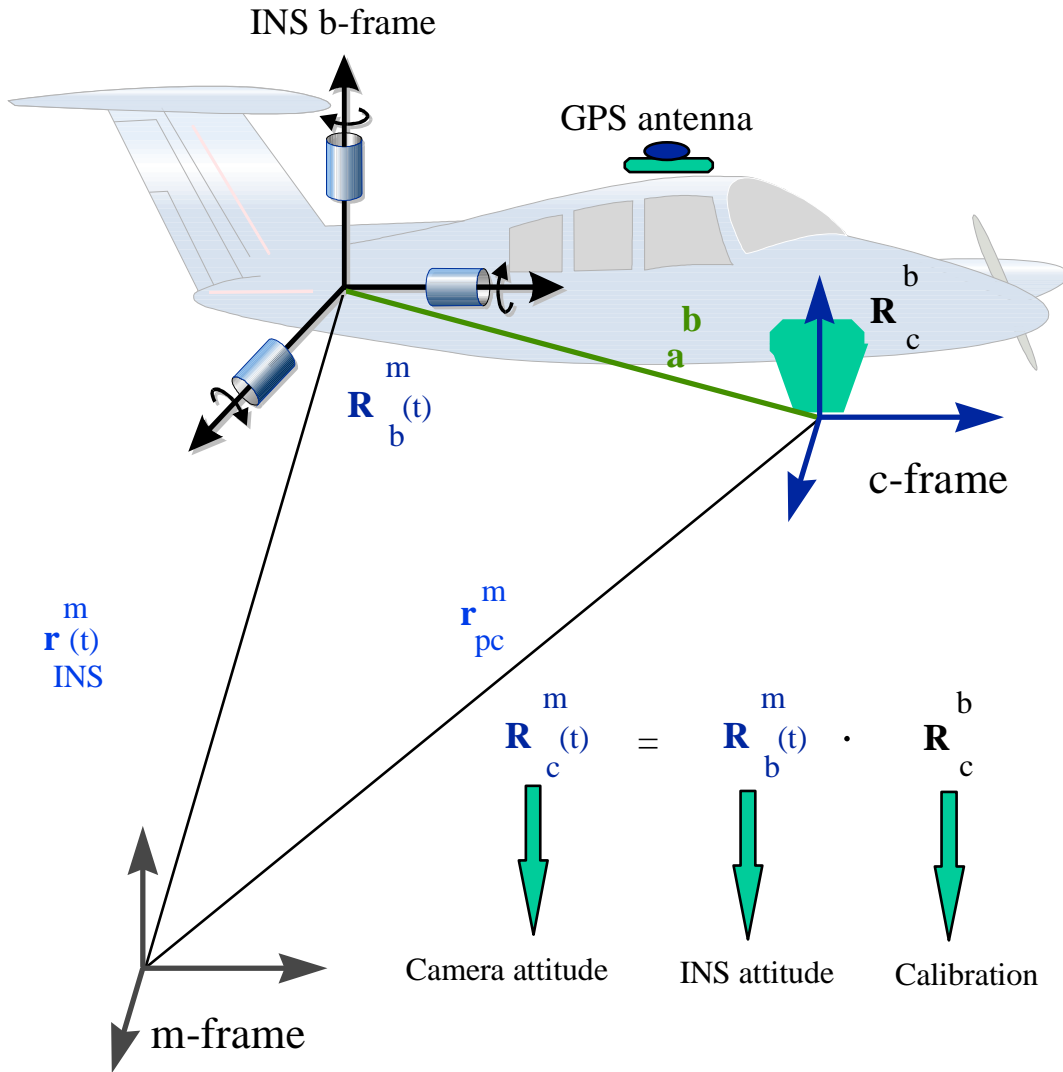
Figure 3.6 : Detailed Diagram of Elements of Georeferencing for the Airborne Case

The INS position r_{INS}^{m} is the position resulting from the INS/GPS integration. In the event of a continuous loss of the GPS signal, the INS will be used in stand-lone mode to extend the mission. The high data rate of the INS, 50 Hz, facilitates the interpolation of camera coordinates.

In addition to transformations between sensors, rotations between different sensor frames have to be taken into account. The INS b-frame (gyro frame) cannot be aligned with the c-frame. The constant rotation R_c^b between the two frames is again obtained by calibration. In this case, $R_c^m(t)$ can be written as:

$$R_c^m(t) = R_b^m(t) \bullet R_c^b . \tag{3.6}$$

where R_c^b is the rotation between the c-frame and the INS b-frame as determined from a calibration process.
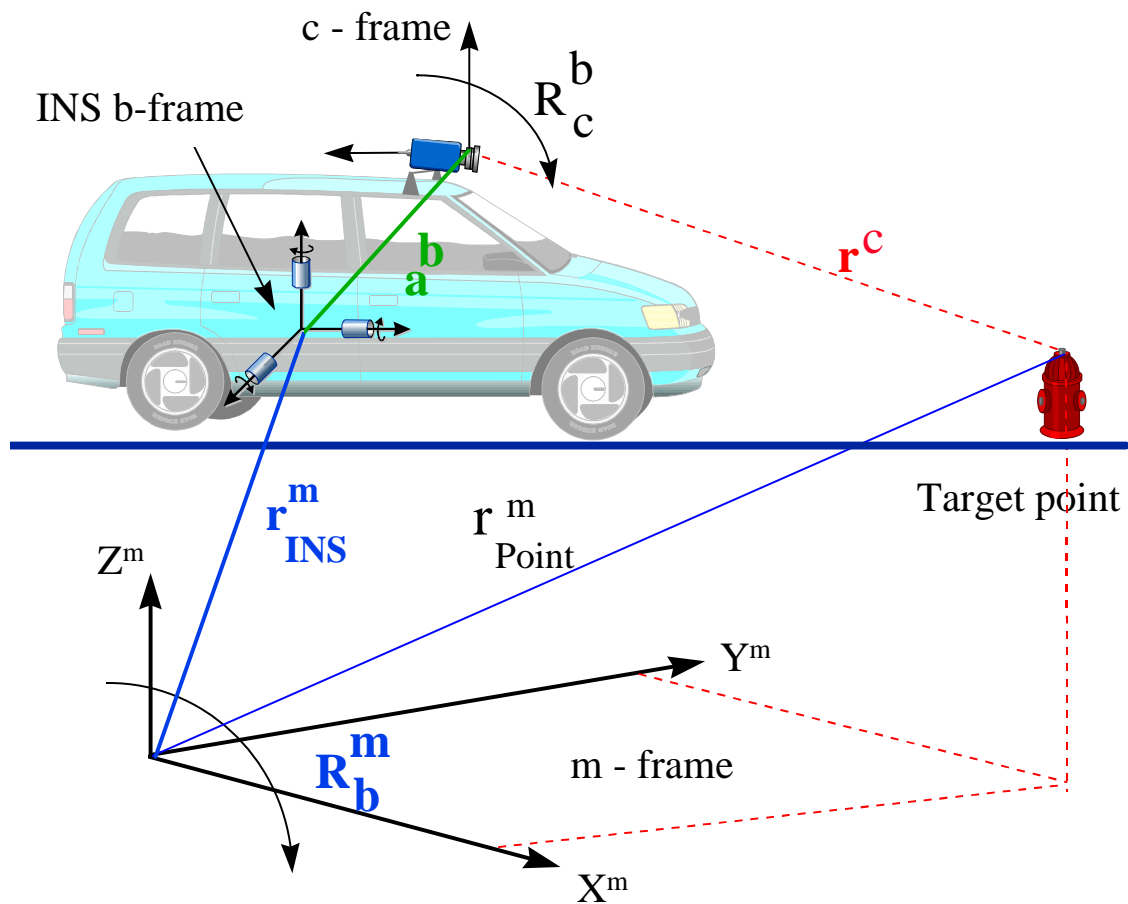
Figure 3.7 : Detailed Diagram of Elements of Georeferencing for the Close-Range Case

Applying Equations (3.5) and (3.6) to Equation (3.4), the final georeferencing formula can be written as :

$$r_i^m = r_{INS/GPS}^m(t) + R_b^m(t) \ [s^i \ R_c^b \ r^c + a^b \ ] \tag{3.7}$$

where R_c^b transforms the vector r^c from the c-frame to the b-frame and $R_b^m(t)$ transforms the vector $[s^i \ R_c^b \ r^c + a^b \ ]$ from the b-frame to the m-frame. R_c^b and a^b are determined through calibration procedures before the survey. Table 3.2 outlines how different quantities are obtained. For more details on the georeferencing process see Schwarz et. al. (1993b) and El-Sheimy and Schwarz (1994).

Table 3.2: Elements of the Georeferencing Formula

Variable	Obtained from
r_i^m	**Unknown** (3)
$r_{INS/GPS}^m(t)$	Interpolated from the GPS/INS positions at the time of exposure(t)
$R_b^m(t)$	Interpolated from INS gyro outputs at the time of exposure(t)
s^i	Determined by stereo techniques, laser scanners or DTM
R_c^b	Calibration
r^c	Measured image coordinates
a^b	Calibration

It should be noted that, the vector $r^m_{INS/GPS}(t)$, as well as the rotation matrix $R^m_b(t)$ are time-dependent quantities while the vectors r^c and a^b as well as the matrix R^b_c are not. This implies that the carrier is considered as a rigid body whose rotational and translational dynamics are adequately described by changes in $r^m_{INS/GPS}(t)$ and $R^m_b(t)$. This means that the translational and rotational dynamics at the three sensor locations is uniform, in other words, differential rotations and translations between the three locations as functions of time have not been modeled. It also means that the origin and orientation of the three sensor systems can be considered fixed for the duration of the survey. These are valid assumptions in most cases, but may not always be true.

The quantities $r^m_{INS/GPS}(t)$, $R^m_b(t)$ and r^c in Equation (3.7) are determined by measurement, the first two in real time, the third in post mission. The quantities R^b_c and a^b, however, are determined by calibration, either before or during the survey. To define R^b_c by calibration, a minimum of three well determined GCPs are required. For more details about the determination of R^b_c, see Cosandier et. al. (1994) and Skaloud (1995) for the airborne case, and El-Sheimy (1996) for the land application case. It should be mentioned that the determination of R^b_c in the land application case is much easier than in the airborne case. This due to the fact that in land applications, the calibration can be performed in static mode where most of the navigation errors can be minimized. Besides,

the decorrelation of the exterior orientation parameters from the sensor dependent parameters by a set of known control points, is much easier in land applications than in airborne applications.

The scale factor s^i, in the airborne case, changes with the flying altitude of the aircraft above ground. It can, therefore, either be approximated by assuming a constant flying altitude, calibrated by introducing a digital terrain model, or determined by measurement, using either stereo techniques or an auxiliary device such as a laser scanner. For precise georeferencing, the latter two techniques are the most interesting to be investigated because they can provide all necessary measurements from the same airborne platform and thus avoid datum problems. In the land applications case, the scale factor s^i, changes with the distance between the object and the sensor. It is therefore, different for each point. It can be determined by measurement, either by using stereo techniques or an auxiliary device such as a laser scanner. The first is the most commonly used technique.

3.6 Data Flow Optimization and Automation

The data flow of a general multi-sensor system is shown in Figure 3.8. At the top level are the user requirements which include type of survey, accuracy, reliability, image coverage, result presentation (e.g., maps, reports, digital output), etc. These user requirements are critical for the survey planning.
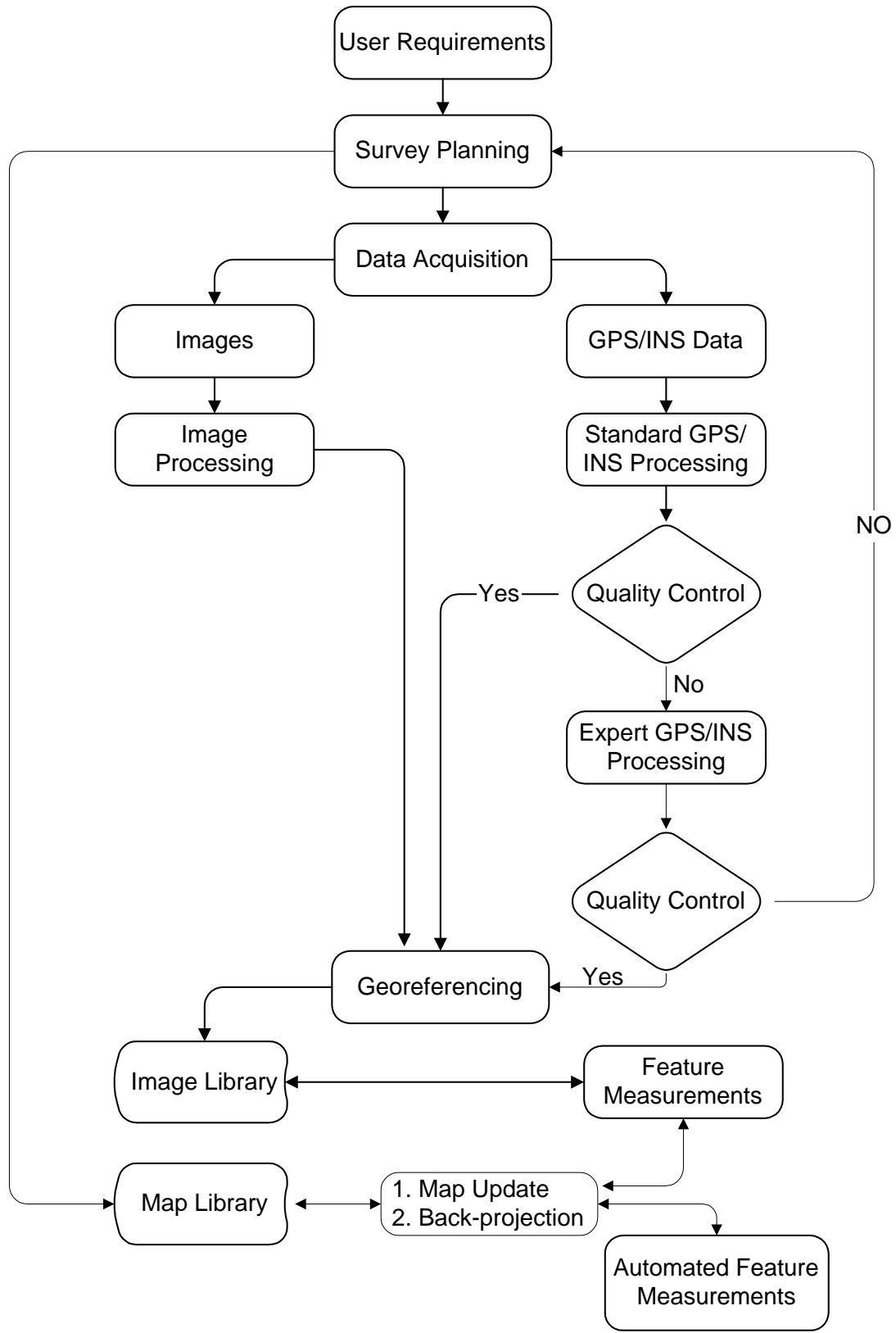
Figure 3.8: Data Flow of Multi-Sensor System

They determine the selection of the survey route according to parameters such as satellite availability, sun direction, road type, tree coverage, buildings, speed limits, traffic density, spacing between exposures, length of survey, and time schedule. To facilitate the set-up of an easy-access survey data base, the survey route is divided into small units which essentially follow the road pattern or other easily identifiable features. The result of optimizing all these factors is expressed in a waypoint file which defines the survey trajectory and the operational constraints (Schwarz and El-Sheimy, 1996).

This file is used to automate the data acquisition stage as much as possible. The driver is guided to the defined waypoints, based on azimuth and distance information contained in the file. The cameras are automatically switched on or off depending on the file information. Alert messages ensure that the data collected are sufficient to provide the user-required accuracy. Vital information is displayed to the survey crew on-line via the navigation control unit. It consists of the camera configuration in use, the number of satellites tracked, the azimuth and distance to the next waypoint, quality control alerts, etc. The information displayed on the navigation control unit is supplemented by spoken messages in critical situations, such as alerts or a change of the survey route.

The images are compressed and downloaded with an identifier which allows easy identification of all images in the same area taken at different times. The navigation data are downloaded after passing through the real-time quality control module. In post-mission, the GPS/INS data are processed first. Typically, the majority of them will pass the quality test after standard processing and will be used for georeferencing the image

data. They will then be stored in the image library. Those parts of the total traverse which do not pass the quality test, are immediately submitted to a more elaborate second stage of processing. In this fully-automated procedure, standard problems, such as those caused by loss of lock, are addressed and automatically resolved. After this stage, most of the data, say 98%, should be available for georeferencing. Those data which still do not satisfy the quality control requirements will either not enter the georeferencing stream or will be subjected to the scrutiny of a human expert who decides on the basis of the processing already done, whether or not further processing is likely to result in a higher percentage of usable data. As the expert knowledge built into the GPS/INS processing software is improved by the analysis of large data sets, the percentage of unusable data will get smaller and smaller. This means that tasks currently performed by a human expert will be taken over by the computer.

After georeferencing and storage in the image library, the images can be used to generate the output requested by the user. This output will obviously be different from one user to the next. In many cases, the user will want to do the feature extraction himself. In that case, the georeferenced images are simply transferred together with a standard report on their quality. In other cases, the user may request specific products which can be handled by dedicated application software. In some cases new software development will be needed. To handle the enormous amount of data and to cover a wide range of diverse applications a structured DBMS is absolutely essential. It must be capable of image selection based on location, time of survey, survey unit, best geometry, etc. On the other hand, utility programs for large groups of applications will also be needed. For many

applications, a partial automation of the measuring process will be highly desirable, such as the automatic measurement of conjugate points using epipolar lines or the automatic identification and measurement of geometrically well-defined objects. For map revision, features such as superimposition and back projection are extremely important. Many of these developments are only in their early stages and will considerably add to the quality of the products to be expected from multi-sensor systems.

CHAPTER 4

SYSTEM CALIBRATION

Highly accurate calibration of all sensors of the integrated system is an essential requirement to ensure accurate 3-D positioning. System calibration includes the determination of the accelerometer biases and gyro drifts of the INS, as well as parameters which define the internal geometry of the camera; these termed the inner orientation parameters. Also, the relative location and orientation between the camera cluster and the navigation sensors (GPS and INS) have to be determined. They will be called relative orientation parameters and will be used in the transformation of the 2-D image coordinates into the 3-D world coordinates through the georeferencing process. In this chapter, an overview of imaging with CCD cameras will be given as an introduction to the general requirements of their calibration. Mathematical models of integrating the navigation sensor output in the calibration procedure will also be discussed.

4.1 CCD in Photogrammetry

Close-range photogrammetry, in the form of film-based systems, has been used for over three decades to derive 3-D coordinates of objects (Karara, 1989). The main constraints for expanding the use of close range photogrammetry were: single-frame, slow-rate

photography, highly specialized processing equipment, and the need for expensive optical hardware for measurement. Close-range photogrammetry has undergone significant changes in recent years by making use of the advent of filmless imaging systems, such as CCD cameras. Digital CCD camera-based photogrammetric systems have the capability to reduce the turn-around time and employ equipment which is steadily decreasing in price.

While conventional cameras provide timing or exposure control using aperture settings (f-stop), shutter time, or flash synchronization, digital sensors additionally offer the possibility of instantaneously controlling the electronic signal amplification (gain control). This technique enables local image contrasts to be adjusted in order to avoid saturation or underexposure of gray level information which affects the geometric quality of the image (Luhman, 1990).

Recent trends in CCD technology are characterized by increased resolution (e.g., 4k x 4k pixels), color image acquisition, and improved radiometric. Standard CCD cameras use sensor chips ranging from 400 to 580 lines and 500 to 780 sensor elements per line. Normally the camera delivers a standard analog video signal (e.g. CCIR, RS-170) or a digital signal.

Another important development which supports the use of CCD cameras in photogrammetric applications is the advancement of fast ADCs. Frame grabbers integrated with high-speed computer buses and processing hardware have become a

standard commodity. Compared to analytical plotters used in conventional photogrammetry, the use of state-of-the-art computer image boards greatly simplifies measurements. They can be made on imported digital images and be displayed on high resolution monitors of a personal computer or workstation.

4.2 Image Acquisition with CCD Cameras

The acquisition and transmission of images taken by CCD cameras depend on the type of camera; namely analog or digital camera. An analog camera transmits an analog video signal and the ADC is carried out by a frame grabber. A digital camera provides a digital signal with the ADC already performed in the camera. The basic functions to be performed in order to obtain a digital image are:

- Signal processing in the camera,

- Data transmission to the frame grabber,

- Analog-to-digital conversion (ADC),

- Data buffering, compression, and storage.

The transmitted signals follow the video standards which are defined by television standards. Standard video signals are actually complex waveforms and contain information about the brightness of the image, along with timing pulses which indicate the end of each display line (horizontal sync " HSYNC") and the end of each display frame (vertical sync " VSYNC"). The first standard for black-and-white television, called

RS-170, was defined in 1941 by the National Television Systems Committee (NTSC) and the Electronics Industries Association (EIA). Another standard was defined in 1950 by the Commite Consultatif International des Radiocommunications (CCIR). The only difference between the two standards are the timing characteristics (see Table 4.1). For more details about different video standards, see Beyer (1992).

Table 4.1 : RS-170 and CCIR Video Signal Standard

(Source : COHU INC., Technical Manual No. 6X-948)

Parameter	RS 170	CCIR
• Frame rate / Field rate	30 / 60 Hz	25 / 50 Hz
• Number of active lines	480	576
• Interlacing	2:1	2:1
• Field time	16.67 ms	20 ms
• Line time	63.49 μs	64 μs
• Line frequency	15750 Hz	15625 Hz
• Aspect Ratio	4:3	4:3

Both standards use the principle of 2:1 interlacing. Interlaced scanning means that an image (frame) consists of two alternating fields. The definition of the field depends on the scanning mode. There are four basic scanning modes (Figure 4.1), which are:

1. **Interlaced frame mode :** In this mode, the sensor integrates each field for 1/30 second, spanning the time of two full video frames. Field-2, even lines, begins integrating midway through integration of field-1, odd lines. Due to the integration process, this mode is more prone to problems in kinematic applications. The main

68

advantage of this mode is that the maximum vertical resolution, about 485 lines, is available.

2. **Non-interlaced frame mode:** The odd lines are used for both fields. Each field is scanned for 1/60 second. Vertical resolution is about 242 lines. This is one-half of that available in the interlaced frame mode.

3. **Interlaced field mode :** The sensor integrates each field for 1/60 of a sec and combines two rows to form the lines. To form field-1, lines one and two are combined, then to form field-2, lines two and three are combined. Because of the 1/60 second field rate, this mode has less lag than the interlaced frame mode. On the other hand, due to the combination of lines, it has less vertical resolution than the interlaced frame mode.

4. **Non-interlaced field mode :** In this mode, the same two lines are combined to produce each line for both fields. This results in a lower vertical resolution of 242 lines. The camera still operates at 1/60 second for each field.

It is clear that due to the 1/60 second difference between the two fields, none of the interlaced frame modes can be used in kinematic applications. Interlaced images, in kinematic applications, suffer from severe blurring. Digital cameras do not have this problem since image acquisition and ADC are performed inside the camera. But they do have a major disadvantage in terms of the time needed to capture and transmit the digitized images. Typical digital cameras, with 1k X 1k resolution, take about 1-2 sec to transmit an image. The trade-off between digital and analogue cameras depends mainly on the application, static or kinematic, and the required image rate.

Scanning	Field - 1	Field - 2
Frame Interlace		
Frame Non - Interlace		
Field Interlace		
Field Non - Interlace		
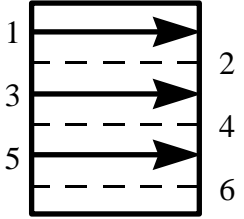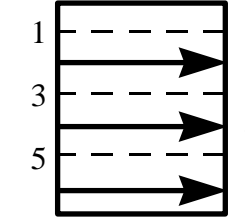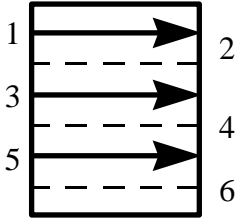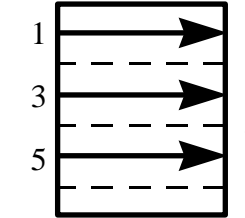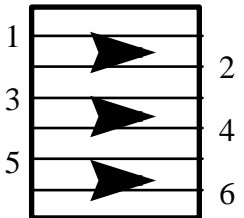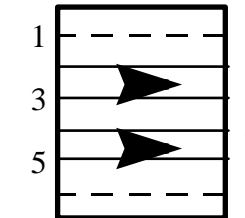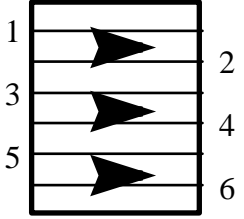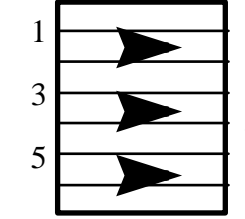
Figure 4.1 : Video Scanning Modes

The frame grabber is the second major component of the image acquisition process. Existing frame grabbers have a multitude of capabilities which are very difficult to generalize. The choice of a frame grabber for photogrammetric applications is likely to be different from that used, for example, in machine vision where target location in pixels is commonly sufficient. Accurate 3-D measurements require excellent stability over the complete image area because even a small localized imperfection can affect the overall measurement precision. Major error sources due to the frame grabber are :

1. Line jitter due to synchronization errors : The vertical and horizontal sync signals associated with the video signals are used to control the timing of the frame grabber. The source of the sync signal can be extracted from either the video input signal, from a separate composite sync input, or from the on-board clock. In the frame grabber, the sync signals are conditioned by a Phase-Locked-Loop (PLL) circuit which corrects for missing, extraneous, or low-level sync pulses - characteristics of many video signals.

The causes of line jitter are well known Lenz (1989), Raynor and Seits (1990)). The problem occurs because in CCD cameras discrete pixels are the originators of the analog signal. The camera clocks the analog data from the CCD chip at a fixed frequency (28.6363 MHz for the RS-170A signal). The PLL controls the timing of the ADC of the video signal based on the frequency that is expected. The ADC takes place after the beginning of a HSYNC signal. Any problems in detecting the beginning of the HSYNC gives rise to line jitter. Line jitter effects could reach 0.1 pixel shift in the x-direction (Beyer, 1992). This shift will introduce about 0.7 cm across-track error and 5 cm along-track error for all objects 35 m away from the van.

The effect of line jitter on the VISAT derived 3-D coordinates of points will depend on the sequence of images used in their computation. If fixed-base cameras are used, both cameras will have the same effect. This is due to the fact that all images taken by the same frame grabber are externally synchronized, using the same timing pulses. Therefore, they have the same line jitter value. Since both images have the same x-shift, only the along-track error will be canceled (see Figures 4.2.a and 4.2.b for a schematic explanation). On the other hand, if consecutive images are used, the error will depend on the magnitude and direction, left or right, of the line jitter. Consecutive images could be from the same camera, from different cameras but the same frame grabber, or from different cameras and different frame grabbers.

There are two methods for minimizing the line jitter effect. The first is based on synchronizing the frame grabber with the pixel clock output, and the second by averaging the images over many frames. The former requires a frame grabber that accepts a pixel clock input. Frame grabbers that accept pixel clock and three synchronized cameras are rare. The latter is suitable for static applications only and, hence, is commonly used in camera calibration and industrial metrology.

(b)

Across-Track Error

Line-jitter
with the same
direction
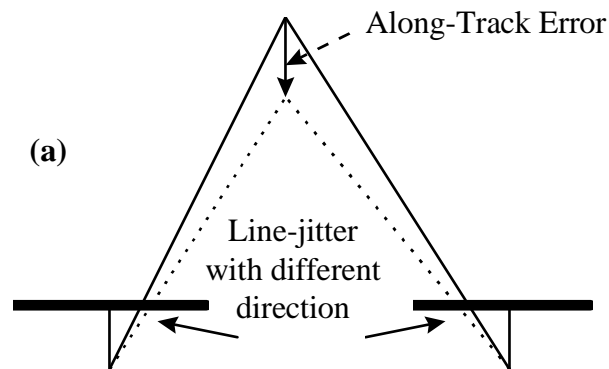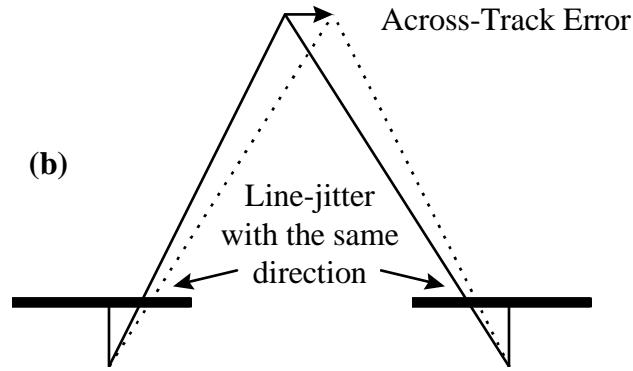
Figure 4.2 : Effect of Line-Jitter on the 3-D Coordinates

2. ADC process : Because most frame grabbers acquire images in real time (that is, 1/30 of a second RS-170 allowance for each video frame), special video speed ADC converters must be used. RS-170 allows 52.59 μsec for each line in the image to be sampled. This is called the active line time. In this time, a 512 x 480 frame grabber, for example, must convert 512 pixels (i.e. perform 512 ADCs). This requires an ADC with a throughput of almost 10 MHz (52.59 μsec divided by 512 equals 103 nsec; 103 nsec is equivalent to 9.74 MHz).

Most of the ADC performance parameters given by the manufactures are either insufficient or unclear for the signal and frequencies used. There are four main sources of error in ADC: quantization, linearity, offset, and gain. Quantization has to do with how accurately a particular digital pixel value represents the brightness of the corresponding location in the original video signal. Brightness resolution is determined by the resolution of the ADC. An 8-bit ADC divides the intensity spectrum from black to white into 256 values ($2^8 = 256$). The last three errors characterize the ADC response to the input

video signal, see Figure 4.3. These errors are temperature-dependent (Wong et. al. (1990)), i.e. the converter functions correctly only at its normal operating temperature. The temperature effects will be discussed in more detail in Chapter 6.
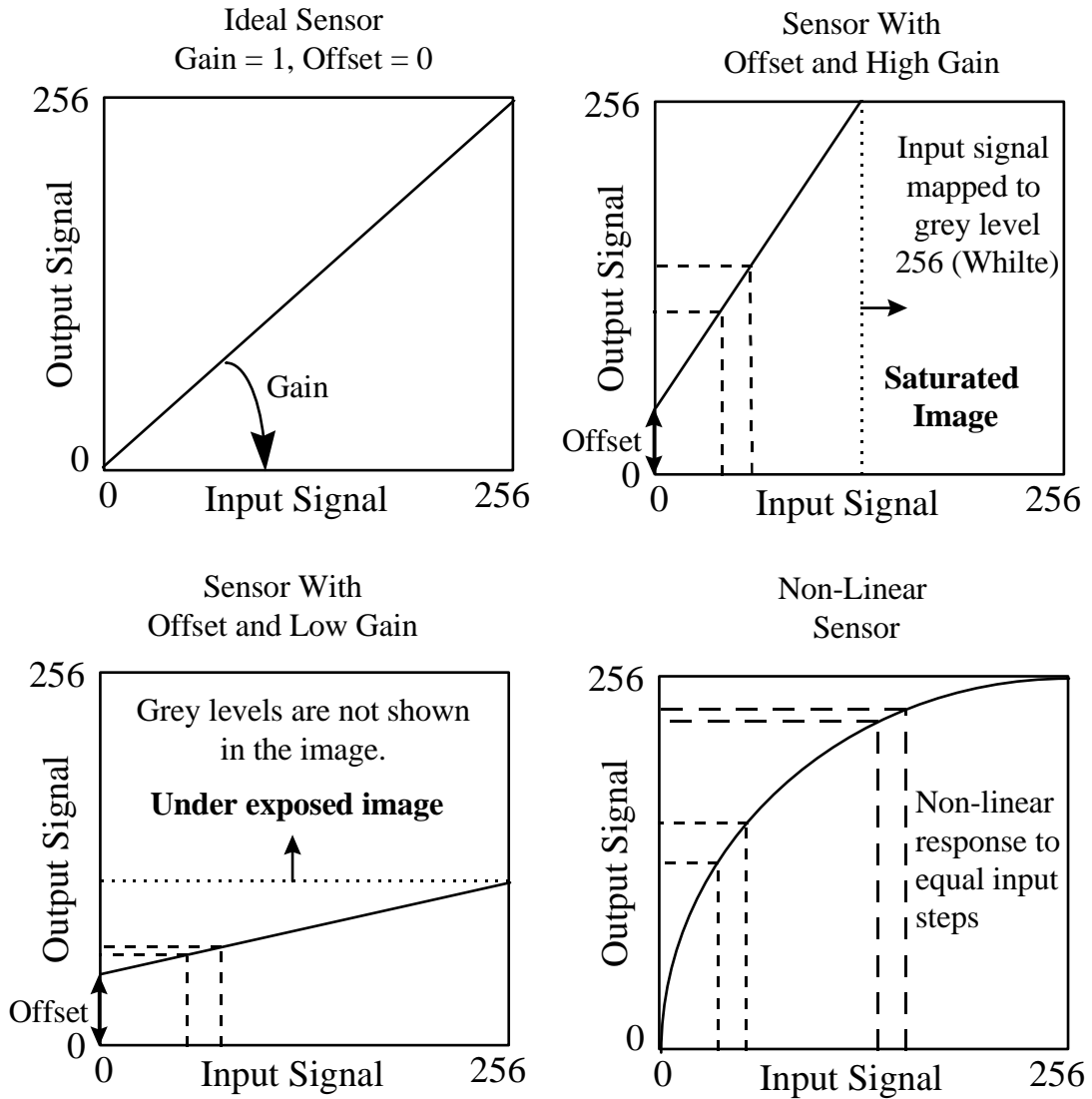
Figure 4.3: Characteristics of ADC Response

4.3 System Calibration

For the integration of analogue video cameras with navigation sensors, the term system calibration is more appropriate than simply camera calibration. On the one hand, this is due to the fact that an additional interior orientation parameter, scale in the x-axis direction of the image space, is also estimated in the calibration procedure. This scale arises from the difference between the camera clock frequency, governing video signal output of the image data, and the frame grabber sampling frequency. Essentially, this creates rectangular pixels, for more details see Lichti and Chapman (1995). On the other hand, the integration of the video cameras with the INS requires the knowledge of the spatial relation between the two system frames. This requires the spatial vector and the relative rotation between the two sensor frames. The system calibration, therefore, includes the calibration of the cameras and the relative orientation calibration.

4.3.1 Camera Calibration

Camera calibration is a standard procedure which has to be performed before using any metric or digital camera in photogrammetric applications. It determines the interior geometry, i.e. the inner orientation parameters, of the cameras. A self-calibration bundle adjustment is used for this purpose (Cosandier and Chapman, 1992). It solves for the four elements which define the inner geometry of the camera, namely principal point coordinates (x_p, y_p), lens focal length (f), y-axis scale factor $(k_y$ - used when pixels are

not square), and the five elements which define the lens distortion characteristics. In addition, the position (X_O, Y_O, Z_O) and the orientation (ω, Φ, κ) parameters for each camera are solved for. These parameters are used to relate the cameras to the navigation sensors.

The principal point coordinates and the y-scale factor relate the computer coordinate system to the image coordinate system. The first is a left-handed coordinate system with the origin at the left topmost pixel of the screen, x-axis parallel to the image lines and the y-axis parallel to columns of the image. The latter, is a right-handed system with its origin at the principal point. Figure 4.4 shows the relation between the two systems. Due to the difference between the two coordinate systems, an additional reflection (-1) must be incorporated into the y-collinearity equation. Therefore, the y-scale factor is simply added to the bundle adjustment to account for both the x-axis scale factor and the reflection. Thus, the y-scale factor is simply the negative reciprocal of the actual x-axis scale factor. The transformation from the computer coordinate to the image coordinate is defined by the following formula:

$$\bar{x} = x_c - x_p,$$

$$\bar{y} = (y_c - y_p) / k_y \tag{4.1}$$

where

$\bar{x}, \bar{y}$ image coordinates,

x_C, y_C computer coordinates,

k_y y-axis scale factor.
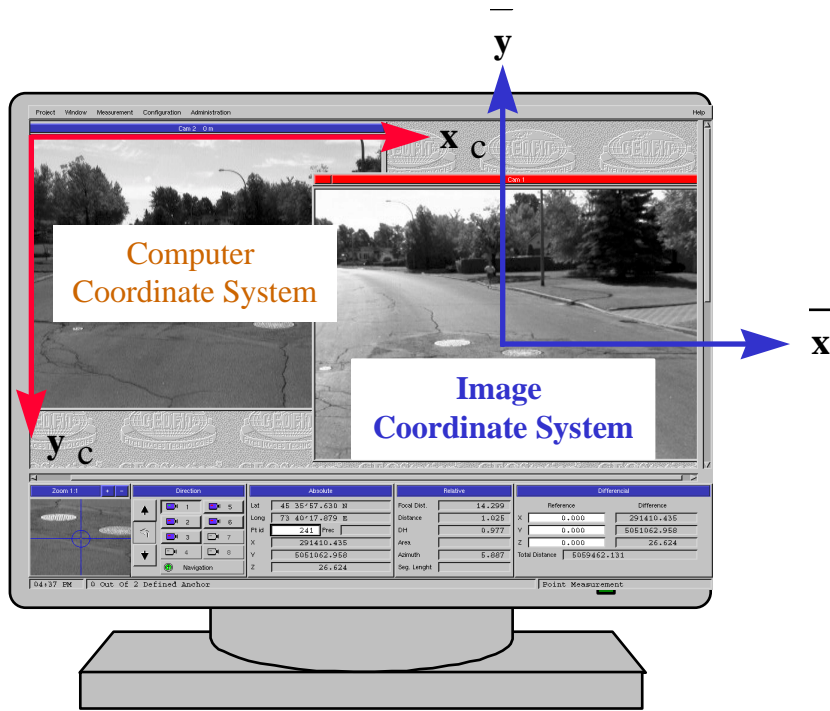
Figure 4.4 : The Computer and Image Coordinate Systems

The mathematical model of the bundle adjustment with self-calibration is based on the collinearity conditions. They are formulated as follows:

$$\bar{x} = -f\frac{U}{V} + \Delta x \,,$$

$$\bar{y} = -f\frac{V}{W} + \Delta y \tag{4.2}$$

Using the auxiliary parameters

$$U = m_{11}(X - X_0) + m_{12}(Y - Y_0) + m_{13}(Z - Z_0) \,,$$

$$V = m_{21}(X - X_0) + m_{22}(Y - Y_0) + m_{23}(Z - Z_0) \,,$$

$$W = m_{31}(X - X_0) + m_{32}(Y - Y_0) + m_{33}(Z - Z_0) \tag{4.3}$$

where

$\bar{x}, \bar{y}$	Image coordinates,
f	Lens focal length,
m_{ij}	Elements of the orthogonal matrix R_m^c defining the rotation between the m-frame and the camera coordinate system (c-frame),
X, Y, Z	Object coordinates in the m-frame,
X_o, Y_o, Z_o	Perspective center coordinates in the m-frame,
$\Delta x, \Delta y$	Correction terms for additional parameters, mainly lens distortion parameters.

Lens distortion can be thought of as the deviation of the image ray from ideal collinearity with the object ray. Lens distortion is due to the imperfection of lens manufacturing. For an ideal lens, the object, the lens perspective center, and the image point, all should lie along a straight line. However, no lens has supports an ideal collinearity behavior and will always have imaging aberrations. Lens distortion is usually divided into two types, radial and tangential. Radial distortion affects the position of the image point on a straight line radiating form the principal point. The tangential distortion magnitude depends on the radial distance of the imaged point to the principal point and the orientation with respect to a reference direction. The three radial lens distortion coefficients (k1, k2, and k3), and two tangential distortion coefficients (p1 and p2) are modeled by (Brown, 1966):

$$\Delta x = \bar{x}(k_1 r^2 + k_2 r^4 + k_3 r^6) + p_1(r^2 + 2\bar{x}^2) + 2 p_2 \overline{xy},$$

$$\Delta y = \bar{y}(k_1 r^2 + k_2 r^4 + k_3 r^6) + 2 p_1 \overline{xy} + p_2(r^2 + 2\bar{y}^2) \qquad (4.4)$$

where

$$r = \sqrt{\overline{x}^2 + \overline{y}^2}$$

Calibration of cameras requires a test field of targets with known coordinates in an arbitrary coordinate system. The UofC 3-D calibration jig has been used. It consists of 28 randomly-spaced targets within a 2 x 1.5 x 1.5 m cube, see Figure 4.5. The 3-D coordinates of the center of each of these targets were determined via angle intersection using a 1 arcsecond electronic theodolite. Estimated 3-D coordinates have been surveyed to an accuracy of 0.1 mm.

In order to achieve sub-pixel accuracy in the calibration results, special techniques for measuring the image coordinates of the test field targets are needed. These techniques make use of circular targets, black circles with white background, made of retro-reflective film. This material has a very important property; it reflects the light directly back towards its source. Therefore, in order to have a good contrast between the targets and the background, a light source was mounted very close to the cameras. The centroid detection algorithm was used to determine the coordinates of the targets. It first creates a binary window around the target using thresholding and then computes the center of gravity of the targets in the computer coordinate system as :

$$\overline{x}_{cg} = \frac{\sum \sum \overline{x} \cdot g(\overline{x}, \overline{y})}{\sum \sum g(\overline{x}, \overline{y})}$$

$$\overline{y}_{cg} = \frac{\sum \sum \overline{y} \cdot g(\overline{x}, \overline{y})}{\sum \sum g(\overline{x}, \overline{y})}$$
(4.5)

where,

x_{cg}, y_{cg} Coordinates of the target center of gravity,

$g(\overline{x}, \overline{y})$ Gray level value of the pixel at location $(\overline{x}, \overline{y})$.
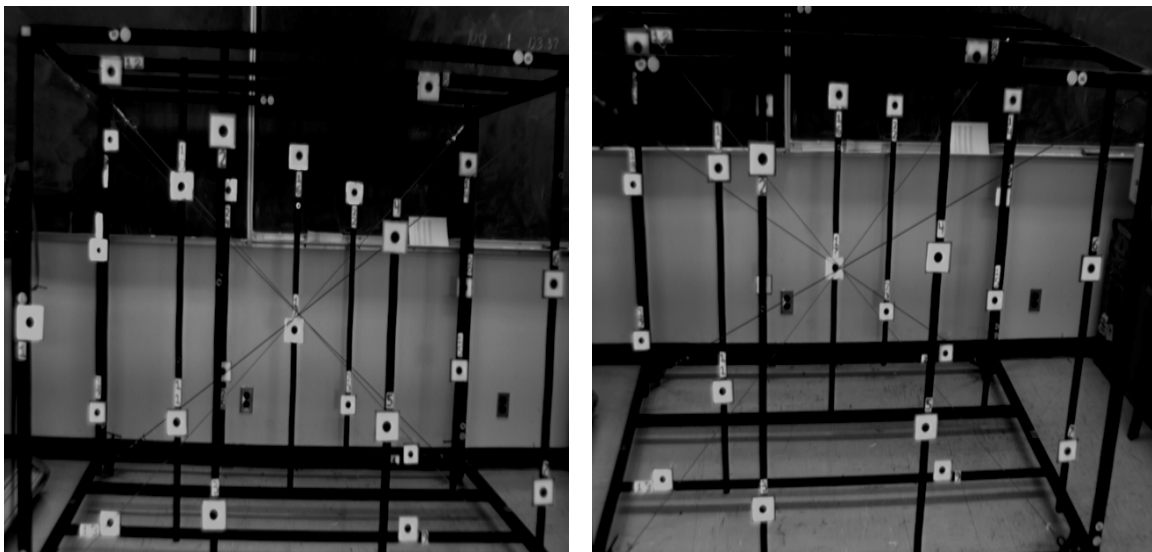
Figure 4.5: The Camera Calibration Jig

4.3.2 Relative Orientation

The imaging component of the VISAT system consists of 8 video cameras with a resolution of 640 x 480 pixels. The cameras are housed in a pressurized case and mounted inside two fixed-base towers on top of the VISAT van (Figure 4.6). This

arrangement eliminate for all practical purposes the chance for the cameras to move during the survey.
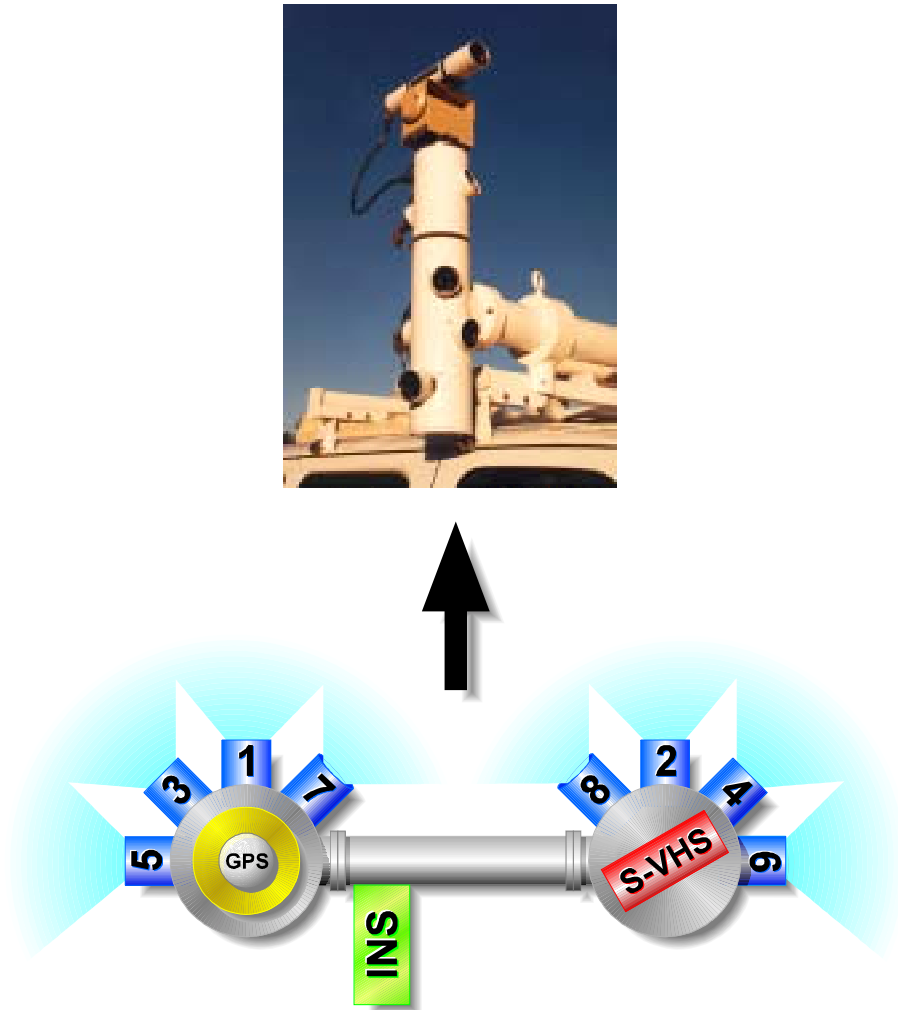
Figure 4.6 : Roof Mount of the Cameras

The relative orientation (RO) parameters can be divided into two groups. The first group contains the parameters which define the relative position and orientation between different stereo pairs. The second group consists of the parameters that define the relative position and orientation between the cameras and the navigation sensors. The latter are

essential for the georeferencing process. To estimate the two groups of parameters, some

constraints are added to the bundle adjustment program (El-Sheimy and Schwarz 1993).

The constraint equations make use of the fact that both the cameras and the INS are fixed

during the mission. This is achieved by acquiring a number of images at different

positions and distances from a test field of GCPs (see Figure 4.7).
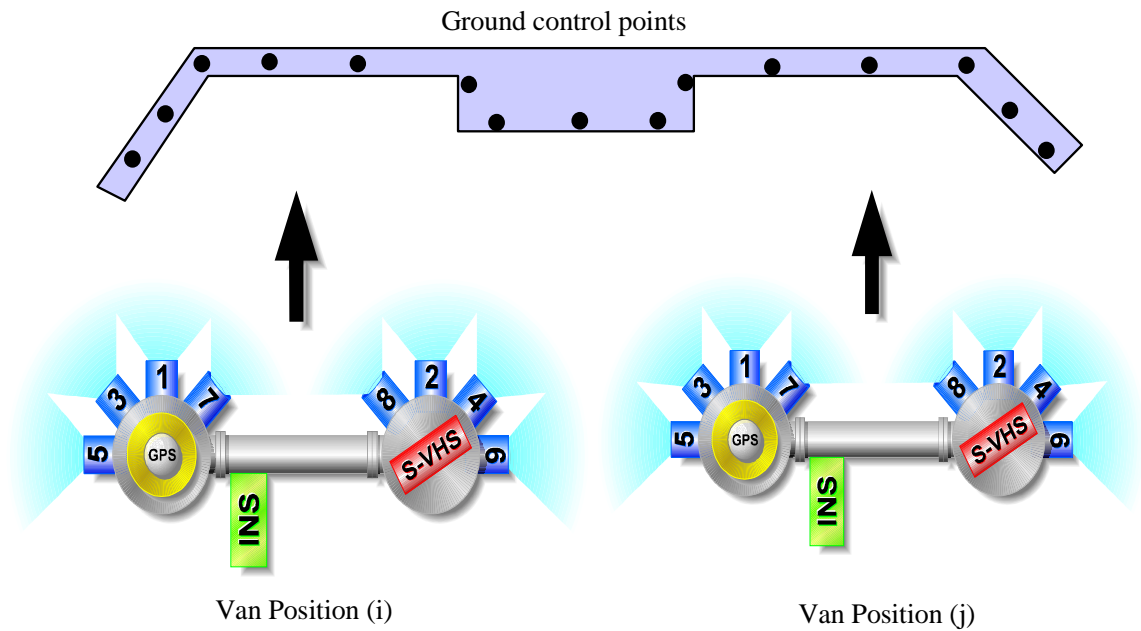
Figure 4.7 : The Test Field for Calibrating the RO Parameters.

These constraints can be written for two van positions (i) and (j) and two cameras (c1)

and (c2) as follows:

- $b^i = b^j,$

- $\Delta R_b^{c1}(i) = \Delta R_b^{c1}(j)$, $\Delta R_b^{c2}(i) = \Delta R_b^{c2}(j)$,

- $\Delta R_{c1}^{c2}(i) = \Delta R_{c1}^{c2}(j)$ (4.6)

For the stereo-pair (i),

- $B^i = \sqrt{(X^{c1} - X^{c2})^2 + (Y^{c1} - Y^{c2})^2 + (Z^{c1} - Z^{c2})^2}$,

- $\Delta R_b^c(i) = R_m^c(i) \cdot R_b^m(i)$,

- $\Delta R_{c1}^{c2}(i) = R_m^{c2}(i) \cdot R_{c1}^m(i)$ (4.7)

where,

b is the base vector between stereo-pair (c1) and (c2),

R_c^m is the rotation matrix between the c-frame and the m-frame, the m-frame is

         the frame in which the test field coordinates are expressed,

R_b^m is the INS attitude matrix between the INS b-frame and the m-frame,

ΔR_c^b is the rotation matrix between the c-frame and the INS b-frame,

ΔR_{c1}^{c2} is the rotation matrix between camera (1) and camera (2), and

X^{ci}, Y^{ci}, Z^{ci} are the coordinates of the camera (ci) perspective center in the m-frame.

The implementation of the constraints requires the knowledge of the exterior orientation parameters (X_O, Y_O, Z_O, ω, ϕ, κ) of the cameras as well as the attitude information of the INS. The latter is estimated after processing the INS data and including them in the bundle adjustment with their proper weights. The exterior orientation parameters are estimated directly form the bundle adjustment program. Once the exterior orientation parameters of each camera are available, the constraints are implemented as follows :

1- The base constraints: each camera will constitute a strip, see Figure 4.8 for a pictorial example of two strips and three van setups. The base vector $\begin{pmatrix} b_x & b_y & b_z \end{pmatrix}$ between each stereo pair are expressed in one of the camera coordinate systems as follows :

$$B_{i,j} = \begin{pmatrix} b_x \\ b_y \\ b_z \end{pmatrix}_{i,j} = R_m^c(i,j)\left[\begin{pmatrix} X_o \\ Y_o \\ Z_o \end{pmatrix}_{i+1} - \begin{pmatrix} X_o \\ Y_o \\ Z_o \end{pmatrix}_i\right] \tag{4.8}$$

where

i   is the number of strips, i.e. the number of cameras, and

j   is the number of van setups , i.e. the number of images in each strip.

2- The relative rotation matrix constraints : The analytical formulation of the constraints is based on the relative rotation matrices ΔR between any two cameras or any camera and the INS b-frame. This can be achieved by keeping the relative rotation angles ($\Delta\omega$, $\Delta\phi$, $\Delta\kappa$) constant in the bundle adjustment. The form of the rotation matrix used is as follows :

$$\Delta R = \begin{pmatrix} C\Delta\phi C\Delta\kappa & C\Delta\phi S\Delta\kappa & -S\Delta\phi \\ S\Delta\omega S\Delta\phi C\Delta\kappa - C\Delta\omega S\Delta\kappa & S\Delta\omega S\Delta\phi S\Delta\kappa + C\Delta\omega C\Delta\kappa & S\Delta\omega C\Delta\phi \\ C\Delta\omega S\Delta\phi C\Delta\kappa + S\Delta\omega S\Delta\kappa & C\Delta\omega S\Delta\phi S\Delta\kappa - S\Delta\omega C\Delta\kappa & C\Delta\omega C\Delta\phi \end{pmatrix} \tag{4.9}$$

Where S and C are the trigonometric functions sine and cosine, respectively.
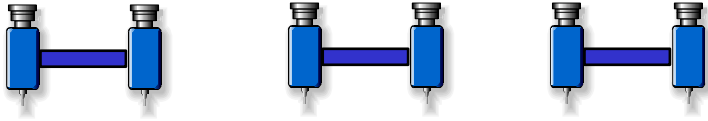
Figure 4.8 : Pictorial Example of the RO Constraints

There are only three independent parameters in the matrix ΔR. Their functional relationship with the matrix elements are as follows :

$$
\begin{aligned}
\tan \Delta\omega &= \frac{\Delta R_{23}}{\Delta R_{33}} \\
\sin \Delta\phi &= -\Delta R_{13} \\
\tan \Delta\kappa &= \frac{\Delta R_{12}}{\Delta R_{11}}
\end{aligned}
\tag{4.10}
$$

Once the relative orientation parameters are available after the first iteration of the bundle adjustment, the constraints can be implemented as follows:

$$
\begin{pmatrix} b_x \\ b_y \\ b_z \end{pmatrix}_{i,j} = \begin{pmatrix} b_x \\ b_y \\ b_z \end{pmatrix}_{i,j+1}
\tag{4.11}
$$

$$
\begin{pmatrix} \dfrac{\Delta \boldsymbol{R}_{23}}{\Delta \boldsymbol{R}_{33}} \\ -\Delta \boldsymbol{R}_{13} \\ \dfrac{\Delta \boldsymbol{R}_{12}}{\Delta \boldsymbol{R}_{11}} \end{pmatrix}_{i,j} = \begin{pmatrix} \dfrac{\Delta \boldsymbol{R}_{23}}{\Delta \boldsymbol{R}_{33}} \\ -\Delta \boldsymbol{R}_{13} \\ \dfrac{\Delta \boldsymbol{R}_{12}}{\Delta \boldsymbol{R}_{11}} \end{pmatrix}_{i,j+1}
\tag{4.12}
$$

The number of constraints added to the bundle adjustment program can be computed using the following formula :

Number of constraints $= (i-1)! \bullet (j-1)!,$ \hfill (4.13)

where (i) is the number of cameras and (j) is the number of van positions setups during the calibration.

After the calibration, the offset vector between the INS and the cameras, expressed in the INS b-frame, can be computed. It should be noted that this is not possible before the calibration, since the cameras perspective centers cannot be physically observed. These vectors are used in the georeferencing equation given in Chapter 3. The offset vectors are computed as follows (Figure 4.9):

$$
\boldsymbol{a}_{ci}^{b} = \boldsymbol{R}_{m}^{b} \cdot \begin{pmatrix} X_{INS}^{m} - X_{ci}^{m} \\ Y_{INS}^{m} - Y_{ci}^{m} \\ Z_{INS}^{m} - Z_{ci}^{m} \end{pmatrix}
\tag{4.14}
$$

$$
\boldsymbol{a}_{GPS}^{b} = \boldsymbol{R}_{m}^{b} \cdot \begin{pmatrix} X_{INS}^{m} - X_{GPS}^{m} \\ Y_{INS}^{m} - Y_{GPS}^{m} \\ Z_{INS}^{m} - Z_{GPS}^{m} \end{pmatrix}
\tag{4.15}
$$
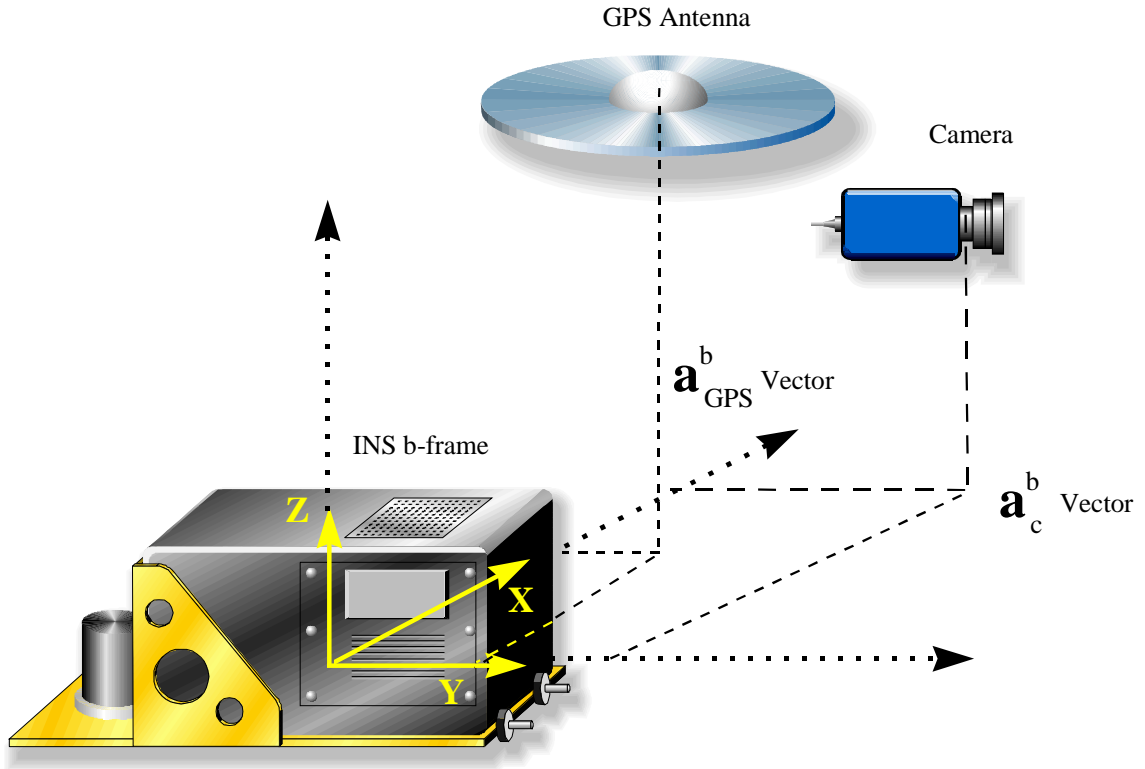
Figure 4.9: The Coordinates of the Cameras and the GPS Antenna in the INS b-frame

4.3.3 INS Calibration

The calibration of the INS system consists of a lab calibration and a field refinement test. The field test will be discussed in more detail in Chapter 6. In the lab calibration, 30-minute samples of stationary INS data in four different directions are collected on a stable and level surface. The azimuths are: $0°$, $90°$, $180°$, and $270°$. Since the INS sits on a level surface during the lab test, the pitch and roll can be assumed to be zero. The INS gyro drift (d) and accelerometer biases (b) can be computed as follows, for more details see Wong (1988) and Savage (1978) :

$$d = \frac{1}{4} \sum_{j=1}^{4} \left(\omega_{ie}^{b} - R_{l}^{b} \omega_{ie}^{l} \right)^{j},$$

$$b = \frac{1}{4} \sum_{j=1}^{4} \left(f^{b} - R_{l}^{b} g \right)^{j} \tag{4.16}$$

where

$$R_{l}^{b} = \begin{pmatrix} \cos(A) & -\sin(A) & 0 \\ \sin(A) & \cos(A) & 0 \\ 0 & 0 & 1 \end{pmatrix}$$

$$\omega_{ei}^{l} = \omega_{e} \begin{pmatrix} 0 \\ \cos\phi \\ \sin\phi \end{pmatrix}$$

where (j) is the sample number, (A) is the sample azimuth, and ϕ is the latitude. Results from the lab calibration show that the gyro drift and accelerometer biases in this particular Honeywell Laser-Ref III are :

$$d = \begin{pmatrix} 0.00864 \\ 0.00071 \\ 0.00914 \end{pmatrix} arc\sec\!\!\Big/_{\!\!\sec} , \text{ and}$$

$$b = \begin{pmatrix} 20 \\ -30 \\ -150 \end{pmatrix} mGal.$$

The parameters estimated in the lab calibration are used as an approximation to the gyro drifts and accelerometers biases, they are further improved by information from a field test which will be discussed in Chapter 6.

4.4 Integrating INS Attitude Data into Bundle Adjustment

The integration of INS attitude data into a bundle adjustment program requires some consideration due to the fact that the INS attitude data normally refer to a local-level frame (LL-frame). The attitude of the INS system, i.e. the orientation of the INS measurement frame (b-frame) with respect to the LL-frame, can be defined by three Euler rotational angles known as roll (r) around the x-gyro axis, pitch (p) around the y-gyro axis, and yaw (y) around the z-gyro axis. Attitude angles are derived from the attitude matrix R_b^{LL}, relating the b-frame and the LL-frame.

In the KINGSPAD processing software, this attitude matrix has been defined according to navigation conventions as follows (Wei and Schwarz (1990b)) :

$$
\begin{aligned}
R_b^{LL} = R_b^m &= R_3(y) \cdot R_1(p) \cdot R_2(r) \\
&= \begin{bmatrix} c(y)c(r) - s(y)s(p)s(r) & -s(y)c(p) & c(y)s(r) + s(y)s(p)c(r) \\ s(y)c(r) + c(y)s(p)s(r) & c(y)c(p) & s(y)s(r) - c(y)s(p)c(r) \\ -c(p)s(r) & s(p) & c(p)c(r) \end{bmatrix}
\end{aligned}
\tag{4.17}
$$

where s and c denote the sine and cosine respectively.

Using Equation (4.17) the attitude angles roll, pitch, and yaw (r, p, y) can be obtained by :

$$
\begin{aligned}
r &= \tan^{-1}\left(-\frac{R_b^{LL}(3,1)}{R_b^{LL}(3,3)} \right) \\
p &= \sin^{-1}\left(R_b^{LL}(3,2) \right) \\
y &= \tan^{-1}\left(-\frac{R_b^{LL}(1,2)}{R_b^{LL}(2,2)} \right)
\end{aligned}
\tag{4.18}
$$

As shown in Equation (3.2), the attitude matrix R_b^{LL} can be obtained by solving the following differential equation :

$$\dot{R}_b^{LL} = R_b^{LL}\Omega_{lb}^b = R_b^{LL}(\Omega_{ib}^b - \Omega_{il}^b)$$

(4.19)

where Ω_{ib}^b is the skew-symmetric matrix for the INS body rates and the Ω_{il}^b is the skew-symmetric matrix for the angular velocities of the LL-frame with respect to the inertial frame.

The solution of Equation (4.19) is given in Savage (1982) and provides the recursive form for the update of the attitude matrix R_b^{LL}. For the b-frame sensed rotation, it takes the following form:

$$R_b^{LL}(t + \Delta t) = R_b^{LL}(t) \cdot \left[I + \frac{1}{\theta}\sin\theta \cdot S + \frac{1 - \cos\theta}{\theta^2} \cdot S^2 \right]$$

(4.20)

where

- $S = \Omega\Delta t$ is the skew-symmetric matrix form of the vector θ given by :

$$\Omega = \begin{bmatrix} 0 & -\theta_z & \theta_y \\ \theta_z & 0 & -\theta_x \\ -\theta_y & \theta_x & 0 \end{bmatrix} = \begin{bmatrix} 0 & -\omega_z\Delta t & \omega_y\Delta t \\ \omega_z\Delta t & 0 & -\omega_x\Delta t \\ -\omega_y\Delta t & \omega_x\Delta t & 0 \end{bmatrix}$$

- θ is the small incremental angular changes of the rotation of the b-frame with respect to the LL-frame over the short time interval Δt. This interval is typically between 16 to 20 msec.

The attitude matrix of the camera is defined according to photogrammetric conventions as the rotation from the mapping frame (m-frame) to the camera frame (c-frame) as:

$$R_m^c = R_3(\kappa) \cdot R_2(\phi) \cdot R_1(\omega) \qquad (4.21)$$

where ω, ϕ, κ are the rotation angles around the x-axis, y-axis, and z-axis of the camera, respectively.

The integration of the INS attitude data into the bundle adjustment, therefore, requires the following steps:

1. For easy operation, the coordinate system of the calibration test field should be based on a mapping coordinate system, e.g. UTM or 3TM, representing a LL-frame. In that case, the INS derived azimuth is directly related to the LL-frame. If a different coordinate system for the test field is used, it will result in different values *for* (ω, ϕ, κ) and, therefore, a different relative orientation between the cameras and the INS system. Thus a constant azimuth has to be made in this case to all maps produced by a GPS/INS system. The azimuth of the network could be determined using a GPS static survey with baselines of about 1 to 2 km in length.

2. The estimation of the relative orientation parameters ($\Delta\omega$, $\Delta\phi$, $\Delta\kappa$) between the INS (b-frame) and the cameras (c-frame) requires the product of the rotation matrices

R_b^m and R_m^c. In order to obtain meaningful values, both rotation matrices must have the same sequence of rotations about the axes x, y and z. It is clear from Equations (4.17) and (4.21) that the two matrices have different sequences of rotations with respect to the m-frame. Therefore, in the implementation of the relative orientation constraints, discussed in Section 4.3.2, both rotation matrices should follow the same rotation sequence. Since the constraints will be implemented in the bundle adjustment program, it is more feasible to follow the camera rotation sequence. That is, the implementation of the relative orientation constraint should take the form :

$$R_b^c = R_m^c \cdot R_b^m = \left[R_3(\kappa) \cdot R_2(\phi) \cdot R_1(\omega)\right] \bullet \left[R_3(y) \cdot R_2(r) \cdot R_1(p)\right] \qquad (4.22)$$

The implementation of Equation (4.22) requires the following steps:

- Extract the INS attitude angles (r, p, y) using Equation (4.18).

- Re-produce the INS attitude matrix using the rotation sequence in Equation (4.22).

- Do the same two steps when implementing the INS attitude matrix in the georeferencing process.

CHAPTER 5

THREE-DIMENSIONAL COMPUTATION USING THE VISAT SYSTEM

The final accuracy of 3-D coordinates computed from the VISAT system is a function of the complete processing chain, which involves GPS position, INS position/attitude, system synchronization, system calibration, pixel size, pointing accuracy, and van speed. These factors are discussed in this chapter. Firstly, the procedures of 3-D coordinate computation will be discussed followed by the factors affecting the accuracy of the VISAT system. The expected accuracy of the 3-D coordinates and how each component contributes to the error budget will be given. The quality control module concept will be discussed in the last section for both the positioning and imaging modules.

5.1 3-D Computation

3-D coordinate computation of any object within the field of view of the cameras requires the following information from at least two images :

- Position of the camera perspective center at exposure time (3 parameters per image), as estimated from the GPS/INS position and the translation component between the INS and the cameras;

- Camera orientation at exposure time (3 parameters per image), as estimated from the INS attitude and the relative orientation parameters between the cameras and the INS;

- Interior geometry of the camera sensor (9 parameters), as estimated from the camera calibration; and

- Image coordinates of the object (2 parameters), as measured from the image in the VISAT Station.

The input information needed is not the direct output from a single module. It includes the data acquisition module using the VLog software, GPS/INS processing using the KINGSPAD software, system calibration using bundle adjustment software, georeferencing using Georef software , and finally the image measurements in the VISAT Station software. The whole process includes the following major steps :

1. Collecting synchronized GPS, INS, and image data using the VLog software. All the data streams are time-tagged with the GPS time with a special file containing the camera exposure time, called "TAG" file.

2. Processing the GPS and INS data using the KINGSPAD software. The software produces a georeferencing file, called the "REF" file. The file contains the GPS time, INS position and attitude, and standard deviation of the output quantities at 50 Hz.

3. Calibrating the cameras and cameras/INS using the bundle adjustment program.

4. Georeferencing the images, which includes the following :

   - Interpolating the INS position and the attitude information from the "REF" file at the time of exposure stored in the "TAG" file. Since the INS data are produced at

50 Hz (1 Hz equals to 33 cm at 60 km/h), a linear interpolation model is enough for the VISAT application.

- Rotating the camera-INS offset vector $\boldsymbol{a}^b$, as estimated by system calibration, from the INS b-frame into the m-frame using the INS attitude matrix $\boldsymbol{R}_b^m(t)$, from the KINGSPAD software, as follows :

$$
\begin{pmatrix} a_x \\ a_y \\ a_z \end{pmatrix}^m = \boldsymbol{R}_b^m(t) \bullet \begin{pmatrix} a_x \\ a_y \\ a_z \end{pmatrix}^b \tag{5.1}
$$

- Computing the perspective center coordinates of the cameras as follows :

$$
\begin{pmatrix} \phi \\ \lambda \\ h \end{pmatrix}_{Camera} = \begin{pmatrix} \phi \\ \lambda \\ h \end{pmatrix}_{INS} + \begin{pmatrix} \dfrac{a_y^m}{R_P} \\[3ex] \dfrac{a_x^m}{R_M \bullet Cos\phi} \\[3ex] a_z^m \end{pmatrix} \tag{5.2}
$$

where $\boldsymbol{R_M}$ and $\boldsymbol{R_P}$ are meridian and prime vertical radii of curvature, respectively.

- Computing the attitude matrices of the cameras using the INS attitude matrix $\boldsymbol{R}_b^m(t)$, as estimated from the KINGSPAD software, and the relative orientation matrix $\boldsymbol{R}_b^c$, as estimated from the system calibration, as follows :

$$
\boldsymbol{R}_m^c(t) = \boldsymbol{R}_b^c \bullet \boldsymbol{R}_m^b(t)
$$

- Storing the georeferencing information in a header in front of each image.

5. Transforming the 2-D image coordinates measured in the computer coordinate frame to the 2-D image coordinates of the camera CCD chip. This step requires the camera principal point coordinates (x_p, y_p) and the scale factor k_y.

$$\bar{x} = x - x_p \ ,$$

$$\bar{y} = (y - y_p) / k_y \tag{5.4}$$

6. Correcting the image coordinates for the lens distortion parameters :

$$\Delta\bar{x} = \bar{x}(k_1 r^2 + k_2 r^4 + k_3 r^6) + p_1(r^2 + 2\bar{x}^2) + 2p_2 \overline{xy}$$

$$\Delta\bar{y} = \bar{y}(k_1 r^2 + k_2 r^4 + k_3 r^6) + 2p_1 \overline{xy} + p_2(r^2 + 2\bar{y}^2) \tag{5.5}$$

where k_i, p_j are lens distortion coefficients as estimated from the camera calibration.

7. Transforming the 2-D CCD chip coordinates to the 3-D c-frame coordinates. This step requires the determination of the focal length (f) of the camera lens.

8. Introducing all the information with the proper weighting into a least squares bundle adjustment. Up to 10 image points can be introduced into the least squares problem.

5.2 Factors Affecting the Accuracy of the VISAT System

The georeferencing model discussed in Chapter 3 contains the measured image data as well as all steps in the processing chain. They include GPS positioning, INS position/attitude determination, system calibration, accuracy of cameras, and the effect of image geometry. This model can, therefore, be used to assess the contribution of measurement and system errors to the 3-D positioning accuracy. The following system

analysis is somewhat simplified because it does not use the explicit model for INS/GPS integration. However, the error model of this integration has been analyzed elsewhere, see for example Schwarz et. al. (1993b), and its characteristic contribution to the error budget is well-known. With this caveat in mind, the model given in Equation (3.7) can be considered as a general model for analyzing the errors in the georeferencing procedure. Its parameters will change from one application to the next. The structure of the error model will, however, be the same.

Using a first-order error analysis of Equation (3.7) and adding one term, $(V+\omega)$. δT to reflect the synchronization error, the following formula is obtained, for more details see El-Sheimy et. al. (1995) and Schwarz and El-Sheimy (1996):

$$
\begin{aligned}
\delta r_i^{\,m} = \ & \delta r_{INS}^{\,m}(t) + \\
& \delta R_b^{\,m}(t) \bullet (S^i \bullet R_s^{\,m} \bullet r^s + a^b) + \\
& R_b^{\,m}(t) \bullet (S^i \bullet \delta R_s^{\,m} \bullet r^s + \delta a^b) + \\
& R_b^{\,m}(t) \bullet (\delta S^i \bullet R_s^{\,m} \bullet r^s + S^i \bullet R_s^{\,m} \bullet \delta r^s) + \\
& (V + \omega) \bullet \delta T
\end{aligned}
\tag{5.10}
$$

where V and ω are the velocity and angular rate of the camera, respectively.

Equation (5.10) contains five major groups of errors that contribute to the final accuracy of the 3-D coordinates. They are the INS/GPS position errors, the INS orientation errors, the calibration errors, the target pointing and geometry errors, and the synchronization errors.

The only potential error which was not included in Equation (5.10) is the instability of the cameras with respect to the navigation sensors. This instability will increase the error level of δa^b and δR_s^b. Experience available at this point does not indicate that these effects are large enough to be above the general noise level. In general, the variation in δa^b is not as critical as that in δR_s^b.

5.2.1 GPS/INS Errors

The accuracy of the GPS/INS system depends on the accumulation of errors in each subsystem and on the effectiveness of the updating procedure in reducing these errors. Typical GPS/INS positional errors for a truck survey over a baseline of 20 km length are shown in Figure 5.1. The number of available satellites during the test was five. The figure confirms that positional errors are in the order of 10 cm with an RMS of 7 cm. Similar results were reported by Lapucha (1990). The largest accumulation of errors occurs during periods of unaided INS operation, that is, upon loss of satellite lock or lack of ZUPTs. During these periods of bridging, the INS is used as a stand-alone positioning system. After re-acquisition of the satellites, its results are used to recover the phase ambiguities.
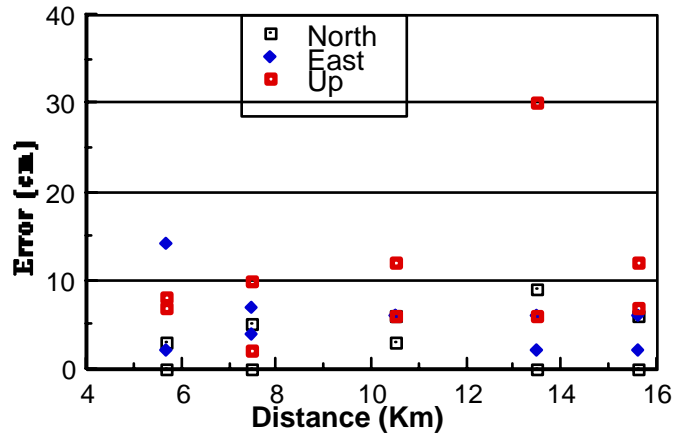
Figure 5.1: GPS/INS Positional Errors.

The basic idea behind INS bridging is the use of the INS-predicted coordinates to reset the position of the GPS receiver after signal re-acquisition. The bottom line, in INS bridging, is that any errors incurred during unaided INS operation should be below a threshold value in order to prevent a bias in the GPS computation following re-acquisition of lock. The threshold value is half a cycle, i.e. 10 cm for single frequency receivers and 40 cm, when wide-laning techniques are used, for dual frequency receivers. The reason for this INS-induced bias is that the inertially-derived position is used in re-computing the phase ambiguities. Errors in the ambiguity determination, due to errors in the INS coordinates, will therefore show up as a constant bias. Should there be a large number of satellites available, the GPS filter will attempt to re-establish precise ambiguity terms in kinematic mode. Although this is not uniformly reliable, since it is geometry dependent, it works well if there is a longer period of uninterrupted GPS observations with at least four satellites.

In stand-alone mode, INS results are mainly affected by the initial position error, the initial velocity error, the initial misalignment, the gyro drifts, and the accelerometer biases. Driven by these error sources, the INS results will have a long-term error behavior dominated by the so-called Schuler oscillations, the period of which is about 84.4 minutes, for more details see Britting (1971). For short periods of time, say bridging of 20 to 30 seconds, the INS position error can be approximated by the following equation (see Figure 5.2):

$$\delta P_{t_2} = \delta P_{t_1} + \delta V_{t_1} \bullet (t_2 - t_1) + \frac{1}{2} \delta a_{t_1} \bullet (t_2 - t_1)^2 + \delta \varepsilon \qquad (5.6)$$

where

δP_{t1} is the position error at time t1,

δP_{t2} is the position error at time t2,

δV_{t1} is the velocity error at time t1,

δa_{t1} is the accelerometers bias at time t1, and

$\delta \varepsilon$ is the effect of platform misalignment errors, which is about 5 mGal/arcsec (Hein, 1995).

Given that typical GPS/INS position errors are within 5 cm (fixed ambiguities) and GPS/INS velocity errors are within 2 cm/sec (GPS double difference), the unmodeled accelerometer bias can reach 10-20 mGal, and the unmodeled misalignment errors can reach 10 arcsec (see Section 6.4), the position error for a bridging period of 20 sec can reach 57 cm, see Equation (5.7).

$$\delta P_{t_2} = 0.05m + (0.02\frac{m}{sec})(20\sec) + \frac{1}{2}(10\times10^{-5}\frac{m}{sec^2})(20\sec)^2 +$$

$$\frac{1}{2}(10\times5\times10^{-5}\frac{m}{sec^2})(20\sec)^2$$

$$\delta P_{t_2} = 0.05m + 0.4m + 0.02m + 0.1m = 0.57m \qquad\qquad (5.7)$$

The contribution of each component in Equation (5.7) clearly shows that the dominant error is the initial velocity error. This error can be minimized by performing a ZUPT which could reduces this error by an order of magnitude. This is possible, when the obstacle causing loss of lock can be identified in advance, such as in case of an overpass.

Bridge

Time (t2)

GPS Signal Blockage

Time (t1)

Positional Error = δP_{t_2}

Positional Error = δP_{t_1}
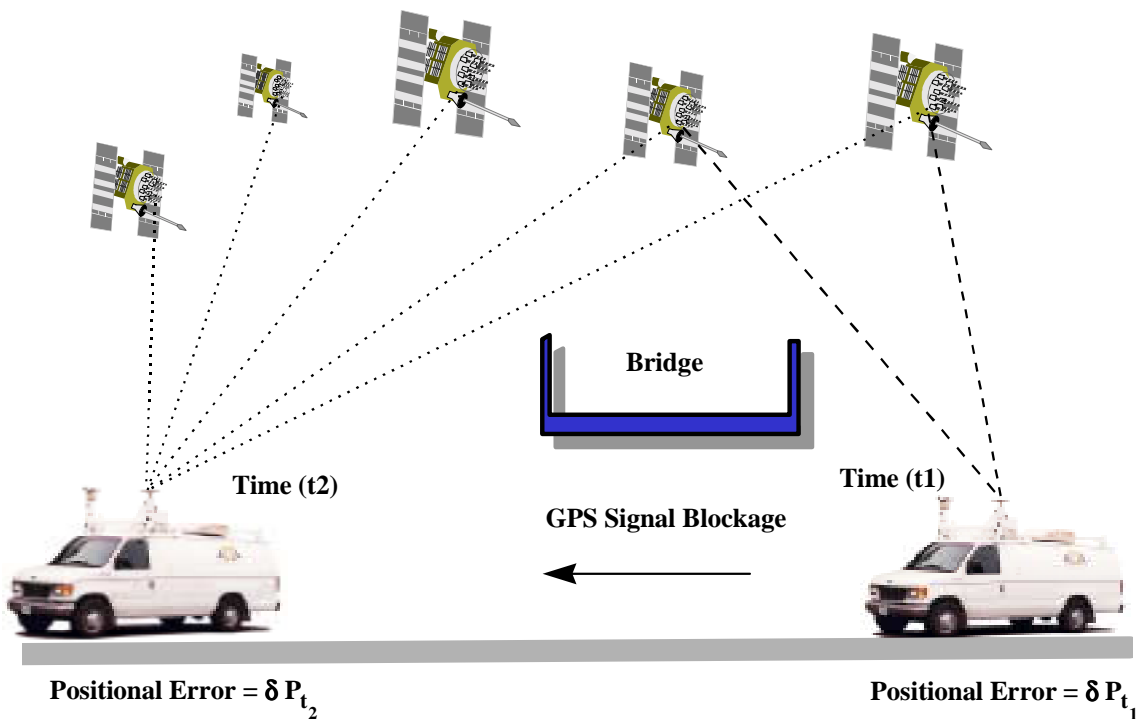
Figure 5.2 : Diagram of INS Bridging Error Sources.

Reliable bridging of GPS outages by INS will, therefore, depend on a reliable short-term error model and long-term INS error estimation during periods when high precision position and velocity information from GPS is available.

GPS errors will be reflected in the behavior of the INS due to the updating process. These errors are, however, not as serious a problem as those described above since they are not time-dependent as with unaided inertial positioning, and bounded in size provided phase lock is maintained. These errors include multipath, which is at the cm-level and usually ignored in kinematic mode, constant bias owing to poor initial ambiguity determination, phase measurement noise due to high dynamics and distortion of the carrier phase due to ionospheric activity.

The constant bias portion of the error is mainly a function of the static initialization time, baseline length, and ionospheric effects, especially if these are unusually severe. Given 20 minutes of alignment during which GPS data are collected, this bias error should be at the level of $\pm$ 5 cm for typical missions if short initial baselines of less than 7 km are used. However, they can be larger given extreme solar activity or longer initial baselines.

Further errors will accumulate during the mission owing to the distortion of the phase measurements by the ionosphere and to the increased phase measurement noise in case of high dynamics. Higher dynamics will cause the GPS tracking bandwidth to increase in order to accommodate vehicle induced Doppler shifts in the signal, followed by an

inevitable reduction in the precision of the phase measurements. For more details about contribution of these errors to error budget, see Zhang (1995).

The effect of GPS/INS position errors on the derived 3-D coordinates of points will depend on the sequence of images used in the computation. If fixed-base stereo pairs are used, see Figure 5.3.a, both cameras obtain the same GPS/INS position plus a constant shift (as determined in the calibration). Therefore, the errors in the GPS/INS position will introduce a constant shift for all points within this stereo-pair and have the same direction as that of the GPS/INS position. On the other hand, if consecutive images are used, and the baseline between them is obtained from INS/GPS positioning, see Figure 5.3.b, the target position error will depend on the magnitude and direction of the baseline error, and the baseline length.
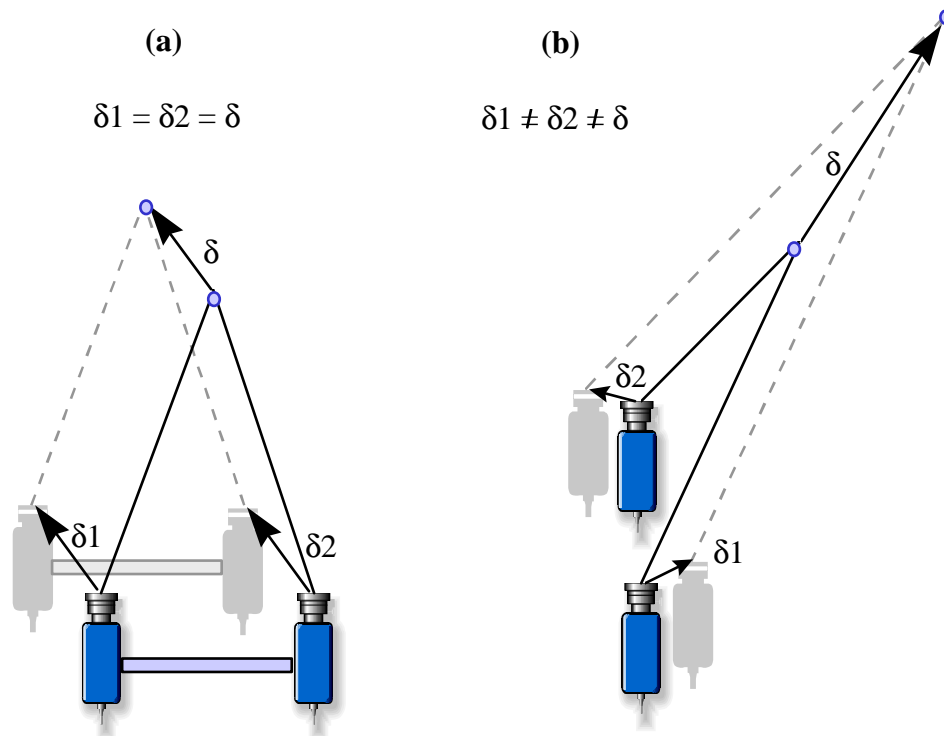
Figure 5.3 : Effect of Baseline Errors on the Final 3-D Coordinates

5.2.2 Calibration Errors

Lever arm corrections, i.e., corrections for the offset between the INS center and both the GPS antenna center and the cameras perspective centers, will affect the accuracy of cycle slip detection and correction, the coordinates of the cameras perspective centers, and the base between the cameras. They consist of a constant bias and a time-dependent term. The constant bias is the result of errors in the original survey performed during the system calibration. When the GPS/INS/camera system is vehicle-mounted, a survey must be performed, once only, in order to compute the local body frame offset components between the GPS antenna, camera perspective centers, and the INS b-frame center, see Section 4.3. The translations are derived by a total station survey as well as a bundle adjustment, while the azimuth rotation is computed by determining the difference between an astronomic azimuth of some chosen lines in the test field and the INS azimuth determined during the alignment procedures.

Given that a typical static alignment can be performed to an accuracy of about 2-4 arc minutes in azimuth (Liu, 1994), the remaining error is of the order of ± 0.25 cm for a lever arm of 2 m. Note that an error of 2 arc minutes in the baseline azimuth will introduce across-track error of 2 cm for all objects 35 m away from the van. On the other hand, a constant bias of 0.2 cm in the fixed base between the cameras, especially the front ones, can introduce an error of 4 cm, mainly along track, for an object 35 m away from the cameras; see Figure 5.4 for the effect of a baseline error of 0.2 cm on the along-track error. The error is computed using the following formula :

$$Y = \frac{f}{P}B$$

$$\delta Y = \frac{f}{P}\delta B = \frac{Y}{B}\delta B \qquad (5.8)$$

where

B is the baseline length,

Y is the distance between the object and the cameras,

P is the photogrammetric parallax.
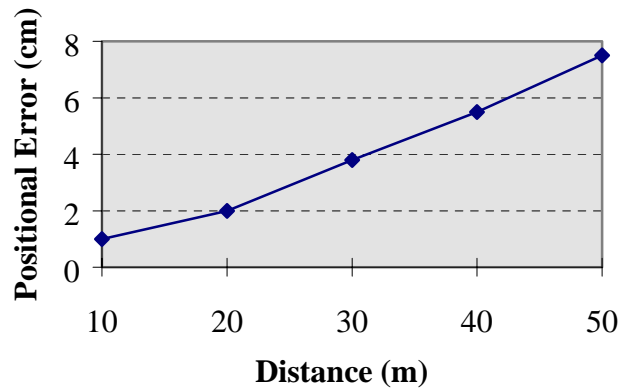
Figure 5.4 : Effect of an Error of 0.2 cm in the Baseline Length on the 3-D Position

A time-dependent term which must be considered in lever arm computation is the drift in roll, pitch, and azimuth incurred during the survey. Following the alignment, these drift terms will increase and may reach several arc minutes per hour, depending on the accuracy of the INS. Since roll, pitch, and azimuth are used at each GPS update epoch (nominally 1 Hz) and each image capture epoch to rotate the original translations vectors described above, time changes in the attitudes have to be considered. The total rotational error can reach 5-10 arc minutes over a long mission. The effect of this error depends on

the distance between the cameras and the object. For objects 35 m away from the cameras, the rotational error will introduce an position error of about 5 cm.

Errors in the inner orientation parameters are another major error source which can contribute to the error budget in the 3-D position. The most critical parameter is the principal point coordinate, more specifically x_p. A half-pixel error in x_p can introduce along-track errors of 28 cm for points 35 m away from the cameras. This highlights the importance of using sub-pixel accuracy in the calibration measurements. A part of this problem is the stability of the CCD chip in different operational environments. The main error source is temperature variation. More details about the effect of temperature on the image coordinates will be given in Chapter 6.

5.2.3 Synchronization Errors

Time synchronization errors between the GPS, the INS, and the video data streams are another possible error source. The synchronization effect appears in both the interpolated vector $\mathbf{r}_{INS}^m(t)$ and the rotation matrix $\mathbf{R}_c^m(t)$. In order to reach the accuracy required for the VISAT system, the synchronization should be accurate to a few milliseconds (one millisecond is equivalent to 1.6 cm position error at a velocity of 60 km/h). The system synchronization is performed using the PPS from the GPS receiver. The PPS interrupts the computer every second through either LPT ports or the COM ports of the host PC .

The interrupt handler gets a computer time tick, T_{pps}^{c}, which corresponds to the PPS signal. From the GPS position record, the time tag in the GPS time, T_{pps}^{GPS}, is already available. The offset between the GPS time frame and the computer time frame is, therefore, $(T_{pps}^{GPS} - T_{pps}^{c})$. Adding this time offset to the camera time tag in the computer frame will result in the camera time tag in the GPS time frame as given by the following equation :

$$T_{camera}^{GPS} = T_{camera}^{c} + (T_{pps}^{GPS} - T_{pps}^{c}) \,. \tag{5.9}$$

If there are no delays from the PPS interrupt service routine or any hardware-related delays, then this time tagging accuracy should be within the PPS timing accuracy. Unfortunately, delays are unavoidable. Synchronization errors can result from the following :

1. Internal hardware delay: This error accounts for the fact that measurements have to be converted, through the ADC process, to a digital format and then transmitted to the communication ports. For example, in the GPS receiver, measurements will be processed to obtain the navigation solution before the GPS raw measurements are sent out to the GPS receiver communication port. The time taken by the receivers is different from one receiver to another and is usually not known to the user.

2. Data Transmission delay: This is the unknown time delay between the sensors and the computer, i.e. the time taken by data to reach the communication boards. For example, the INS communication board (Arinc-429) will wait till it receives a complete record

before it issues an interrupt to the computer. The delay will depend on the data transmission rate from the INS. If this time is constant, this error can be treated as a deterministic constant.

3. <u>Time Tagging Delay:</u> In the data logging software of the PCs that handle multi-data streams, the use of interrupt service routines (ISR) is essential for avoiding data losses. The number of ISR in a logging software depends on the number of sensors; it should not exceed the interrupt vector available in the PC. Since the CPU responds to interrupts in a priority order, called the Interrupt Request Service (IRQ), it is very likely that one interrupt is blocked by another of higher priority for some unknown time before it is serviced. Other system resources are also likely to block the sensors ISR, such as hard disk accessing and writing. In general this error is unpredictable and very hard to determine.

4. <u>Computer Clock Reading Error:</u> This type of error is due to the fact that the PC timer chips (8253 for XT and 8254 for AT) keep the time of the day with a counter that has 18.2 Hz ticks, equivalent to 55 msec. With such a coarse resolution, synchronization errors in position could reach 1.55 m (1 msec = 3 cm for 60 km/h speed). In order to reach higher clock resolution, channel 0 of the timer has a two byte register for counting the fractional part of 55 msec. For example, by using the first 10 bits in this counter the resolution will be increased by a factor of 1024, that is to 53.78 μsec. The final computer time will be the coarse time ticks plus the high resolution fraction of the ticks. An error from clock reading could happen when the minor time counter is full and the time-of-the-day counter is read before its counter has been incremented.

The main effect of delays (1) and (2) is that the solution cannot follow the trajectory of the system. Time tagging errors of types (3) and (4) can be corrected by matching the period between the measurements with a redefined acquisition interval. Obviously, effects of the time tagging error are proportional to the speed of the vehicle, and thus requirements for time tagging accuracy will change for different applications and hardware configurations. In land vehicle applications, synchronization errors will introduce an along-track error. For a vehicle traveling at 60 km/h, a time-tagging error of 1 msec will cause an error in position of 1.6 cm. For an airplane traveling at 150 m/sec, the same synchronization error will cause an error in position of 15 cm.

Synchronization errors could be dramatically reduced by using either low-level coding software techniques or centralized hardware integration techniques. In the former, the real-time clock (RTC) of the host PC is a typical example. The AT and higher-end models each have a battery-operated RTC on the main circuit board. The clock contains 64 bytes of battery backup RAM. This RAM accepts clock data and system configuration. The 64 bytes RAM is divided into four registers which can be accessed like any other memory location. The first register, register A, is of particular interest for RTC programming. Figure 5.5 gives a description of the status register A.

The interrupt frequency 4-bit field of this register has a default value of 0110 (binary). This value results in an interrupt frequency of 1024 interrupts per second (i.e., an interrupt every 0.967562 msec). The interrupt frequency field can also be programmed by changing the value of the 4-bit field. The programmed frequency can reach 8192

interrupts per second, that is an interrupt every 0.122978 msec. Therefore, a synchronization error of one tick (0.122978 msec) will cause an error in position of 0.2 cm for a vehicle traveling at 60 km/h. For more details about the RTC registers, see Tischer (1994).
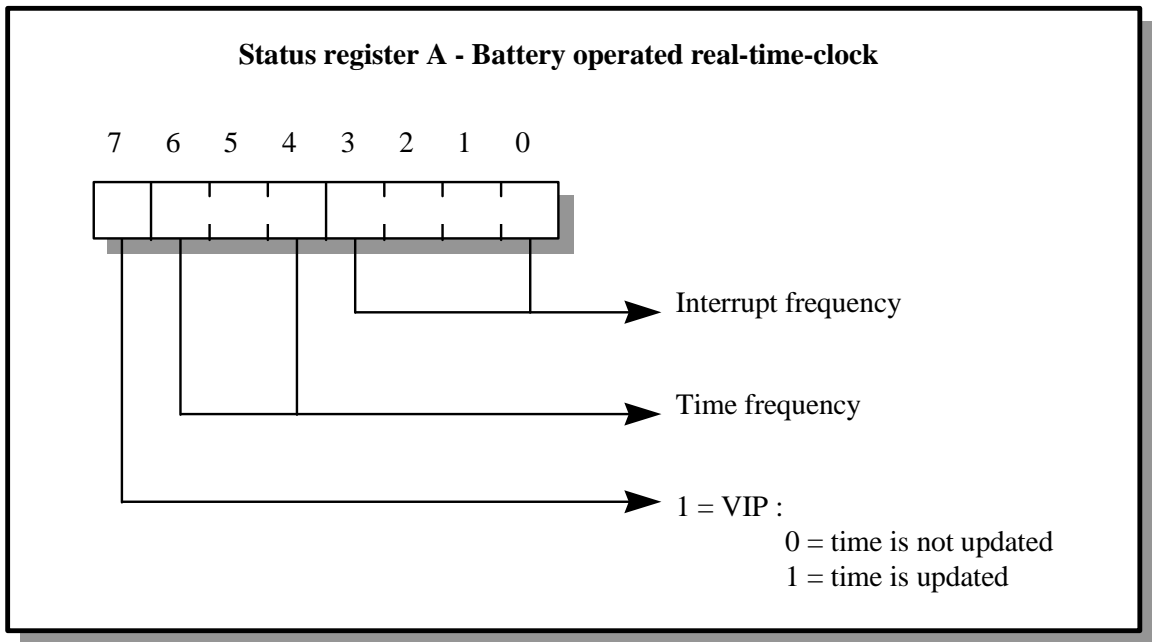
Figure 5.5 : RTC Status Register A

The second method for improving the system synchronization is to integrate the hardware in a single centralized interfacing board. Such a board is being developed for integrating GPS, INS, ABS, GPS PPS, and the camera capture pulse, see Figure 5.6 for schematic explanation of the concept. The board has a time capture module which uses a 10 MHz master VCXO (Voltage Controlled Crystal Oscillator) to provide time as a 28 bits fraction (100 nanosecond resolution). The GPS PPS signal is used to synchronize the board timing with the GPS epoch at the rising or falling edge (programmable) of the PPS

signal. The timing accuracy of this board is essential for high-dynamic airborne applications such as helicopter mapping applications.
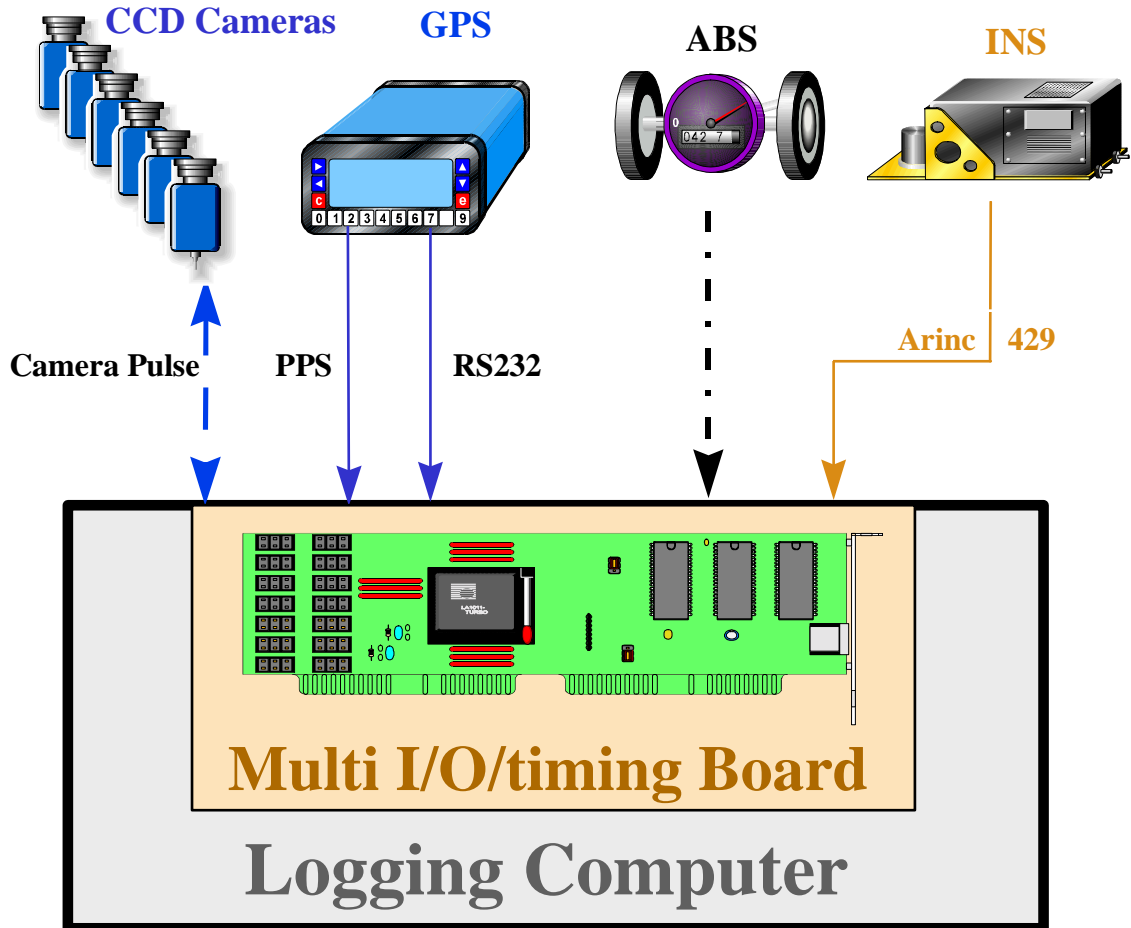
Figure 5.6 : Decentralized Hardware Configuration

5.2.4 Error Budget

Table 5.1 summarizes how each term in Equation 5.10 contributes to the final accuracy of the 3-D coordinates. The table indicates that all but one error source contribute less than 10 cm, and most of them only a few centimeters. The one major exception is the scale

factor error δs^i in along-track direction, which is due to the poor geometry in that direction and obviously depends on the distance between the camera and the target. It should be noted that there is no general distance-dependent error of this magnitude, but that it only occurs when the target is in this direction. Fortunately, under normal operation, a target in this direction can be seen on a large number of images and the unfavorable geometry can thus be excluded by operational procedures.

5.3 Practical Considerations

5.3.1 Quality Control of the System Positioning Module

The quality control of the system positioning module consists of a real-time alert system for those situations where the overall performance specifications of the system are not likely to be met, and a post-mission suite of programs for cycle slip correction, INS bridging, and backward smoothing in case of GPS outages. The major task of this segment is real-time quality assurance, i.e. the certainty that a specified percentage of the stored INS and GPS data are of sufficient quality to allow continuous computation of the vehicle trajectory within the specified accuracy limits. For example, the requirement to achieve a standard deviation of 30cm in position for 98% of the post-mission trajectory computation would be such a specification.

Table 5.1 : Error Sources of The VISAT System and Their Magnitude

Error in	Expected Magnitude	Contribution to $\delta \mathbf{r}_i^m$	Characteristics
• 1st term (INS/GPS position) δr_{INS}^m	5-10 cm	5-10 cm	Constant for all points in the same image.
• 2nd term (INS attitude) $\delta R_b^m(t)$	1-5 arcminutes	1-4 cm at 30 m	Function of the distance between the camera and the object.
• 3rd term (Calibration) 1. δR_s^b 2. δa^b	1 - 3 arcminutes 0.1 - 0.3 cm	1-2.5 cm at 30 m 2-6 cm at 30 m (fixed base)	1- Constant for the whole mission. The effect on 3-D coordinates depends on the distance between the camera and the objects. 2- Depends on the camera configuration used in 3-D computation. Critical for fixed-base cameras.
• 4th Term (Target pointing and Geometry) 1. δr^s 2. δs^i	0.5 pixel 0.5 pixel	0.5 cm at 7 m 2.5 cm at 30 m 2.5 cm at 7 m 16 cm at 30 m	1- Depends on the camera configuration used in 3-D computation. Introduces across-track error. 2- Depends on the camera configuration used in 3-D computation. Introduces along-track error. Critical for fixed-base cameras.
• 5th Term (Synchronization) 1. $V \delta T$ 2. $\omega \delta T$	1 - 2 msec 1 - 2 msec	1.8 - 3.6 cm for V= 60 km/h 1.8 - 3.6 arcmin for ω= 30 deg/sec (1.5 - 3 cm at 30 m)	1- Introduces along-track error. Can be reduced by using the PC RTC or special timing boards 2- Introduces across-track error. Error magnitude function of the distance between the camera and the objects. Maximum along curves.

Since this accuracy can always be achieved for good satellite coverage and signal reception, quality control is mainly concerned with countermeasures for cases of poor GPS satellite geometry, signal blockage, or cycle slips. INS aiding of GPS plays a major role in all of these countermeasures. Since they have to take effect before GPS positioning accuracy deteriorates beyond half a cycle, a real-time system for the detection of such situations is needed to alert the operator. In addition, expert knowledge on INS bridging and backward smoothing are important parameters for real-time decision. The application of these techniques is, however, done in post-mission. The real-time alert will, therefore, be discussed first, before bridging and backward smoothing procedures are presented.

Poor satellite geometry is not a problem if it only increases GPS white noise. Integration with INS and proper weighting will usually alleviate the problem. If, as is often the case, poor satellite geometry generates correlated position errors, regular INS ZUPTs are needed in addition to GPS to maintain the required accuracy level. Since real-time monitoring of deteriorating satellite geometry can be done via the dilution of precision (DOP) numbers, an alert for such situations can be given.

Signal blockage by houses and trees or a complete loss of lock are indicated by the receiver hardware. Thus, real-time detection of these events is not a problem and an alert can always be given. Fixing ambiguities afterwards is an involved process which depends very much on the specific situation. Countermeasures are INS bridging and smoothing,

ambiguity resolution on the fly (OTF), or a combination of all of these. Details will be discussed in the context of post-mission procedures.

Cycle slip detection can be done in near real-time by predicting the GPS triple phase difference $\delta\nabla\Delta\varphi_{predicted}$ from INS coordinates. By computing the cycle slip difference $\mathbf{v}$ between the predicted and the measured value of the triple difference, it is possible to detect cycle slips by the formula:

$$\mathbf{v} = \delta\nabla\Delta\varphi_{predicted} - \delta\nabla\Delta\varphi_{measured}, \text{ with}$$

$$\delta\nabla\Delta\varphi_{predicted} = (\nabla\Delta\rho(t) - \nabla\Delta\rho\,(t-1)),$$

$$\delta\nabla\Delta\varphi_{predicted} = (\nabla\Delta\varphi(t) - \nabla\Delta\varphi\,(t-1)) \tag{5.1}$$

where,

t   is the current epoch,

(t-1)   is the previous epoch,

$\nabla\Delta\rho$ is the double difference range obtained from the INS predicted coordinates,

$\nabla\Delta\varphi$ is the phase double difference obtained from GPS phase measurements.

In terms of cycle slip detection and correction, there is no conceptual difference between using the centralized or the decentralized Kalman filter, as shown in Figure 5.7.
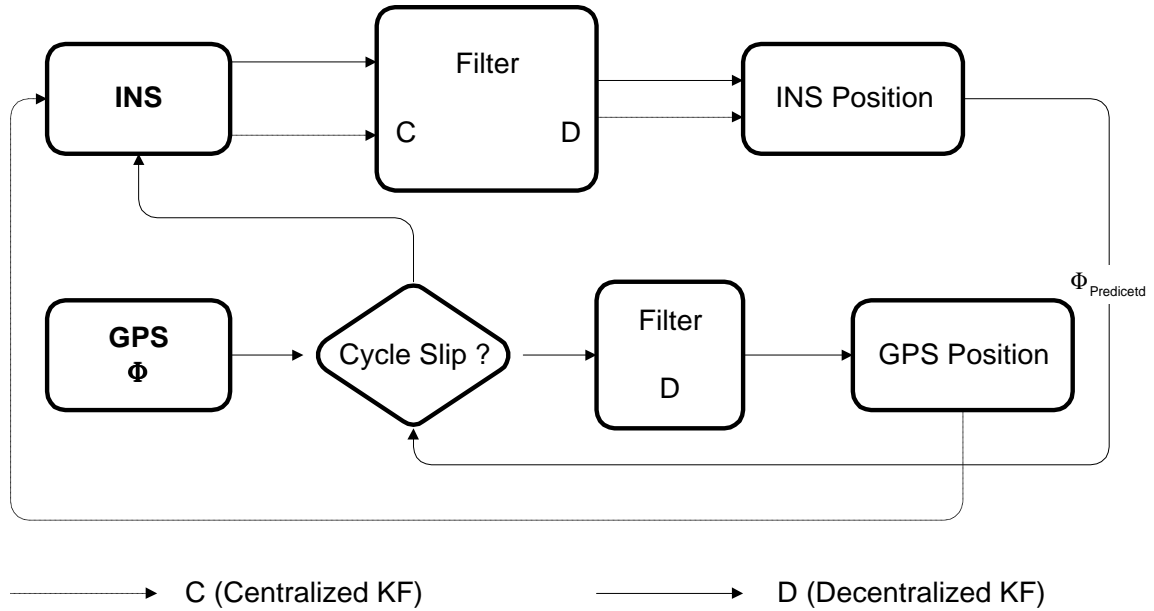
Figure5.7: Cycle Slip Detection and Correction in Centralized and Decentralized Kalman

Filtering

The cycle slip detection node accepts both the raw GPS phase measurements and the predicted phase measurements. The only difference is that for centralized filtering, the predicted phase data are derived from the central filter which accepts GPS raw measurements as update information, while for decentralized filtering, the predicted phase data are derived from the master filter which takes GPS filter output as the update information. Note that the data rates of the two systems are quite different and synchronization and interpolation are problems that have to be addressed in the integration process.

For precise positioning with GPS/INS the values $\mathbf{v}$, expressed in cycles, will be close to zero and continuous with respect to time. The noise in $\mathbf{v}$ is due to the estimation error of

the integrated INS and the measurement noise of the GPS receivers. Since ν is the change of the double difference from one epoch to the next, noise from common error sources is greatly reduced. A simple method of fixing cycle slips is the continuos monitoring of ν in time. By computing its effect on the triple differences via Equation 5.11, cycle slip recovery for the phase triple difference can be obtained in real time. If post-mission recovery is sufficient, the influence of noise can be reduced by modeling ν as a function of time through the use of all available information before and after the cycle slip. In this case, the double difference observation can directly be used without the additional time differentiation for the triple differences. This reduces the measurement noise considerably; for some further discussion, see Schwarz et. al. (1994).

In case of loss of lock and cycle slips, it is usually not necessary to fix the problem in real time. Therefore, INS bridging and backward smoothing, which make use of the additional information obtained from the INS, are typical post-mission procedures. The basic idea behind INS bridging is the use of INS-predicted coordinates to reset the position of the GPS antenna after loss of lock and signal re-acquisition. Such bridging will result in correct ambiguities if all errors incurred during unaided INS operation remain below half a cycle. If they are larger, constant biases will be generated following re-acquisition of lock. Since ambiguities are constants, errors in the ambiguity determination, due to errors in the INS coordinates, will also show up as constants.

Such biases can be eliminated subsequently by an OTF procedure in real time or a similar method in post-mission. The advantage of using INS bridging beforehand is the

determination of very good approximate values for the ambiguities. Thus, convergence of OTF procedures will be considerably faster. From an operational point of view, it is important to decide which period can be bridged by INS alone without subsequent OTF procedures and in which cases it will be safer to apply them. This will affect the real-time decision on vehicle stops for additional ZUPTs.

In general, INS bridging is used as a prediction method only, i.e., current filter estimates are used to predict position from INS observations. Due to errors in the Kalman filter states and the data, the length of the bridging interval is limited, depending on the quality of the INS. For navigation grade systems, typical intervals are 20 - 30 seconds. These intervals can be considerably extended if prediction is combined with smoothing after signal re-acquisition, this principle is shown in Figure 5.8.
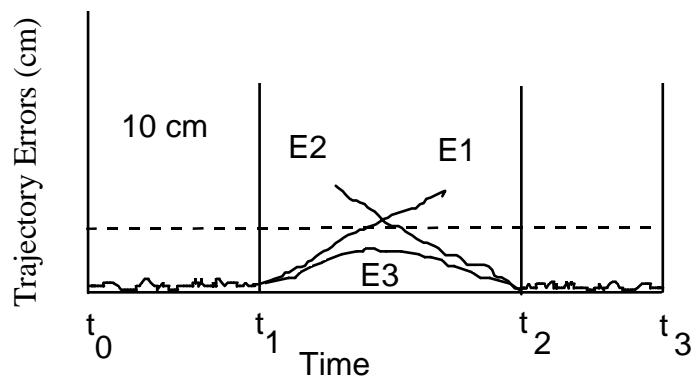
Figure 5.8 : INS Bridging with Forward-Backward Prediction and Smoothing

In the forward prediction process, GPS information up to the time epoch t1, at which the GPS signal is lost, is used to predict the trajectory during the period t1 to t2 in which no GPS data are available. This results in the error curve E1. Due to the double integration of errors at time t1, the error curve E1 increases rapidly. Using the information in time

sections t2 to t3 after GPS signal re-acquisition, a backward prediction can be used for the t1-t2 section, resulting in the error curve E2. In a statistical sense, E2 is the mirror image of the error behavior of E1. A smoothing procedure combines both the forward prediction and the backward prediction optimally and gives an improved estimation of the trajectory with the error curve E3. As can be seen, the bridging interval is greatly extended by using this procedure.

It should be noted that INS bridging by prediction can be used as a real-time method, while bridging by prediction and smoothing is clearly a post-mission method. In the VISAT system, these procedures are currently used in post-mission. Their real-time use does not promise major advantages and is currently not planned.

A further extension of the bridging interval can be achieved if dual frequency GPS receivers are employed. By using wide-laning techniques, the accuracy required from the INS stand-alone solution is 43 cm instead of 10 cm. Thus the bridging interval, for which the INS solution is valid, is considerably longer. For more details about INS bridging accuracy and results see Lapucha (1990) and Cannon (1991).

The quality control component gives real-time alerts to the operator in situations where the specified trajectory quality can most likely not be achieved. These alerts are determined by the computer which monitors data accuracy of GPS and INS, tracks signal blockage for each satellite, and introduces expert knowledge on INS bridging (smoothing), and the convergence time of OTF ambiguity resolution techniques into the

process. In those cases, where an alert is given, the vehicle is stopped to either allow an additional ZUPT, or, in more critical cases, an independent ambiguity resolution. Using these additional measurement periods, the required post-mission trajectory accuracy can be obtained in the specified number of cases and resurveys can be avoided.

5.3.2 Quality Control of the Image Measurement Module

5.3.2.1 Epipolar Geometry

Automatic data capture from the image cluster is one of the most important tasks in reducing the time required for image measurement. Epipolar geometry forms the foundation of any matching algorithm used in known camera configurations because it substantially reduces the search window, eventually confining it to an epipolar line.

Figure 5.9 shows a stereo-pair in epipolar geometry with Ci and Cj being the perspective centers of cameras (i) and (j). The epipolar plane is defined by the object point (P) and the two perspective centers C^i and C^j. The epipolar plane intersects the two images along epipolar lines Li and Lj. Ideally, the image points Pi and Pj must lie on the epipolar lines. To find a conjugate for a point on the epipolar line Li, it is necessary to search along the corresponding epipolar line Lj. The obvious advantages of using epipolar geometry is that the conventional 2-D correlation can be completely substituted by 1-D correlation along

epipolar lines, for more details about the correlation along epipolar lines see Zhang (1988) and Yan and Zuxun (1988).
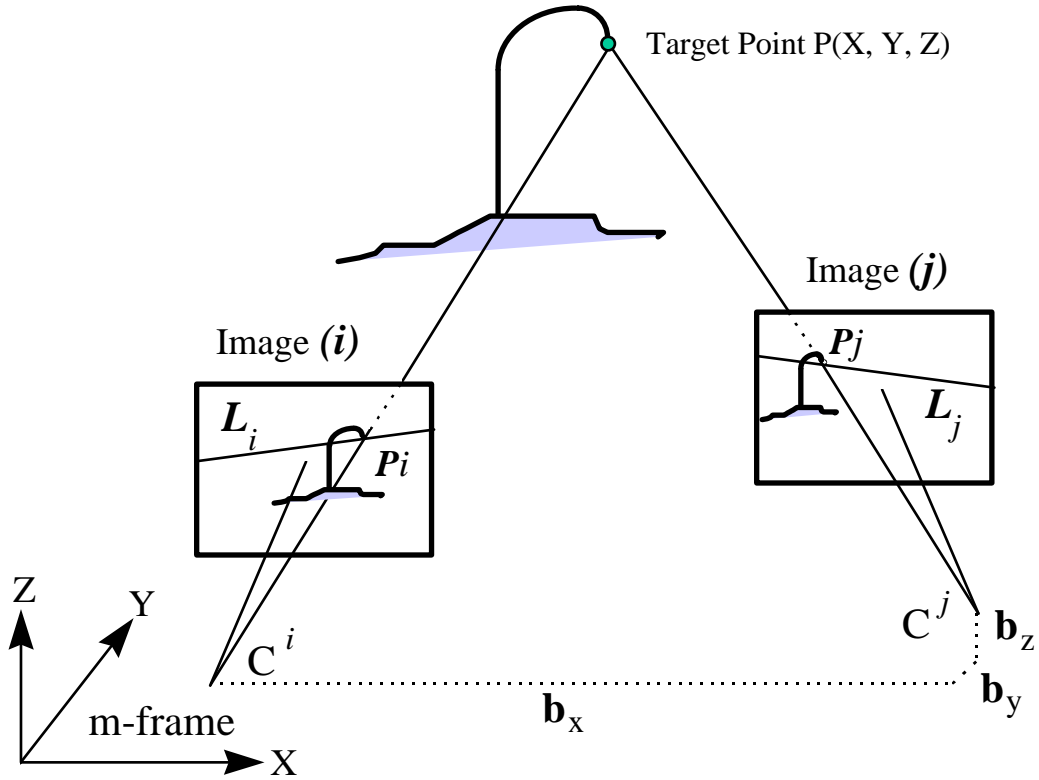
Figure 5.9 : Epipolar Geometry

The derivation of the epipolar line equation is based on the coplanarity condition. It makes use of the fact that each pair of bundle rays must be coplanar with the base. The coplanarity condition of image (i) is given as follows :

$$
\begin{vmatrix}
b_x^{ci} & b_y^{ci} & b_z^{ci} \\
\overline{x}_{pi}^{ci} & \overline{y}_{pi}^{ci} & -f^{ci} \\
\overline{x}^{ci} & \overline{y}^{ci} & -f^{ci}
\end{vmatrix} = 0 \tag{5.12}
$$

where,

R_m^{ci} is the rotation matrix between the m-frame and the c-frame of

camera (i),

f^{ci} is the focal length of camera (Ci),

$\bar{x}^{ci}, \bar{y}^{ci}$ are the image coordinates for any point on the epipolar line L_i,

$\bar{x}_{pi}^{ci}, \bar{y}_{pi}^{ci}$ are the measured image coordinates of point (P) on the epipolar

line L_i,

$$\begin{pmatrix} b_x^{ci} \\ b_y^{ci} \\ b_z^{ci} \end{pmatrix} = R_m^{ci} \bullet \begin{pmatrix} b_x^{m} \\ b_x^{m} \\ b_x^{m} \end{pmatrix}$$ is the base vector in the coordinate system of camera (i), and

$$\begin{pmatrix} b_x^{m} \\ b_x^{m} \\ b_x^{m} \end{pmatrix}$$ is the base vector between the stereo-pair (i) and (j) in m-frame.

The epipolar line L_i can be derived from Equation (5.12) as :

$$\bar{y}^{ci} = \frac{f^{ci}b_x^{ci} + \bar{x}_{pi}^{ci}b_z^{ci}}{f^{ci}b_x^{ci} + \bar{x}_{pi}^{ci}b_z^{ci}} \bar{x}^{ci} + \frac{\bar{y}_{pi}^{ci}b_x^{ci} - \bar{x}_{pi}^{ci}b_y^{ci}}{f^{ci}b_x^{ci} + \bar{x}_{pi}^{ci}b_z^{ci}} f^{ci} \qquad (5.13)$$

Similarly, the coplanarity condition for image (j) can be written as :

$$\begin{vmatrix} b_x^{cj} & b_y^{cj} & b_z^{cj} \\ x_{pi}^{cj} & y_{pi}^{ci} & z_{pi}^{ci} \\ \bar{x}^{cj} & \bar{y}^{cj} & -f^{cj} \end{vmatrix} = 0 \qquad (5.14)$$

where

$$\begin{pmatrix} x_{pi}^{cj} \\ y_{pi}^{cj} \\ z_{pi}^{cj} \end{pmatrix} = R_{ci}^{cj} \bullet \begin{pmatrix} \overline{x}_{pi}^{ci} \\ \overline{y}_{pi}^{ci} \\ -f^{ci} \end{pmatrix}$$

are the coordinates of photo point (pi) in the coordinate

system of camera (CJ)

The equation of the epipolar line L_j is thus given by :

$$\overline{y}^{cj} = \frac{y_{pi}^{cj}b_z^{cj} - z_{pi}^{cj}b_y^{cj}}{x_{pi}^{cj}b_z^{cj} - z_{pi}^{cj}b_x^{ci}}\,\overline{x}^{cj} + \frac{y_{pi}^{cj}b_x^{cj} - x_{pi}^{cj}b_y^{cj}}{x_{pi}^{cj}b_z^{cj} - z_{pi}^{cj}b_x^{ci}}\,f^{cj}$$
(5.14)

5.3.2.2 The Use of Constraints in VISAT Applications

The discussion so far has centered on the use of georeferenced images for 3-D object coordinate determination. Geometric information in the images can be used to enhance coordinate determination and to achieve a more reliable solution of higher quality. Such information may be the fixed relative position and orientation of cameras on a stable base or known geometric features of objects in the images.

1. Camera Relative Orientation Constraints : Making use of the fact that the cameras are mounted on a stable base, the length of the base and the fixed relative orientation of the cameras can be used as constraints. These constraints are very useful in calibrating the systems as was discussed for the relative orientation constraint in Chapter 4.

Epipolar geometric constraints are another example of using this general technique for 3-D computations. Epipolar geometry is also the foundation for any matching techniques performed with cameras in a known geometric configuration. It essentially reduces the search window to an epipolar line.

2. Object-Space Geometric Constraints : Any known geometric configuration of points in the object space can be used to put additional constraints on the solution. A common example are straight lines which may occur as vertical lines, as for instance a telephone pole, or as horizontal lines, as for instance lane markings or edges of buildings. For a vertical line, the constraint for two points on the line can be written as:

$$X_i - X_j = Y_i - Y_j = 0 \tag{5.15}$$

Parallel lines provide a powerful orientation constraint for images. By writing a constraint for each line and then adding a constraint forcing the two direction cosines to be the same, redundancy for the short-term attitude can be obtained and the INS attitude can be checked.

The use of horizontal line constraints in the image measurements of road centerlines could serve as a first step in the automatic extraction of road features from a sequence of close-range images. For more details about the automatic extraction of line features from a sequence of close-range images, see Xin (1995).

Triangulation between images is a very useful feature for complementing GPS/INS data. In theory, it can bridge between images where georeferencing data have poor quality due to long GPS signal blockage. In this aspect all the above constraints could help in extending the bridging length.

CHAPTER 6

RESULTS AND ANALYSIS

So far, the theory, concept, and problems of integrating and calibrating the VISAT system have been discussed. The objective of this chapter is to evaluate the calibration results and positioning accuracy of the system. First, the calibration of the imaging component is presented in three parts: the camera calibration, the relative orientation calibration, and the temperature effect. Then, results of quality control are presented in terms of the INS bridging interval, cycle slip detection and correction, and the potential of using the INS results in reducing the OTF time. Finally, the system's relative and absolute accuracy are presented and the error propagation with distance is discussed.

6.1 Camera Calibration

The camera calibration procedures include: capturing images of the test field from different positions and orientations, measuring the image coordinates of the target, and estimating the camera parameters by performing bundle adjustment computations.

In all interior orientation calibrations, six convergent images of the 3-D calibration jig are taken with the cameras mounted on tripods. Convergent imagery is utilized to reduce the

correlation between the perspective center coordinates and the interior orientation parameters. Other correlation, e.g. between the ω and Φ rotation angles and between the principal point coordinates (x_p, y_p) along with the decentering lens distortion parameters (*p1, p2*) are suppressed by incorporating images with orthogonal κ rotation angles into the bundle adjustment. The camera stations are arranged at two different vertical levels, the first with the tripod at its lowest level and the second with the tripod extended to its maximum height. Therefore, a vertical base of about 1-1.2 m is obtained. Horizontally, the camera stations are arranged as shown in Figure 6.1. At each camera station there are 15 parameters to solve for. The first six parameters are the camera exterior orientation parameters (X_O, Y_O, Z_O, ω, Φ, κ) which are station-dependent. The rest, are the nine parameters of interior orientation and the lens distortion parameters (*x_p, y_p, f, ky, k1, k2, k3, p1, p2*), which are station-independent unknowns. The adjustment solves for the set of additional parameters at each camera setup and constrains them to the same value. This adds some constraints to the adjustment.

On average there are at least 20 target points visible in each image. This results in high degrees of freedom and, therefore, a reliable error analysis. In order to avoid the problem of highly correlated parameters such as *k1, k2*, and *k3* or *p1, f*, and *x_p*, the first ten parameters, i.e. all parameters excluding the lens distortion parameters, are solved for in the first run. This improves the approximate values so that in the second run all 15 parameters can be solved for with a minimum number of iterations.
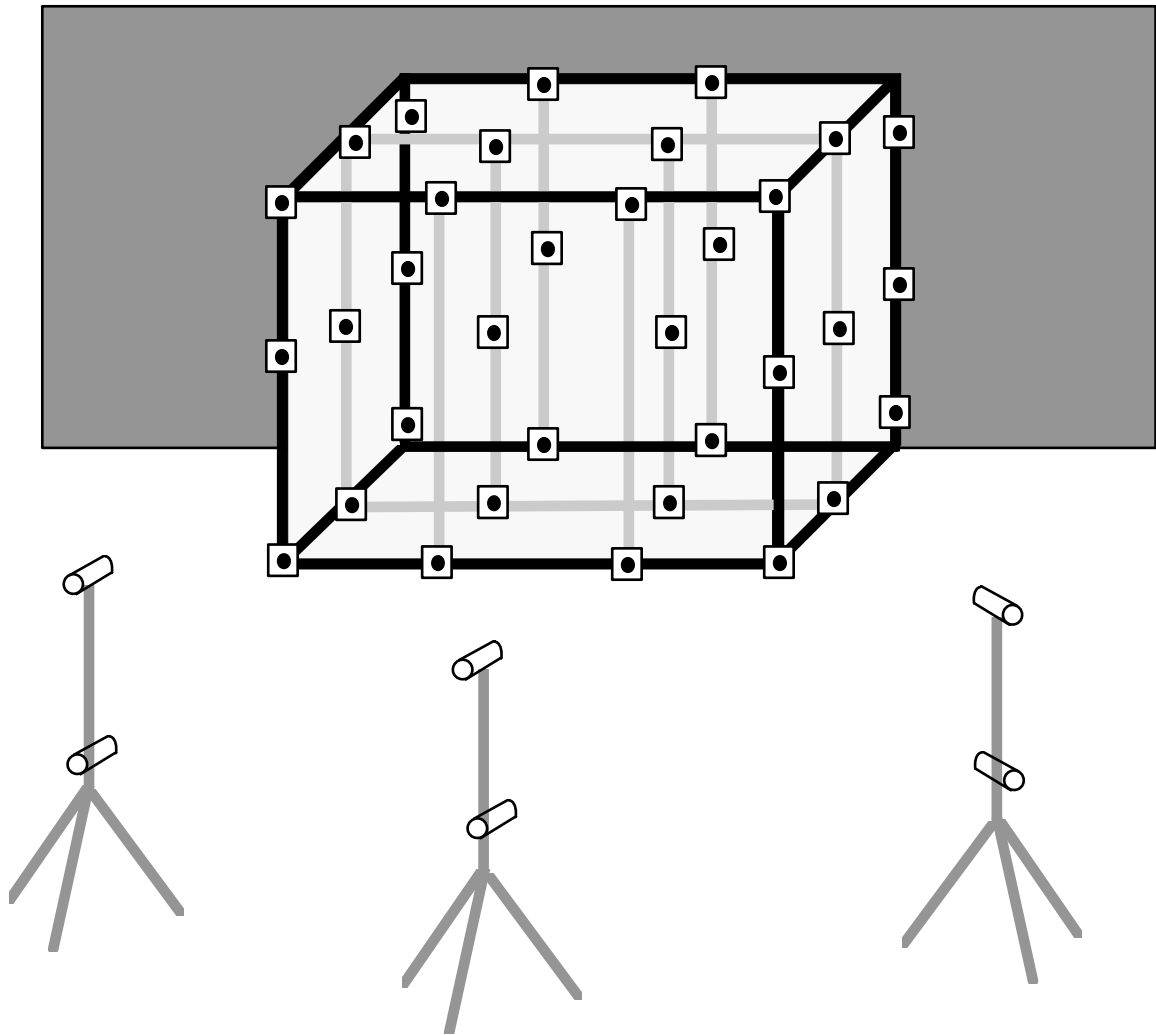
Figure 6.1: Schematic Diagram of Camera Setup

Table 6.1 summarizes the results for one of the cameras, the results for the others are similar. The table confirms that the results are better in the direction of the y-axis than for the x-axis. This is most likely due to line jitter as discussed in Chapter 4. The addition of the lens distortion parameters improves the results by five times. This indicates that the lens distortion model is viable. The results also indicate that additional improvement is achieved by letting the control points float freely in the adjustment. This strongly indicates that the calibration jig is stable and the target coordinates are of acceptable

accuracy. A five times improvement was reported by Cosandier and Chapman (1992) for

a 24 mm lens (the VISAT cameras have 8 mm lenses).

Table 6.1 : Bundle Adjustment Results - 8 mm Lens Camera

	Without lens distortion model Control held fixed	With lens distortion model Control held fixed	With lens distortion model Control let to float
x (pixels) RMS	0.535	0.116	0.098
y (pixels) RMS	0.423	0.085	0.074
No. of camera stations	6	6	6
No. of observations	207	232	232
No. of unknowns	60	90	171
Degrees of freedom	147	142	61

In order to confirm that the camera parameters were correctly estimated. Another set of

images of the calibration jig was taken from different locations. Another adjustment was

executed in which the jig targets were used as check points in the adjustment. Table 6.2

lists the results of the adjustment, where δX, δY, and δZ are the differences between the

estimated coordinates, from the adjustment, and the known coordinates of the 10 control

points. The results agree well with those of the first adjustment. It should be mentioned

that an error of 1 mm is equivalent to 0.25 pixel at the image scale.

Table 6.2 : The Camera Calibration Residuals at Check Points

Point Number	δ X (mm)	δ Y (mm)	δ Z (mm)
3	1.23	1.41	0.54
5	-2.14	1.21	0.78
6	-1.78	-2.16	-0.87
11	0.67	0.98	1.23
14	-0.98	0.76	0.65
16	-2.56	-0.54	2.01
19	-1.23	-0.49	-0.66
20	1.45	0.97	-0.92
23	1.43	0.36	1.12
24	-0.57	-1.01	0.43
Mean (mm)	1.523	1.110	1.017
RMS (pixels)	0.392	0.277	0.254

6.2 Relative Orientation Calibration

A test field of ninety evenly distributed circular targets was established for calibrating the offsets and misalignments of the complete system, see Figure 6.2 for the test field. The coordinates of these targets were determined using a network of six points, determined by GPS, as base stations for a total station survey. A baseline of 1.3 km was used to estimate the azimuth of the network using a GPS static survey.
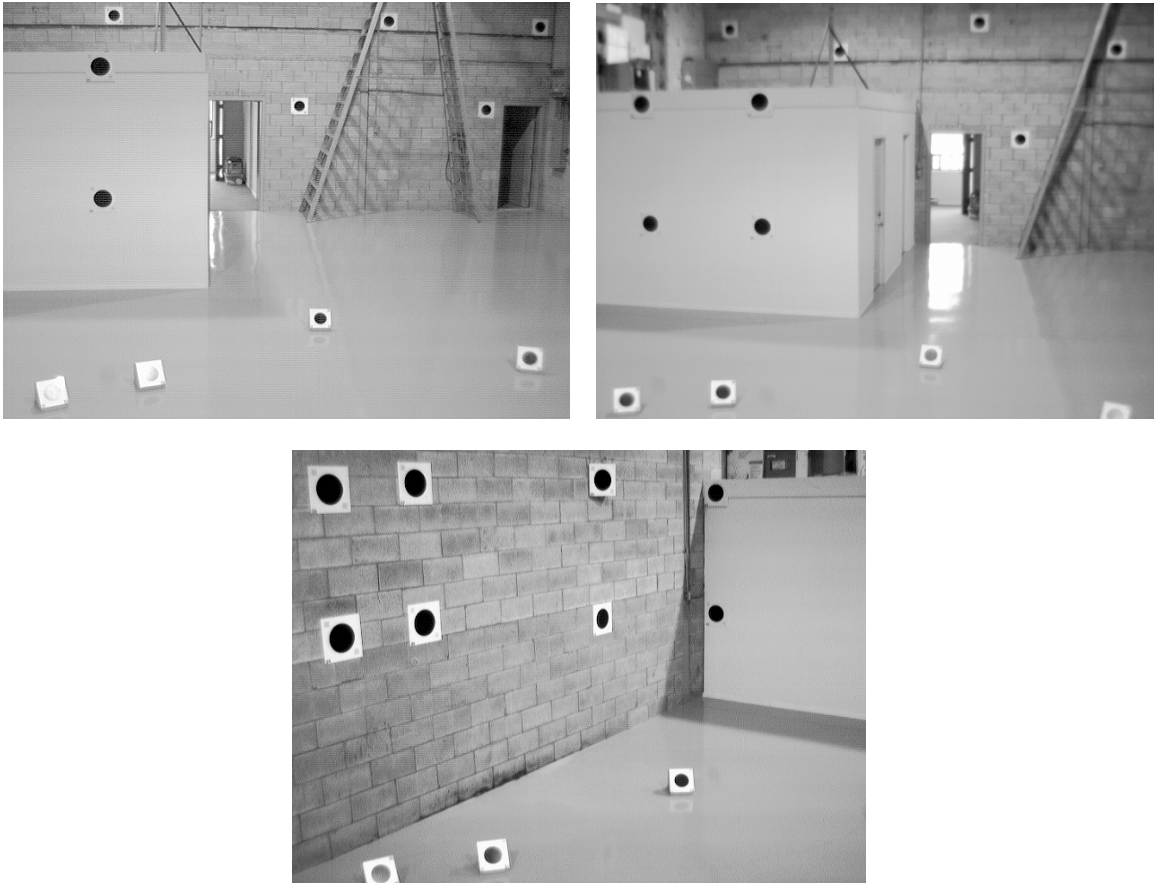
Figure 6.2 : Images of the Relative Orientation Test Field

System calibration was performed three times at one-month intervals. In each calibration test, eight images were grabbed from at least five different van positions. For each calibration test, the adjustment was calculated twice, with and without the relative orientation constraints. Table 6.3 lists the second calibration results for cameras (1) and (2) without the relative orientation constraints, where ($\Delta\omega$, $\Delta\Phi$, $\Delta\kappa$) are the relative orientation angles between the cameras and the INS b-frame. Similar results were obtained for calibrations (1) and (3). The results indicate that the relative orientation parameters are different and have an accuracy of $\pm$ 4 mm for the base vector and $\pm$ 3 arc minutes for the relative orientation angles. The reason for having large corrections for the

relative orientation angles is due to the fact that the accuracy of aligning the INS is about 2-4 arc minutes. This adds more distortion to the bundle adjustment, which is then reflected in the large corrections to the relative orientation parameters. Table 6.4 summarizes the final results of the three different calibrations for camera (1) and camera (2) after applying the relative orientation constraints. It is obvious that even with a one-month difference between the three calibrations, the changes in the base vector and the relative orientation angles are about $\pm$ 2 mm and $\pm$ 2 arc minutes, respectively. The probable error due to system calibration at a distance of 35 m is about 3 cm (35 m x tan 2 arc minutes = 3 cm) for the relative orientation angles. On the other hand, a constant bias of 2 mm in the base between the cameras, especially the forward looking ones, can introduce an error of 7 cm, mainly along-track, for an object 35 m away from the cameras. For more details about the contribution of calibration errors to the error budget see El-Sheimy (1996).

Table 6.3. The Relative Orientation Parameters of Calibration (2) Without Applying
Relative Orientation Constraints (Results of Camera (1) and Camera (2))

Calibration No. 2	B (cm)	$\Delta\omega$ (deg.)		$\Delta\Phi$ (deg.)		$\Delta\kappa$ (deg.)	
		cam (1)	cam (2)	cam (1)	cam (2)	cam (1)	cam (2)
Van set-up 1	182.71	80.4003	81.3991	0.1379	0.7130	-7.8114	9.2847
Van set-up 2	183.21	80.3921	81.4491	0.1535	0.7021	-7.8303	9.2422
Van set-up 3	182.44	80.4064	81.3714	0.1464	0.6200	-7.8164	8.9672
Van set-up 4	183.98	80.4453	81.3655	0.1849	0.7349	-7.6452	9.2266
Van set-up 5	182.91	80.4495	81.4095	0.1478	0.6639	-7.7682	9.1123

Table 6.4 : The Relative Orientation Parameters of Three Different Calibrations After
Applying Relative Orientation Constraints (Results of Camera (1) and Camera (2))

Calibration	B	$\Delta\omega$ (deg.)		$\Delta\Phi$ (deg.)		$\Delta\kappa$ (deg.)	
	(cm)	cam (1)	cam (2)	cam (1)	cam (2)	cam (1)	cam (2)
No. 1	183.47	80.4691	81.4191	0.1691	0.6313	-7.8631	9.1923
No. 2	183.12	80.4325	81.3991	0.1603	0.6778	-7.8484	9.2010
No. 3	183.33	80.4495	81.3723	0.1642	0.6538	-7.8521	9.1892

6.3 Temperature Effects

To analyze the effect of a change in temperature of the camera and the frame grabber on the image coordinates, a number of tests were performed. The first test was conducted by allowing the cameras and the frame grabber to warm up for a period of two hours. The cameras and the computer were switched on at the same time. During the two-hour period, a series of images were grabbed every 10 minutes for a test field of circular targets. During the test, the van and, therefore, the cameras were firmly held in the same position. The targets in each image were measured by the centriod sub-pixel algorithm discussed in Chapter 4. Figures 6.3 and 6.4 show the change in coordinates for one of the targets, with the coordinates of the first image taken as the reference. Similar results were obtained for all other target points. It should be mentioned that the results in Figure 6.3 are for a target appearing in images of camera (2) which is connected to the imaging board (1), while the results in Figure 6.4 are for camera (5) which is connected to board (2). Both figures confirm that the coordinate shift, which is predominantly in the x-direction, becomes stable after approximately 80 minutes and is more or less identical for

133

both boards. The total RMS warm-up shift is as large as 0.4 pixel. Since the error is identical for both boards, it will not affect the 3-D coordinates because it will cancel out, on the other hand, in calibration mode, it will not cancel. Therefore, it is recommended to warm up the system for 80 minutes before performing the calibration test.
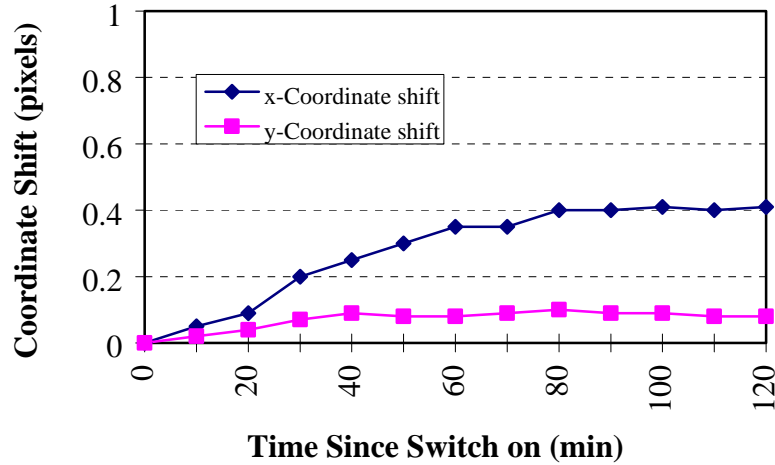
Figure 6.3 : Coordinate Shift Over the Period of Warm-Up for Both the Camera and

Frame Grabber (1)
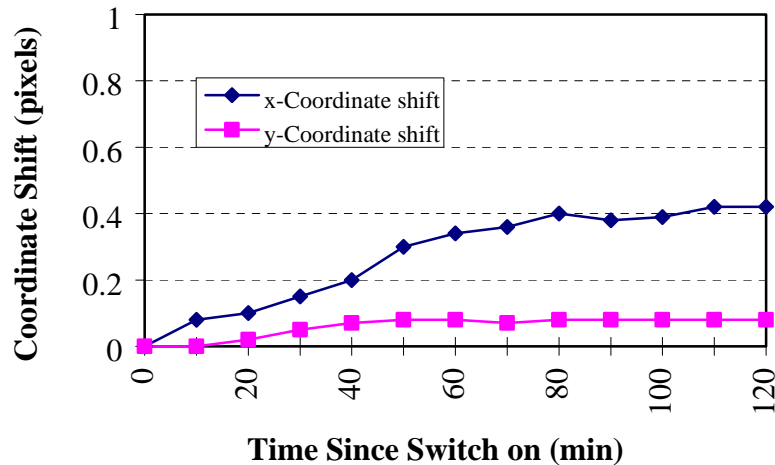
Figure 6.4 : Coordinate Shift Over the Period of Warm-Up for Both the Camera and

Frame Grabber (2)

The experiment performed does not allow a conclusion to be reached on the source of the warm-up effect, i.e. whether it is due to the frame grabber or the cameras. Hence, two further tests were conducted in exactly the same manner as the previous tests, except that either the frame grabber or the cameras were switched on one hour before the other component was switched on. Figure 6.5 shows the results for the temperature-related drift in the camera alone. The figure confirms that the camera drift is very small and similar in both x and y coordinate directions, i.e. it does not contribute in a major way to the observed coordinate shift. This is different for the frame grabber, which displays the same shift during the warm-up period as observed previously, see Figure 6.6. The conclusion therefore is that the scale changes in the x-direction during warm-up are largely frame grabber-related and similar for both frame grabbers. However, they can be practically eliminated by warming up the system for about 80 minutes before starting the survey. It should be mentioned that the typical time for initializing the INS and performing the GPS static initialization is about 30 minutes.
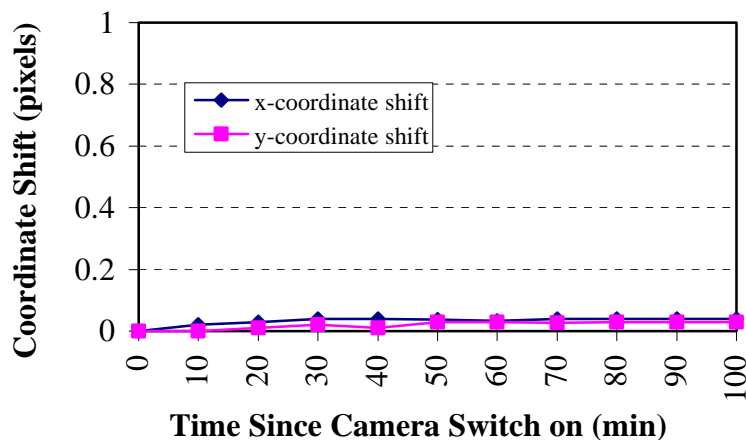
Figure 6.5 : Coordinate Shift for the Period of Camera Warm-Up Only
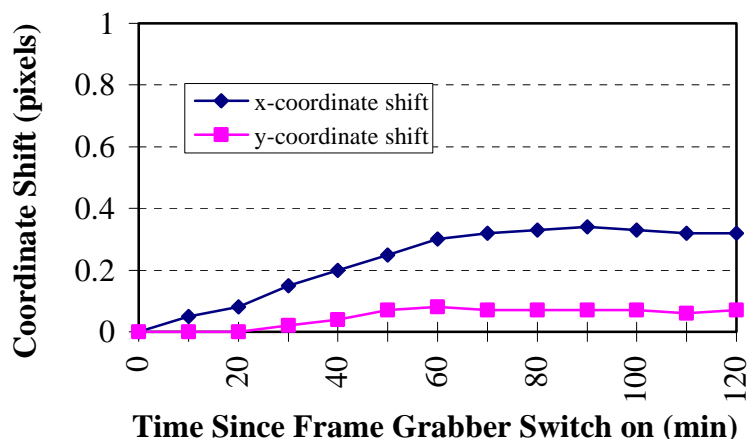
Figure 6.6 : Coordinate Shift Over the Period of Frame Grabber Warm-Up Only

6.4 Quality Control Results

As has been pointed out in Chapter 5, the real-time alerts which are essential for maintaining a uniform positioning accuracy under varying external conditions are dependent on expert knowledge. Some of this knowledge can only be gained empirically. In this Section, current results on INS bridging, backward smoothing, and OTF ambiguity resolution will therefore be presented.

6.4.1 INS Bridging Accuracy

To test the INS bridging accuracy, two field tests of the VISAT navigation component were carried out in May, 1995 and April, 1996. The first test took place along an L-shaped baseline in Calgary, while the second one is along a trajectory of circular shape.

The objective of the first test was to refine the INS-calibrated parameters, estimated from lab calibration, and to estimate the sensor performance in INS stand-alone mode (ZUPT mode). The reason for using an L-shaped baseline is that some INS errors are azimuth-dependent and will only show up in such a test design. On a straight traverse, these errors are usually buried in the larger time-dependent errors and are removed along with them. The objective of the second test was to confirm the calibration results obtained from the first test.

Figure 6.7 depicts the error behavior of the INS in stand-alone mode during the May test. GPS observations were removed from the data for a 100 second period and the INS data were processed in stand-alone mode. The truth model of this diagram was obtained by using the trajectory computed from the original GPS/INS measurements. Its accuracy is good to a few centimeters. The INS stand-alone positioning results stay below the half cycle level (10 cm for L1 and 43 cm for wide lane) for about 31 seconds for L1 and 52 seconds for the wide lane. Thus, bridging by INS would have given correct results in this case for up to 30 seconds when L1 was used and up to 50 seconds for L1/L2. It should be noted that this is valid only for this class of inertial hardware (Honeywell LaserRef III strapdown system), i.e. an INS rated at one nautical mile per hour at 95% CEP in unaided navigation mode. It also should be mentioned that the accuracy shown in Figure 6.7 is not consistently achieved in all runs; a more typical time interval for reaching the half cycle level is 20 seconds for L1 and 30 seconds for wide lane.
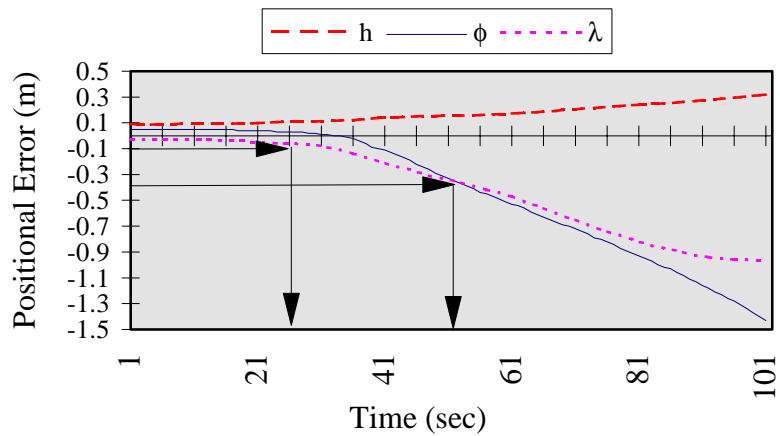
Figure 6.7: INS Error Behavior in Stand-alone Mode

The output from the Kalman filter was processed again by the Rauch-Tung-Striebel (RTS) optimal smoother, for more details about the RTS optimal smoother, see Gelb (1979). The results of the smoothing are plotted in Figure 6.8, it has been assumed that there is a GPS position update at the end of the 100 sec. The truth model of this diagram was obtained by using the trajectory computed from the original GPS/INS measurements. They show that the smoother has improved the accuracy and that the INS bridging interval is extended to 41 seconds for L1 and to 100 sec for the wide-lane case. It also shows that the time interval for the wide lane could be further extended.
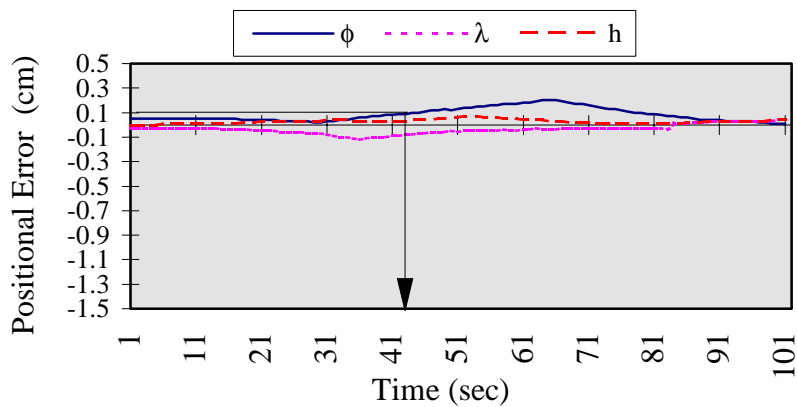
Figure 6.8: INS Error Behavior in Stand-alone Mode After Backward Smoothing

As mentioned in Section 4.3.3, the INS field calibration is the refinement of the bias parameters determined from the lab calibration. This is normally done by estimating the residual drifts and biases in the corrected sensor output via a Kalman filter. The residual gyro drifts and accelerometer biases were estimated to be :

$$d = \begin{pmatrix} -0.007 \\ 0.009 \\ 0.006 \end{pmatrix} arc\sec\!\Big/\!\sec$$

and

$$b = \begin{pmatrix} 5 \\ -10 \\ -17 \end{pmatrix} mGal.$$

The predictable position error of such residuals is about 20 cm, as estimated from Equation (5.7), after 60 sec of INS stand-alone mode. The estimated residual drift and biases were then added to those obtained from the lab calibration. Four more surveys were conducted along a 5 km long circular baseline (Figure 6.9) to test these estimated bias terms. In these tests, the van was driven with constant velocity of 40 km/h with regular stops at 50 sec intervals for 20 sec ZUPTs. Each survey took about 20 minutes to complete. Figure 6.10 shows the difference between the INS stand-alone solution and the GPS/INS solution. The figure confirms that the position between ZUPTS grows to about 0.2 to 0.3 m in 60 sec. It is usually not cumulative which indicates that there is no long term error trend, i.e. the van's dynamics is correctly modeled and the INS bias terms are correctly estimated with residual errors of about 10 mGal.
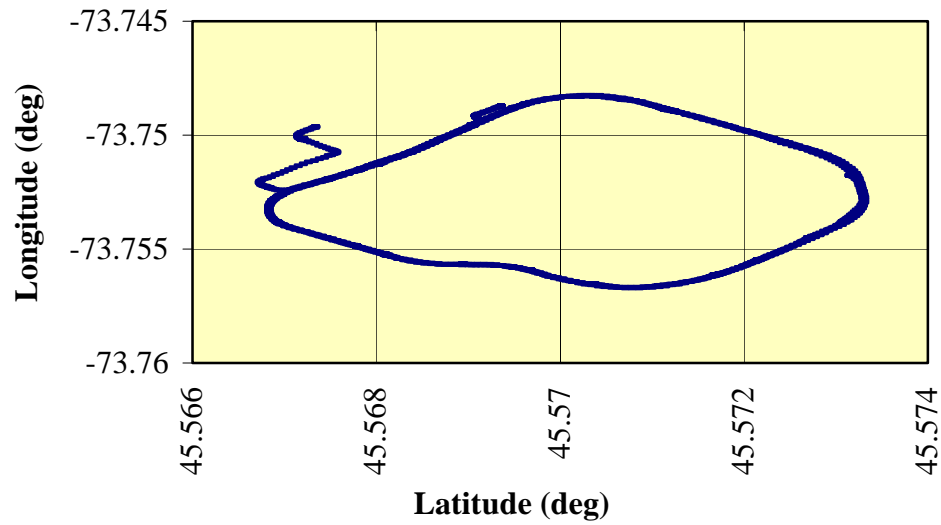
Figure 6.9 : INS Trajectory During a Stand-alone Test Along a Circular Trajectory
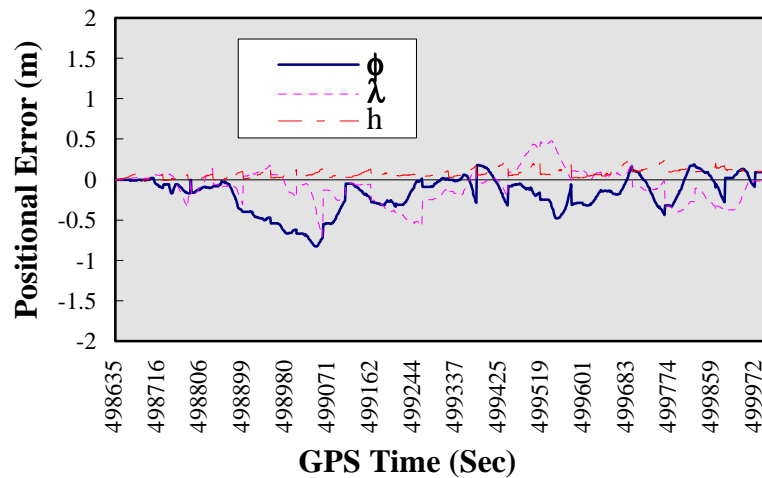
Figure 6.10 : Difference Between INS and GPS/INS Results Along a Circular Trajectory

6.4.2 GPS Cycle Slip Detection and Correction Using INS Coordinates

There are a number of ways to assess the usefulness of the INS predicted coordinates for cycle slip detection and correction. Table 6.5 gives the statistical summary of the difference between the GPS position and the INS solution predicted over one second. To

obtain statistically significant results, a sample size of eight hundred was computed from the two runs of the April test. The mean values are close to zero which indicates that the Kalman filter correctly models the vehicle dynamics and systematic errors. The values for the standard deviation (σ) are within the 3-cm range. Similarly, the maximum values are typically below 5 cm. These results show the reliability of INS for cycle slip detection over short periods and the effectiveness of using the high INS data rate (50 Hz) in interpolating the camera coordinates at the time of exposure.

Table 6.5: GPS Versus INS Prediction In Kinematic Mode

(Sample size = 800 sec)

Run No.	Coordinate	Mean (cm)	Standard deviation (σ) (cm)	Max difference (cm)
1	ϕ	1.2	2.1	3.1
	λ	1.4	2.0	-2.4
	h	-3.3	2.7	-5.1
2	ϕ	-2.2	1.9	3.1
	λ	1.1	2.2	4.2
	h	-2.1	1.7	-2.6

Another method of assessing the INS predicted accuracy is by monitoring the values of $\mathbf{v}$, i.e. the difference between the INS predicted double difference phase $\nabla\Delta\varphi_{predicted}$ and the measured double difference phase, $\nabla\Delta\varphi_{measured}$. Table 6.6 lists the mean and standard deviation of $\mathbf{v}$ values for different satellites and sample sizes during the April test. The listed standard deviation values indicate the threshold for cycle slip detection,

i.e. the value below which no cycle slips can be detected. This indicates that in general a cycle slip of ½ cycle can be detected by using INS measurements.

Table 6.6: Difference Between $\nabla\Delta\varphi$predicted Using INS Predicted Coordinates and $\nabla\Delta\varphi$measured using GPS (Sample size = 800 sec).

SV Number	Mean (cm)	St. dev. (σ) (cm)
26	-1.9	1.5
6	2.1	2.9
16	1.4	1.4
17	3.0	1.9
9	2.9	2.3
23	-1.8	2.1
12	2.7	2.5

A third method of assessing the INS cycle slip fixing capability is the prediction of the ambiguities of emerging satellites by INS and the comparison with the measured GPS results (using the computed position from tracked satellites). Table 6.7 lists the ambiguities for a number of satellites in one of the August runs as determined from GPS and as estimated from the INS predicted coordinates. The maximum difference in cycles agrees with the standard deviation values of Tables (6.5) and (6.6). This confirms that both solutions are essentially identical and that the Kalman filter results correctly model the van dynamics.

Table 6.7 : Difference Between Estimated $\nabla\Delta N$ From GPS and INS

SV Number	$\nabla\Delta N$ INS	$\nabla\Delta N$ INS	Difference in Cycles
6	-1748369	-1748369.1	0.1
16	-1938404	-1938403.8	0.2
17	833425	8344425.1	-0.1
27	-802652	-802651.7	0.3
23	879599	879598.8	0.2

In order to test the accuracy of using INS predicted coordinates to fix the GPS coordinates after signal blockage, a test along a highway with a number of bridges was performed. In this test, the van was stopped for about 600 sec after passing under a bridge. This is not necessary for GPS/INS integration. However, the static period can be used for ambiguity fixing, so that truth values are available to assess the accuracy of the ambiguities obtained by INS bridging. GPS blockage while passing under the bridges was between 10 and 30 seconds. During this time, the INS filter continues in prediction mode. Table 6.8 shows some of the wide-lane ambiguity values estimated from the INS predicted coordinates, and compares them to those fixed by the OTF technique.

Table 6.8 : Ambiguity Estimation Using INS Predicted Coordinates.

SV Number	Blockage Interval (Sec)	$\nabla\Delta N$ GPS	$\nabla\Delta N$ INS	Difference (cm)
6	13	-2804419	-2804419.1	-8.62
16	16	-2423079	-2423079.1	-8.62
17	17	833425	833424.85	12.9
23	18	2351363	2351362.9	8.62
12	23	272884	272884.2	-17.2

The coordinate differences are larger than before, although still well within the half cycle range of 43 cm for wide-lane. The larger differences can be explained by the higher noise level in wide-lane and by the satellite geometry during this test.

6.4.3 INS Supporting OTF Ambiguity Resolution

The reliability of INS bridging depends on the accumulation of errors in each subsystem and on the effectiveness of the updating procedure in reducing these errors. The largest accumulation of errors occurs during periods of unaided INS operation, that is, upon satellite loss of lock or absence of sufficient ZUPTs. During these periods, the INS is used as a stand-alone positioning system. After re-acquisition of the satellites, INS results are used to fix the phase ambiguities. In general the ambiguities fixed by the INS are float. Following that, the GPS filter will attempt to re-establish fixed ambiguity terms while in kinematic mode. This, however, is not uniformly reliable since it is geometry

dependent. In general, the INS predicted coordinates will reduce the time required to fix the ambiguities due to the good approximate coordinates after the bridging process.

Figure 6.11 shows the ambiguity fixing interval as a function of the number of satellites. The first column presents the time required when the OTF technique alone is used, the second column when the INS predicted coordinates are used as an approximation before the OTF procedure is applied, and the third column when the INS predicted coordinates are directly used after a 10 second ZUPT. The results indicate that by using the INS predicted coordinates, the time required to fix the ambiguities is reduced by 80% to 95% for poor satellite geometry and by 20% to 60% for good satellite geometry. This indicates that the INS constant bias terms (mainly accelerometer biases) are well estimated, and that the two systems are accurately synchronized. Similar results were obtained for L1 ambiguities where more time for ambiguity fixing is needed when using only the GPS. An efficient operational procedure to deal with the bridging problem after passing under a bridge is therefore to use wide-lane GPS data processing and then to rewind the GPS and INS files to start at the epoch of signal re-acquisition. This eliminates the errors in the trajectory after signal re-acquisition and ambiguity fixing. The same principle can be used for backward smoothing the INS trajectory during periods of signal blockage.

These results indicate the importance of frequent ZUPTs, when the system alert for loss of lock is on, and of static re-initialization of the system in case of long satellite blockage in urban centers. Static re-initialization will give the GPS filter time to converge after being reset by the INS filter.
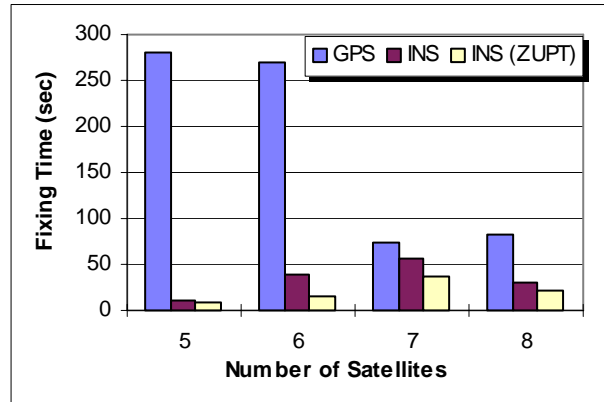
Figure 6.11: Effect of Using the INS Predicted Coordinates in

Speeding Up Ambiguity Fixing

6.5 SYSTEM TESTING

The production system was tested in Montreal and Quebec City in September 1995. The test areas included open areas, urban centers with narrow roads, and minor and major highways with a number of overpasses. Some of the Montreal City test results will be presented in this section. They are in six sectors, about 180 km, surveyed in five days. The sectors were surveyed such that the results in all sectors could be used to evaluate the system repeatability in forward and backward runs on the same day as well as on different days.

6.5.1 Relative Accuracy

The system's relative accuracy can be estimated by the day-to-day and run-to-run repeatability or the accuracy of measuring known distances. In order to test the system repeatability, some well-defined landmarks along the test course were used for comparison. Figure 6.12 shows results of a comparison of different runs in both forward and backward directions on the same day, taking the forward runs as the reference. Figure 6.13 shows the relative accuracy of the same landmarks for day-to-day repeatability, by taking the results of one day as a reference.
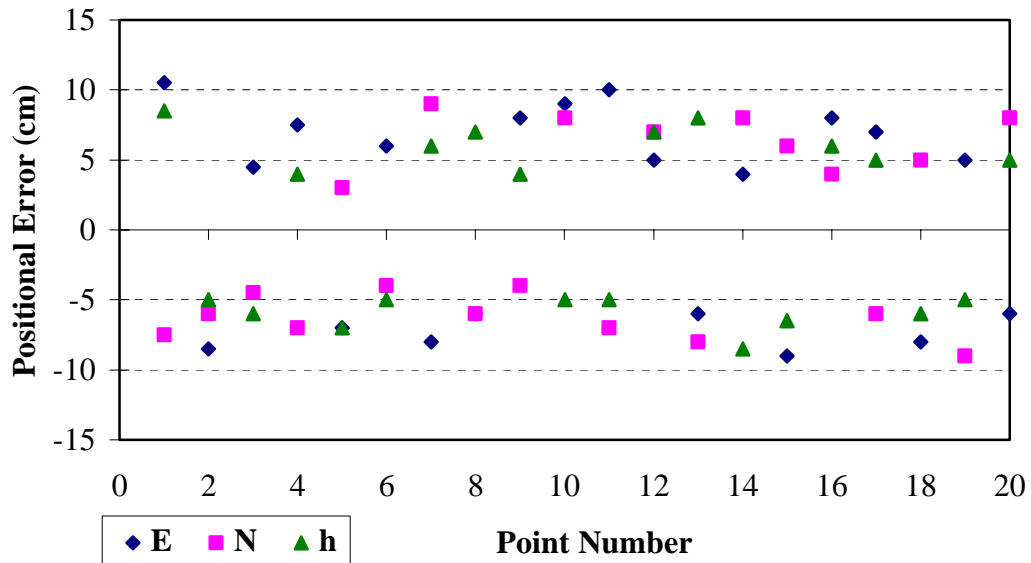
Figure 6.12. Repeatability of Forward-Backward Runs on the Same Day
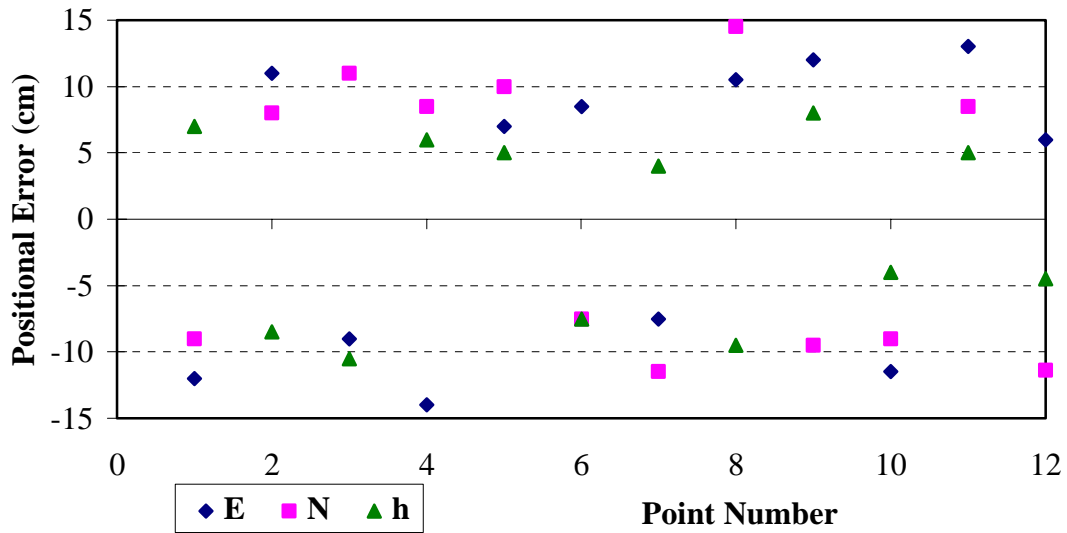
Figure 6.13 : Repeatability of Forward-Backward Runs on Different Days

Table 6.9 summarizes the system repeatability as obtained from the tests described above.

The RMS(E, N) is the composite horizontal error, computed from:

$$RMS(E,N) = \sqrt{(\delta E)^2 + (\delta N)^2}$$, where δE and δN are the errors in the East and North

coordinates.

Table 6.9: Statistical Summary of the System Repeatability

Repeatability	RMS (E, N) (cm)	RMS (h) (cm)
Forward-backward, same day	± 8	± 5
Same direction, different days	± 6	± 4
Forward-backward, different days	± 10	± 7

The results in height indicate that the GPS/INS positioning component is working at the centimeter level of accuracy. Since the height component in GPS is the weakest, it can be expected that the X and Y components are at least of the same accuracy. The increase in errors for the horizontal components must, therefore, be due to the camera array. The most likely explanation is that the increase in RMS(E, N) as compared to RMS(h) is due to the along-track error caused by the errors in determining the base between the cameras. The across-track error should be small and comparable in size to the height error. Another explanation would be a poor synchronization between the GPS/INS component and the camera component. This would result again in an along-track error. Repeatability in the same direction, even on different days, seems to be consistently better than the repeatability between forward and backward runs. The RMS values of 10 cm in the horizontal and 7 cm in the vertical directions are still reasonable, considering the fact that the errors in forward-backward direction should be $\sqrt{2}$ times the errors in the same direction.

The accuracy of measuring distances with the VISAT system is another way of testing the system's relative accuracy. For this purpose a special test was done by measuring the length of some well-defined features along the test course and taking images of these features in kinematic mode. Figure 6.14 shows the difference between the VISAT computed distances and the known distances. As expected, the figure shows that the errors are distance-dependent and reach a magnitude of 10-14 cm for objects 30 m away from the van.
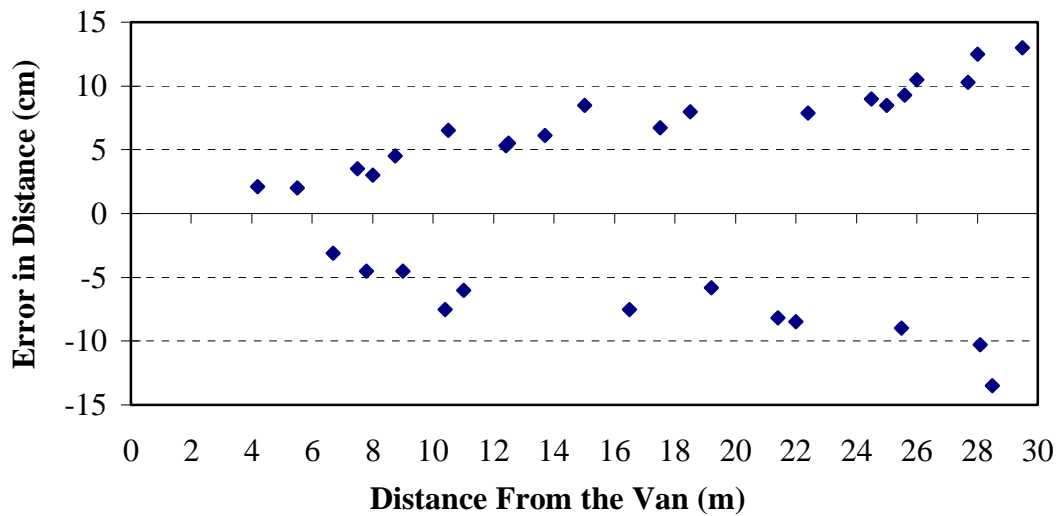
Figure 6.14 : The Accuracy of Measuring Distances with the VISAT System

6.5.2 Absolute Accuracy

The main objective of the VISAT system is the determination of the 3-D coordinates of all objects within the video cameras' field of view. Absolute accuracy is defined as the difference between the VISAT-derived 3-D coordinates and given control. As mentioned previously, the final accuracy of the 3-D coordinates is a function of the complete processing chain which involves GPS positions, INS position/attitude, target localization in the images, and system calibration. Figure 6.15 shows the errors in the computed 3-D coordinates of 14 control points located along one of the test sectors. The 3-D coordinates were computed from two images using the georeferencing formula described in Section 3.5. The distance between the control points and the cameras was approximately 10-30 m. The figure shows that an RMS of 16 cm in the horizontal coordinates and 7 cm in height are achievable for distances of up to 30 m away from the van.

150
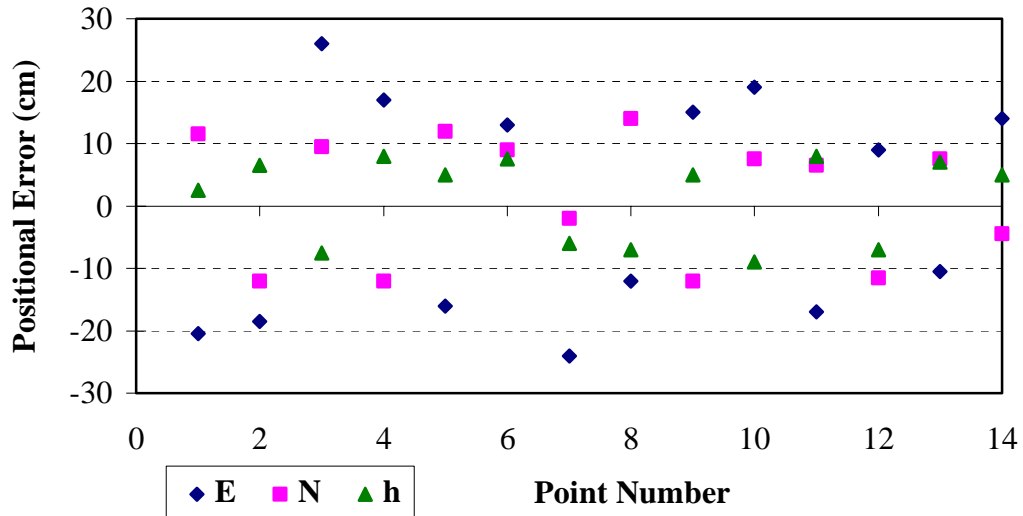
Figure 6.15. Absolute Accuracy of the VISAT System

6.5.3 Error Propagation With Distance and Effect of Geometry Optimization

As mentioned in Chapter 5, most of the system errors are distance-dependent. Therefore, it was necessary to investigate the error propagation with distance and how this error could be minimized by using redundant information in the 3-D coordinate computation. The georeferencing equation contains four unknowns (three coordinates and one scale factor) in three equations. Using an exposure interval of 5 m, the same object will appear in four to six consecutive images. Having N images of the same scene will add 3N extra equations and N unknowns (scale factors) for the same point (i). This adds redundancy to the spatial intersection problem. A least squares solution of the space intersection between the N rays is computed with (3N - 3 - N) degrees of freedom.

151

Figure 6.16 shows the position error for various distances for one specific ground target. This target appears in seven consecutive images (camera 1/camera 2). The position error is defined as the difference between the system coordinates and the known coordinates. The VISAT system was used, in this case, to get the measurement data, but the principle applies to any close-range measurement system of this type. As is obvious from Figure 6.16, the errors in the N-direction (along track) are larger than those in the E and h directions. This is mainly due to the scale factor error discussed previously. By using exposures with good geometry, errors in the N-direction will remain small. Thus by automatically selecting those images which optimize the geometry for all three coordinate directions, positions of consistent accuracy can be obtained.
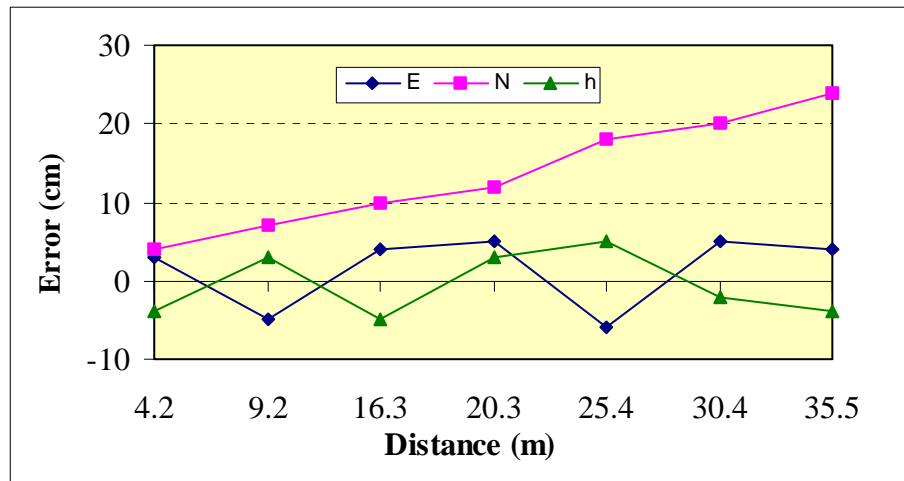
Figure 6.16: Error Propagation with Distance

Figure 6.17 shows the effect of reducing the errors in the 3-D coordinates by adding redundancy and by improving geometry. The solution of the first stereo-pair is used with each consecutive stereo-pair in the spatial intersection problem. The comparison of

Figures 6.16 and 6.17 indicate that by adding stereo-pairs to the spatial intersection solution, the along-track positional errors are considerably improved.
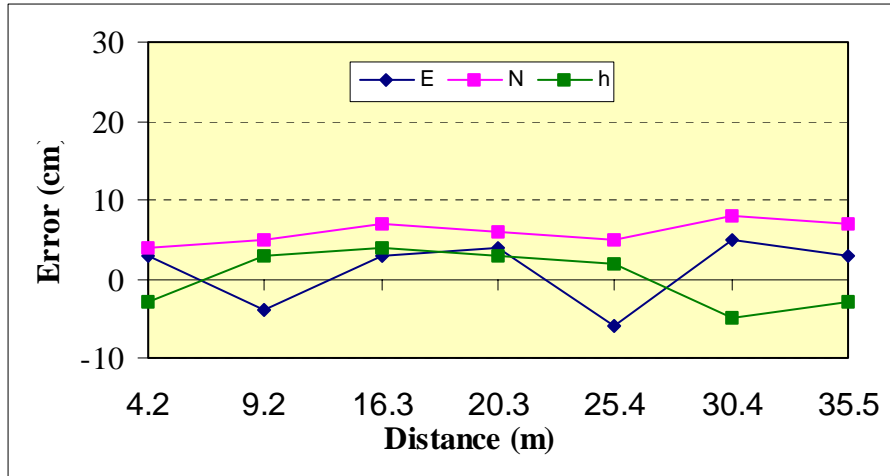
Figure 6.17 : Effect of Geometry on Positional Error

This opens interesting possibilities for a mobile system with centimeter level accuracy. Such accuracy is usually needed for specific targets of economic importance, such as property corners. Figure 6.18 shows, based on the VISAT system camera configuration, the principle of reducing the effect of geometry on the derived 3-D coordinates by combining data from different runs, surveys, and days. Thus, it is possible to design an operational procedure which optimizes the imaging geometry and the distance to the target based on collinearity error analysis. This will usually be sufficient to reduce the total positioning error to 5-10 cm (RMS). If objects are targeted and cameras with higher resolution are used, it might be possible to reduce the total error to RMS values below 5 cm.

The results of using images from different runs for the determination of the 3-D coordinates of one GCP are listed in Table 6.10. In this table, δ is the difference between the GCPs known coordinates and the VISAT-derived coordinates. It should also be mentioned that the poor horizontal accuracy for the image combination (4) is purely due to bad geometry, as supported by the fact that the height accuracy is below the decimeter level. This is due to the fact that the two cameras and the object point lie on a straight line. In practice, such situations can be avoided. The VISAT station software will not allow the user to use such a combination of images, and will propose other combinations which may be obtained from different runs and could result in the best geometry possible for the particular case.
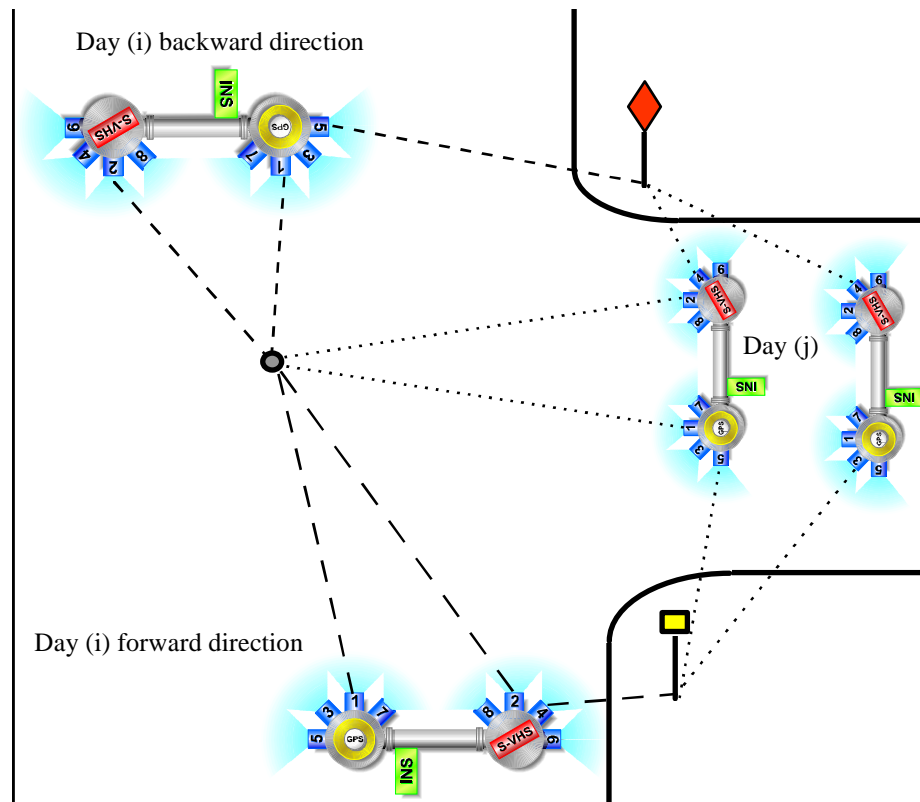
Figure 6.18: Principle of Using Images From Different Surveys and Days

Table 6.10 : The Effect of Using Images From Different Runs on the Accuracy of the 3-D

Coordinates

Camera Configuration and Sequence of Measurements	δ(X,Y) (m)	δ (Z) (m)	Comments
1. Cam. 5 and Cam. 3 with Cam. 5 being 5 m ahead of Cam. 3	0.20	0.03	Day (i), Forward direction
2. Cam. 3 and Cam. 5 with Cam. 5 being 5 m ahead of Cam. 3	0.19	0.02	Day (i), Forward direction
3. Cam. 5 and Cam. 2 with Cam 5 being 10 m ahead of 2	0.23	0.4	Day (i), Forward direction
4. Cam. 3 and Cam. 2 with Cam. 3 being 5 m ahead of Cam. 2	2.58	0.07	Day (i), Forward The software give a bad geometry warning message. The cameras and the object are almost along a straight line
5. Cam. 3 and Cam. 1 with Cam. 3 being 5 m ahead of Cam. 1	0.39	0.01	Day (i), Forward The software give a bad geometry warning message
6. Cam. 1 and Cam. 2 Fixed base	0.16	0.01	Day (j), Backward direction
7. Cam. 2 and Cam. 1 Fixed base	0.17	0.04	Day (j), Backward direction
8. Cam. 1 and Cam. 5	0.09	0.01	Cam. 1 Day (i) Cam. 5 Day (j)
9. Cam. 2 and Cam. 3	0.08	0.02	Cam. 2 Day (i) Cam. 3 Day (j)

CHAPTER 7

SUMMARY, CONCLUSIONS AND RECOMMENDATIONS

7.1 Summary

The development of VISAT, a mobile highway survey system for road inventory and general GIS applications, was the major objective of this research and was successfully achieved. Such a development was necessary because many of the existing classical methods of acquiring GIS data are no longer meeting current needs of data acquisition because they are too slow, labor intensive, and often do not provide the attribute information required for a dedicated GIS. The main objective of this research, the development and testing of a precise multi-sensor mobile mapping system, named VISAT, for operation in urban centers, has been met successfully. The VISAT system can be operated continuously under diverse operational conditions to generate georeferenced digital images. The VISAT Station environment permits user-friendly viewing of the imagery containing recent information for a user prescribed area. The image database provides a flexible information media which can be used in decision making, answer

queries, and more generally, in updating maps and GIS systems. It has been also demonstrated that the system is more accurate than initially anticipated, and can meet the more stringent accuracy requirements for highway and general GIS applications.

The system, consisting of differential GPS, a strap-down INS, an ABS pick-up, and eight CCD cameras, has been extensively tested in different operational environments. Test areas include open areas, urban centers with narrow roads, and minor and major highways with a number of overpasses.

A software package for the integration of GPS serial data, INS Arinc data, and video digital data has been developed using decentralized integration. The synchronization of images is at the 1 msec level. The program has a modular structure that can be easily and quickly modified to accommodate data from new auxiliary measurement systems, e.g. another positioning system such as GLONASS.

The theoretical framework of georeferencing multi-sensor data, more specifically video images, using GPS/INS data has been derived, and considerable emphasis has been given to system calibration and its importance in the georeferencing process. The formulation of the extraction of 3-D coordinates from multi-georeferenced images has also been presented.

7.2 Conclusions

The following conclusions can be drawn from this research :

1. **Absolute accuracy:** The analysis of the system's absolute accuracy was based on a comparison with "ground truth" that was independently determined with an accuracy of 1-2 cm. Agreement with pre-surveyed control points was generally better than 30 cm and had an **RMS** value of **16 cm** in the horizontal coordinates and **7 cm** in height. In general, the results of the system testing show that the absolute accuracy surpasses the development objectives for the prototype system.

2. **System repeatability**: The system repeatability also has been investigated based on run-to-run and day-to-day results. Run-to-run and day-to-day repeatability achieved in the system testing are about **7 cm** (**RMS**) horizontally and about **4 cm** (**RMS**) vertically. There is no significant difference between run-to-run and day-to-day results. This indicates that the GPS/INS component works at a consistent level from day to day and that the GPS can be used as a coordinate reference independent of local control.

3. **Operating speed:** Results indicate that highway velocities of **60 km/h** can be maintained with adequate data transfer and target positioning in post-processing mode at the VISAT Station.

4. **Redundancy:** Further improvement in 3-D coordinate accuracy has been achieved by using redundant measurements instead of individual image pairs and by applying geometric constraints. The use of multi-images in the 3-D computation reduces along-track error propagation with distance as well as extends the 3-D measurement operational distance. By applying these techniques together with point targeting, position accuracy of better than 5 cm (RMS) seem feasible.

5. **Temperature effect:** The effects of temperature change during the warm-up period on the CCD cameras are scale changes in the x-direction. The effects are largely frame grabber related and similar for both frame grabbers. Therefore, it will not affect the 3-D coordinates because it will cancel out. On the other hand, in calibration mode , it will not cancel out, but they can be practically eliminated by warming-up the system for about 80 minutes before starting the calibration.

6. **Synchronization:** In order to reach the accuracy required for VISAT applications, the synchronization should be accurate to a few milliseconds (one millisecond is equivalent to 1.8 cm positional error at a velocity of 60 km/h). This accuracy has been achieved with the current hardware configuration. Synchronization errors introduce an along-track error. Synchronization errors could be dramatically reduced by using either low-level coding software techniques, or centralized hardware integration techniques. The first technique could be applied to the real time clock of the host PC, the second to hardware integration in a single board (centralized interface board).

7. **Calibration:** Lens distortion and y-scale factor determination was necessary for the calibration of non-metric CCD cameras. The calibration requires a number GCPs. A test field of circular reflective targets of 5 inch diameter were used. An automatic detection method is necessary to estimate the target centers to an of accuracy **0.1 pixel**. The calibration is quite stable. Even with a one-month interval between the three performed calibrations, the changes in the base vector and the relative orientation angles were only ± **2 mm** in position and ± **2 arc minutes** in orientation. The orientation error due to system calibration results in a position error of about 3 cm over a distance of 35 m (35 m x tan 2 arc minutes = 3 cm). On the other hand, a constant bias of 2 mm in the base between the cameras (especially the forward looking ones) can introduce an error of 7 cm mainly along-track, for an object 35 m away from the cameras.

8. **INS Bridging:** Tests using the Honeywell LaserRef III INS indicate that stand-alone positioning errors stay below the half cycle level (10 cm for L1 and 43 cm for wide-lane) for about 31 sec for L1 and 52 sec for the wide-lane case. With the use of the RTS optimal smoother, the INS bridging interval can be extended to 41 sec for L1 and 100 sec for the wide-lane case, respectively.

9. **INS cycle slip detection and correction:** The difference between the GPS position and the INS solution over a one second interval was used to assess the potential of the INS to detect and fix GPS cycle slips. The statistical mean of these values was always close to zero which indicates that the Kalman filter correctly models the vehicle

dynamics and systematic errors. The values for the standard deviation were within the **3 cm** range. These results show the reliability of INS for cycle slip detection over short periods and the effectiveness of using the high INS data rate (50 Hz) in interpolating the camera coordinates at the time of exposure.

10. **INS Supporting the OTF:** Test results indicate that the time for OTF ambiguity resolution can be considerably reduced by using the INS predicted coordinates as an approximation before the OTF procedure is applied. The time required to fix the ambiguities is reduced by 80% to 95% for poor satellite geometry and by 20% to 60% for good satellite geometry. This indicates that the INS constant bias terms (mainly accelerometer biases) are well estimated and the two systems are accurately synchronized.

7.3 Recommendations

Based on the work done in this research, the following recommendations for future research are proposed:

Data Logging Software (VLog) :

- Implementation of real-time quality control module: The main function of the real-time quality control component is to give real-time alerts to the operator in situations

where the specified trajectory quality can most likely be not achieved. These alerts are determined by the computer which monitors data accuracy of GPS and INS, tracks signal blockage for each satellite, and introduces expert knowledge on INS bridging (smoothing) and the convergence time of OTF ambiguity resolution techniques into the process. In such cases, where an alert is given, the vehicle is stopped to either allow an additional ZUPT, or, in more critical cases, an independent ambiguity resolution. Using these additional measurement periods, the required post-mission trajectory accuracy can be obtained in the specified number of cases and resurveys can be avoided.

- Investigation of the effect of using a single board for the integration of GPS/INS/ABS/PPS data and its effect on synchronization errors: This implementation will be essential for airborne applications where µsec synchronization accuracy is required. It can be achieved by using the centralized hardware integration scheme discussed in Chapter 5.

Calibration :

- Investigation of another way for simplifying field procedures for the determination of the relative orientation parameters. Cameras could be calibrated inside the tower first, and then the two towers could be calibrated with the INS. Using such a procedure, it would be possible to calibrate the two towers in a lab environment. This has the advantage that fewer GCPs can be used in the second step.

GPS/INS :

- Modeling work should be focused on the investigation and improvement of the accuracy of the INS prediction during data gaps. Another form of the Kalman filter, based on adaptive filtering, might offer a promising approach.

- Implementing a pot-mission quality control module which uses all available resources to obtain the best possible trajectory. This includes: the use of INS data for bridging GPS outages; the use of backward smoothing procedures and OTF ambiguity resolution; the automatic elimination of bad satellites; automatic rewinding of files after fixing the ambiguities; applying no GPS update in periods of bad DOP; omitting bad ZUPTs etc.

- Some additional tests are necessary to investigate the system performance for longer GPS differential baselines. The optimal static initialization time should also be examined.

- Another attractive research area is the use observations from emerging new satellite systems such as GLONASS and STARFIX. The redundant observation would help to reduce problems with GPS signal blockage.

- The integration of ABS data into KINGSPAD as an additional measurement for bridging GPS outages and extending the INS bridging interval should be studied.

Cameras :

- Investigating the use of one control unit for all cameras for better camera-to-camera synchronization.

- Investigating the use of digital or progressive scan cameras and their effect in increasing the vertical resolution of the images.

- Investigating the use of real-time compression of the images and its effect on increasing the rate of the captured images.

VISAT Station :

- Investigating the use of back-projection and feature superimposition and its importance for map revision.

- Investigating the integration of INS data and relative positions obtained from triangulation with image data and implementation of map matching using existing digital maps form an attractive research area.

- Investigating the use of shape detection for automatic detection of road signs and special geometric features. Having identified similar (objects) shapes on stereo pairs of images, and matching constraints (e.g., epipolar lines) can be used to automatically position objects using conjugate imagery. When image resolution permits, character recognition can be employed to identify a specific sign function. This information coupled with line-of-sight data can be used to determine if a sign is in the appropriate position and, if not, where it should be relocated.

- The configuration of the images used in 3-D computation should be optimized in order to form a suitable imaging geometry in the existing system.

New mapping sensors :

- The incorporation of sonar or laser ranging devices would open a number of new applications for the use of mobile mapping systems in transportation applications. The information from these sensors, the distance between the sensors and the road surface, could be used to control the INS vertical channel drift.

These problems will provide challenges for years to come. Solving these problems will be an enormous extension of mobile mapping from vans and the fusion of such data with other multi-sensor data.

REFERENCES

Abousalem, M.A. (1993), "Development of A Robust GPS Kinematic Positioning Module for Automatic Vehicle Location and Navigation", M.Sc. Thesis, Department of Geomatics Engineering, The University of Calgary, Calgary, Canada, UCSE Report No. 20077.

Ackermann, F. (1995), "Sensor-and-Data Integration - the New Challenge", Integrated Sensor Orientation, Wichmann, ISBN 3-87907-279-5, Eds. Colomina/Navaro, pp. 2-10.

Ash, T., Silva, R., Brown, A., and LaMance, J. (1995), "GPS/Inertial Mapping (GIM) System for Real Time Mapping of Roadways Using WADGPS", Proceedings of the Institute of Navigation, ION GPS-95, Palm Springs, CA, USA, September 12-15, pp. 1825-1830.

Baraniak, D. W. (1994), "Creating High Accuracy Digital Maps Using GPS and Stereo Digital Imaging Technologies", Wisconsin Professional Engineer, Published by The Wisconsin Society of Professional Engineers, May/June 1994, Vol. 35, No. 4, pp. 12-14.

Beyer, H.A. (1992), "Geometric and Radiometric Analysis of a CCD-Cameras Based Photogrammetric Close Range System", Ph.D. thesis, ETH-Honggerburg CH-8093 Zurich, ISBN 3-906513-24-6, May 1992.

Blaho, G. and Toth, C. (1995), "Field Experience With a Fully Digital Mobile Stereo Image Acquisition System", The Mobile Mapping Symposium, Columbus, OH, USA, May 24-26, 1995, pp. 97-104.

Bossler J. D, Goad, C. and Novak, K. (1993), "Mobile Mapping Systems; New Tools for the Fast Collection of GIS Information", GIS'93, Ottawa, Canada, pp. 306-315, March 23-35.

Britting, K.R. (1971), " Inertial Navigation Systems Analysis", Wiley-Interscience, New York.

Brown, Duane C. (1966), " Decentering Distortion of Lenses", Photogrammetric Engineering, Vol. XXXII, No. 3.

Cannon, M. E. (1987), "Kinematic Positioning Using GPS Pseudoranges and Carrier Phase Observation", M.Sc. Thesis, Department of Geomatics Engineering, The University of Calgary, Calgary, Canada, UCSE Report No. 20019.

Cannon, M.E. (1991), "Airborne GPS/INS With An Application To Aerotringulation", Ph.D. Thesis, Department of Geomatics Engineering, The University of Calgary, Calgary, Canada, UCSE Report Number 20040.

Cannon, M.E., Schleppe, J., Mclellan, J.F., and Ollevier, T.E. (1992), "Real-Time Heading Determination Using An Integrated GPS-Dead Reckoning System", Proceedings of the Institute of Navigation, ION GPS-92, Albuquerque, New Mexico, September 16-18.

Cohen, C.E. and Parkinson, B.W. (1992), " Aircraft Applications of GPS-Based Attitude Determination", Proceedings of the Institute of Navigation, ION GPS-92, Albuquerque, New Mexico, September 16-18.

COHU INC. (1993), "Installation, Operation and Maintenance Manual for 4990 Series RS-170 &CCIR CCD Monochrome Cameras", Technical Manual No. 6X-948.

Cosandier, D. and Chapman, M. A. (1992), "High Precision Target Location for Industrial Metrology", Videometrics, SPIE OE/Technology, Boston, November.

Cosandier, D., Ivanco, T. A., Chapman, M.A. and Dylke, M. (1994), " The Integration of a Digital Elevation Model in Casi Image Geocorrection", The First International Airborne Remote Sensing Conference, Strasbourg, France, 11-15 September.

El-Mowafy, A. and Schwarz, K.P.,(1994), "Epoch by Epoch Attitude Determination Using A Multi-Antenna System in Kinematic Mode", Proceedings of the International Symposium on Kinematic Systems in Geodesy, Geomatics and Navigation, KIS-94, Banff, Canada, pp. 331-340, August 30 - September 2.

El-Sheimy, N., Schwarz, K.P. (1993), "Kinematic Positioning In Three Dimension Using CCD Technology", VNIS93 Conference, Ottawa, Canada, October 12-15, pp. 472-475.

El-Sheimy, N., Schwarz, K.P. (1994), "Integrating Differential GPS Receivers with an Inertial Navigation System (INS) and CCD Cameras for a Mobile GIS Data Collection System", ISPRS94, Ottawa, Canada, June 6-10, pp. 241-248.

El-Sheimy, N., Schwarz K.P., and Gravel, M. (1995), "Mobile 3-D Positioning Using GPS/INS/Video Cameras, The Mobile Mapping Symposium", Columbus, OH, USA, pp. 236-249, May 24-26.

El-Sheimy, N. (1996), "A Mobile Multi-Sensor System For GIS Applications In Urban Centers", ISPRS 1996, Commission II, Working Group 1, Vienna, Austria, July 9-19, 1996,

Gelb, A. (1974), " Applied Optimal Estimation", The M.I.T. Press, Cambridge, Mass., USA, Fourth Print.

Goldstein, H. (1980), " Classical Mechanics", Addison-Wesley, Massachusetts, USA, 1980

Halverson, G. (1992), "A Company Tries to Map Every Block in America", Business Week, 1992, No. 3293.

Harris, C.B. (1989), "Prototype For A Land Based Automatic Vehicle Location and Navigation System", M.Sc. Thesis, Department of Geomatics Engineering, The University of Calgary, Calgary, Canada, UCSE Report Number 20033.

Hashemipour, H. R., Roy, S. and Laub, A. J. (1988), "Decentralized Structures for Parallel Kalman Filtering", IEEE Trans. Automatic. Control., Vol. AC-33, 1988, pp. 88-94.

Hein, W. G. (1995), "Progress in Airborne Gravimetry: Solved, Open and Critical Problems", IAG Symposium G4, IUGG XXI General Assembly, Boulder, Colorado, July 2-14, 1995, pp. 3-11, Published by Department of Geomatics Engineering, UofC, Calgary, Canada, Report Number 60010.

Karara, H. M. (1989), "Non-Topographic Photogrammetry", Second Edition, American Society for Photogrammetry and Remote Sensing, Virginia , USA.

Krakiwsky, E.J. (1991), "GPS and Vehicle Location and Navigation", Innovation Column, GPS World, May 1991, Vol. 2, No. 5, Advanstar Communications, Eugene, Oregon, USA.

Krakiwsky, E.J., Abousalem, M.A., Szabo, D.J., and Bullock, J.B. (1995), "IVHS Navigation Systems Database ™", Version 4.5, Department of Geomatics Engineering, The University of Calgary.

Lachapelle, G. (1995), "GPS Theory and Applications", ENGO 625 Lecture Notes, Department of Geomatics Engineering, The University of Calgary, Calgary, Canada.

Lapine, L. (1990), "Analytical Calibration of the Airborne Photogrammetric System Using A Priori Knowledge of the Exposure Station Obtained from Global Positioning System Technique", Department of Geodetic Science and Surveying, The Ohio State University, UMI Dissertation Services, Publication No. 9111738, Ann Arbor, MI 48109.

Lapucha, D. (1990), "Precise GPS/INS Positioning for Highway Inventory System", M.Sc Thesis, Department of Geomatics Engineering, The University of Calgary, Calgary, Canada, Report No. 20038.

Lapucha, D., Schwarz, K.P., Cannon, M.E., and Martell, H. (1990), "The Use of INS/GPS in a Kinematic Survey System", Proc. IEEE PLANS 1990**,** Las Vegas, pp. 413-420, March 20-23.

Lenz, R. (1989), "Image Data Acquisition With CCD Cameras", Optical 3D Measurement Techniques, Applications in Inspection, Quality Control and Robotics. p. 22-34., Weichmann, Vienna, September 1989.

Li, R., Chapman, M. A., Qian, L., Xin. Y., and Schwarz, K. P. (1994), "Rapid GIS Database Generation Using GPS/INS Controlled CCD Images", ISPRS 94 GIS/SIG, June 6-10, Ottawa, Canada.

Lichti, D. D., and Chapman, M.A. (1995), "CCD Camera Calibration Using the Finite Element Method", Proceedings of SPIE Intentional Symposium on Intelligent Systems and Advanced Manufacturing, Philadelphia, Vol. 2598, October 22-2, pp. 23-43.

Liu, Z. (1994), "Comparison of Statistical Methods for the Alignment of Strapdown Inertial Systems", M.Sc Thesis, Department of Geomatics Engineering, The University of Calgary, Calgary, Canada, Report No. 20047.

Luhman, T. (1990), "Image Recording Systems for Close-Range Photogrammetry", SPIE vol. 1395, Close-Range Photogrammetry Meets Machine Vision, Zurich, Switzerland, SPIE Vol. 1395, September 3-7, pp. 86-95.

Pottle, D. (1995), " New Mobile Mapping Systems Speeds Data Acquisition", International Journal of Geomatics (GIM), September 1995, pp. 51-53.

Raynor, J.M., and Seits, P. (1990), " The Technology and Practical Problems of Pixel-Synchronous CCD Data Acquisition for Optical Metrology Applications", Close Range Photogrammetry meets machine vision , Zurich, Switzerland, SPIE Vol. 1395, September 3-7, pp. 96-103. 1990.

ROADWARE Corporation (1994), " Data Collection Technologies", Paris, Ontario, Canada.

Savage, P.G. (1978), "Strapdown Inertial Sensors-Theory and Applications-Introduction and Review", AGARD Lecture Series, No. 95.

Schwarz, K.P., Fraser, C.S., and Gustafon, P.C. (1984), "Aerotringulation Without Ground Control", Int. Arch. of Photogrammetry and Remote Sensing, 25 (Part A1), Rio de Janeiro, Brazil.

Schwarz, K.P., Cannon, M.E., and Wong, R.V.C. (1989), "A Comparison of GPS Kinematic Models for the Determination of Position and Velocity along a Trajectory", Manuscripta Geodaetica, 1989, 14(2), pp. 345-353.

Schwarz, K.P., Lapucha, D., Cannon, M.E., and Martell, H. (1990), "The Use of GPS/INS in a Highway Inventory System", Proc. FIG XIX Congress, Helsinki, Finland, Vol. 5, paper 508.4, pp. 238-249, May 10-19.

Schwarz, K. P., Martell, H., El-Sheimy, N., Li, R., Chapman, M., and Cosandier, D. **(1993a),** "VISAT- A Mobile Highway Survey System of High Accuracy", VNIS Conference '93 Conference, Ottawa, October 12-15, pp. 476-481.

Schwarz, K.P., Chapman, M.A, Cannon, M. W., and Gong, P. **(1993b),** "An Integrated INS/GPS Approach to the Georeferencing of Remotely Sensed Data", PE&RS Vol. 59, No. 11, November 1993, pp. 1667-1674.

Schwarz, K.P., Chapman, M., Cannon, M., Gong P., and Cosandier D. (1994), "A Precise Positioning/Attitude System in Support of Airborne Remote Sensing", ISPRS94, Ottawa, Canada, June 6-10, pp. 241-248.

Schwarz, K.P (1995) , "Integrated Airborne Navigation Systems for Photogrammetry" The Wichmann Verlag, ISBN 3-87907-277-9, Photogrammetric week'95, Stuttgart, Oberkochen, Germany, pp. 139-153.

Schwarz, K.P. and El-Sheimy, N., (1996), "Kinematic Multi-sensor Systems For Close Range Digital Mapping" , ISPRS 1996, Commission V, Working Group III, Vienna, Austria, July 9-19, 1996, **Invited Paper**.

Seige, P. (1993), " MOMS : A Contribution to High Resolution Multispectral and Stereoscopic Earth Observation From Space", Proceeding of the Photogrammetric Week '93, Stuttgart, Oberkochen, September, 1993, pp. 109-120.

Skaloud, J, Cosandier, D., Schwarz, K.P., Chapman, M.A. (1994), "GPS/INS Orientation Accuracy Derived From A Medium Scale Photogrammetry Test", Proceedings of the International Symposium on Kinematic Systems in Geodesy, Geomatics and Navigation, KIS94, Banff, Canada, pp. 341-348, August 30-September 2.

Skaloud, J. **(1995),** "Strapdown INS Orientation Accuracy with GPS Aiding", M.Sc. Thesis, Department of Geomatics Engineering Report Number 20079, The University of Calgary, Calgary, Canada.

Tischer, M. (1994) , "PC Intern System Programming", Abacus, Grand Rapids, MI, USA.

Tudhope, R. L. (1988), "Dynamic Aerial Camera Calibration Combining Highly Convergent and Vertical Photography", M.Sc. thesis, Department of Geodetic Science and Surveying, Ohio State University, Columbus, OH, 1988.

VISAT Station User Manual (1995), GEOFIT Inc., Laval, Quebec, Canada.

VISAT Van Operation Manual (1995), GEOFIT Inc., Laval, Quebec, Canada.

Wagner, M. J. **(1995),** "Seeing in 3-D Without the Glasses", Earth Observation Magazine (EOM), July, 1995, pp. 51-53.

Wei, M. and Schwarz, K.P. (1990a), "Testing a Decentralized Filter for GPS/INS Integration", Proc. IEEE PLANS 1990, Las Vegas, USA, March 20-23, pp. 429-435.

Wei, M. and Schwarz, K.P. (1990b), "A Strapdown Inertial Algorithm Using an Earth-Fixed Cartesian Frame", Navigation, Vol. 37, No. 2, pp.153-167 .

Wei, M. and Schwarz, K.P. (1995), " Analysis of GPS-derived Acceleration From Airborne Tests", IAG Symposium G4, IUGG XXI General Assembly, Boulder, Colorado, July 2-14, 1995, pp. 175-188. Published by Department of Geomatics Engineering, UofC, Report Number 60010.

Wells, D.N., Beck, N., Delikaraoglu, D., Kleusberg, A., Krakiwsky, E., Lachapell, G., Langely, R., Nakiboglu, M., Schwarz, K.P., Tranquilla, J., and Vanicek P. (1986), "Guide to GPS Positioning", The University of New Brunswick, Fredericton, New Brunswick, Canada, December 1986.

Wong, K.W., Lew, M., and Ke, Y. (1990), "Experience with two vision systems", Close Range Photogrammetry meets machine vision, , Zurich, Switzerland, SPIE Vol. 1395, September 3-7, pp. 3-7.

Wong, R.V.C. (1988), "Development of a RLG Starpdown Inertial Survey System", Ph.D. Thesis, Department of Geomatics Engineering, The University of Calgary, Calgary, Canada, Report Number 20027.

Wong, R.V.C., Schwarz, K.P., and Cannon, M.E. (1988), "High Accuracy Kinematic Positioning by GPS-INS", Navigation: Journal of The Institute of Navigation, Vol. 35, No.2, pp. 275-287

Xin, Y. (1995), "Automating Procedures on A Photogrammetric Softcopy System", M.Sc. Thesis, Department of Geomatics Engineering, The University of Calgary, Calgary, Canada.

Yan, L. and Zuxun, Z. (1988), " Fast Implementation For Generating Epipolar Line Images With One-Dimensional Resampling", Eidgenossiche Technische Hocheshule Zurich, Institut fur Geodasie und Photogrammetrie., Bericht Nr. 145, April 1988.

Zhang, J.Q. (1995) "Development of a GPS-Aided Inertial Platform for an Airborne Scalar Gravity System", Report No. 20090, Department of Geomatics Engineering, The University of Calgary, Calgary, Canada.

Zhang, Z. (1988), "A New Approach of Epipolar-line Matching for Improving the Performance of SODAMS system", ISPRS 16th, Commission III, Kyoto, Japan, 1988.